Biomimetic Models of [FeFe]-hydrogenase: Utilization of peptides and redox non-innocent ligands in synthetic catalysts

by

Souvik Roy

A Dissertation Presented in Partial Fulfillment
of the Requirements for the Degree
Doctor of Philosophy

Approved September 2013 by the
Graduate Supervisory Committee:

Anne Jones, Chair
Ryan Trovitch
Thomas Moore

ARIZONA STATE UNIVERSITY

December 2013

ABSTRACT

[FeFe]-hydrogenases are enzymes for the reduction of protons to hydrogen. They rely on only the earth abundant first-row transition metal iron at their active site (H-cluster). In recent years, a multitude of diiron mimics of hydrogenases have been synthesized, but none of them catalyzes hydrogen production with the same exquisite combination of high turnover frequency and low activation energy as the enzymes. Generally, model complexes fail to include one or both of two features essential to the natural enzyme: an intricate array of outer coordination sphere contacts that constrain the coordination geometry to attain a catalytically optimal conformation, and the redox non-innocence of accessory [FeS] clusters found at or near the hydrogen-activating site. The work presented herein describes the synthesis and electrocatalytic characterization of iron-dithiolate models designed to incorporate these features. First, synthetic strategies are developed for constructing peptides with artificial metal-binding motifs, such as 1,3-dithiolate and phosphines, which are utilized to append diiron-polycarbonyl clusters onto a peptide. The phosphine-functionalized peptides are shown to be better electrocatalysts for proton reduction in water/acetonitrile mixtures than in neat acetonitrile. Second, we report the impact of redox non-innocent ligands on the electrocatalytic properties of two types of [FeFe]-hydrogenase models: dinuclear and mononuclear iron complexes. The bidentate, redox non-innocent α-diimine ligands (N-N), 2,2'-bipyridine and 2,2'-bipyrimidine, are used to create complexes with the general formula (μ-SRS)$Fe_2(CO)_4$(N-N), new members of the well known family of asymmetric diiron carbonyls. While the 2,2'-bipyridine derivatives can act as electrocatalysts for proton reduction, surprisingly, the 2,2'-bipyrimidine analogues are found to be inactive towards

catalysis. Electrochemical investigation of two related Fe(II) complexes, (bdt)Fe(CO)P_2 for bdt = benzene-1,2-dithiolate and P_2 = 1,1'-diphenylphosphinoferrocene or methyl-2-{bis(diphenylphosphinomethylamino}acetate, related to the distal iron in [FeFe]-hydrogenase show that these complexes catalyze the reduction of protons under mild conditions. However, their reactivities toward the external ligand CO are distinguished by gross geometrical differences.

To my parents for their endless encouragement and support,
and to my wife who has put up with me for reasons not always obvious.

ACKNOWLEDGMENTS

First and foremost, I would like to acknowledge my advisor Prof. Anne K. Jones for giving me the opportunity to delve into the depths of science. Your knowledge, guidance, patience and experience have been hugely influential to my scientific career as well as my personal life. You have been an amazing mentor and it has truly been a privilege to work for you. I would also like to thank my committee members Prof. Ryan Trovitch and Prof. Tom Moore for their valuable help and guidance. I must thank all the current and past members of the Jones group including Arnab, Clelsea, Patrick, Bi, David, Joe, Nick, Lu, Angelo, John and many more for their unending help in the lab. You have been the most awesome colleagues one can ask for. Finally a special thanks to Manas, Basab, and Dinesh for always being up for the moral-boosting happy hour. You will all be missed.

Funding: US Air Force Office of Scientific Research (award number FA9550-08-1-0116), DOE funded Center for Bio-Inspired Solar Fuel Production (award number DE-SC0001016) and Arizona State University must be acknowledged for providing the financial support for this work.

TABLE OF CONTENTS

LIST OF FIGURES

LIST OF TABLES

LIST OF SCHEMES

LIST OF ABBREVIATIONS

Abbreviation	Extended version
bdt	Benzene-1,2-dithiolate
bpy	2,2'-bipyridine
bpym	2,2'-bipyrimidine
DCM	Dichloromethane
DIEA	Diisopropylethylamine
DMF	N,N-dimethyl formamide
ESI-MS	Electron-spray ionization mass spectrometry
Fmoc	9-fluorenylmethoxycarbonyl
FTIR	Fourier transformed infra-red
HATU	Methanaminium-2-(1H-7-Azabenzotriazol-1-yl)--1,1,3,3-tetramethyl uronium hexafluorophosphate
HBTU	O-Benzotriazole-N,N,N',N'-tetramethyluronium hexafluorophosphate
HPLC	High performance liquid chromatography
MALDI-TOF	Matrix assisted laser desorption/ionization mass spectrometry
NMR	Nuclear magnetic resonance
PyBOP	(Benzotriazol-1-yloxy)tripyrrolidinophosphonium hexafluorophosphate
TCEP	Tris(2-carboxyethyl)phosphine
TFA	Trifluoroacetic acid
TIPS	Triisopropylsilane
TMS	Tetramethylsilane
UV-Vis	Ultraviolet-visible

Chapter 1

Introduction: An overview of hydrogenases, active site analogues of [FeFe]-hydrogenases, and the summary and scope of this dissertation

Introduction

The utilization of hydrogen by micro-organisms as a fuel or usage of protons as terminal electron acceptors (producing hydrogen gas) is catalyzed by a class of metalloenzymes named hydrogenases.[1, 2] Hydrogenases harbor earth-abundant transition metal clusters that have the ability to activate or produce hydrogen. The relevance of this reaction towards building a future hydrogen economy has spurred widespread interest in these enzymes.[3, 4] Hydrogen is a carbon neutral, environmentally friendly fuel that is poised to become a major energy carrier in the future by virtue of its clean combustion to water in fuel cells,[5] and direct production of hydrogen from water using solar energy is appealing.[6] However, owing to the intrinsic stability of the hydrogen molecule, both production and oxidation of hydrogen at ambient temperatures require efficient electrocatalysts, and the current industry standards are mostly based on expensive noble metals such as platinum or palladium, the sustainability of which on a global scale is doubtful.[7, 8] Hydrogenases offer a possible alternative to precious metal catalysts because they can operate with very high turnover frequencies at low electrochemical overpotential, and their catalytic activity relies on active sites composed of first row transition metals such as nickel and iron.[9, 10] Therefore, understanding the mechanism of

these enzymes and expanding that chemistry by constructing biomimetic molecular catalysts or artificial metalloenzymes has become a significant research goal.

Overview of Hydrogenases

Hydrogenases can be classified into three types depending on the metal content of the active site: [NiFe]- and [FeFe]-hydrogenases, which produce or oxidize hydrogen, and a third type, referred to as [Fe]-hydrogenases, which can activate hydrogen in the presence of an organic cosubstrate but do not mediate redox reactions of protons or hydrogen.[11] Although phylogenetically unrelated, [NiFe]- and [FeFe]-hydrogenases share several common features. In both enzymes, the hydrogen producing (or oxidizing) bimetallic active site is buried deeply in a naturally engineered cavity of the protein and connected to the surface *via* a series of iron-sulfur clusters that serve as a conduit for fast electron transfer.[12, 13] As shown in Figure 1-1A, the active site of [FeFe]-hydrogenases, commonly referred to as the H-cluster, is composed of two sub-sites connected *via* a bridging cysteinyl thiolate: a redox active [4Fe4S] cubane which operates as a redox-buffer by delocalizing and transferring electrons, and a biologically unusual [2Fe2S] unit where the catalytic reaction takes place.[14-17] The [2Fe2S] subunit consists of two iron centers that are bound by a combination of five diatomic CN^- and CO ligands and connected by a unique non-proteinaceous bridging dithiolate, SCH_2XCH_2S, where the bridgehead atom, X, is likely a nitrogen (NH).[18-21] The iron adjacent to the cubane is thought to be a six coordinate, low spin Fe(II) center, and the iron distal to the cubane is a five coordinate Fe center with an open coordination site at which the substrate turnover is believed to take place. The [NiFe] active site features a heterobimetallic assembly with remarkable similarity to the [2Fe2S] cluster of [FeFe]-hydrogenases (Figure 1-1B). It also contains a

low spin Fe(II) center bound to CO and CN^- ligands that is bridged to a nickel center through two cysteinyl thiolates.[22-24] The nickel first coordination sphere is completed by two terminal cysteine thiolates. Theoretical and experimental studies indicate that the Fe(II) center remains redox-silent throughout the enzymatic cycle, and the oxidation state of the nickel center varies between Ni(II) and Ni(III).[25, 26] The third type, [Fe]-hydrogenases, is structurally distinct from the other two types since it contains a mononuclear iron complex as active site and no iron-sulfur clusters.[27] Nonetheless, the active site of [Fe]-hydrogenases bears some resemblance to those of the bimetallic enzymes in that it also possesses a low spin Fe(0) or Fe(II) center coordinated to two CO ligands, one thiolate and one N/O ligand (Figure 1-1C).[28-30] The similarity in the ligand sets present in the organometallic active sites of all three types of hydrogenases implies that these ligands play a critical mechanistic role that facilitates proton reduction and hydrogen activation at the iron or nickel center under ambient conditions.

Active site models of [FeFe]-hydrogenases

Although natural hydrogenase enzymes are excellent catalysts for proton reduction (or hydrogen activation), their utility in bio-fuel cell application has been limited by a number of factors. First, isolation of these enzymes in large quantities from natural sources is difficult. Second, utilization of enzymes as electrocatalysts in bio-fuel cells requires high loadings on electrodes which may prove impossible to achieve. Third, the extreme sensitivity of these enzymes toward small molecules such as oxygen and carbon monoxide makes them unsuitable for long term use in any device. These limitations have prompted the development of model organometallic complexes that are inspired by the biomechanistic insights obtained by studying the enzymes and built from inexpensive

first-row transition metals. The elucidation of atomic level crystal structures of the hydrogenases and the surprising chemical similarities of the active sites of these evolutionarily unrelated enzymes to each other and to well known classes of organometallic compounds have led to the synthesis of a multitude of model complexes. In this dissertation, we will focus specifically on organo-iron models of [FeFe]-hydrogenases and discuss the major features thought to be essential in functional mimics of this enzyme.

The [2Fe2S] subsite of the H-cluster in [FeFe]-hydrogenases is reminiscent of rudimentary 'CO mobilized' iron-sulfur complexes of the form $(\mu\text{-SRS})\{Fe(CO)_3\}_2$ where R denotes organic groups. Derivatives of this class of diiron compounds, synthesized by modification of the bridging dithiolate and substitution of one or more carbonyls with donor abiological ligands, have provided a library of structural and functional models of the [2Fe2S] subunit.[31-33] However, it is worth noting that although several of these diiron models display moderate electrocatalytic activity towards proton reduction, they require significantly higher overpotential, exhibit slower catalytic rates and are rarely bidirectional compared to the native enzymes.[34] Several structural and functional differences are responsible for the poor catalytic performances of these complexes. First, in contrast to the enzymatic catalysis in which the cluster operates in the Fe^IFe^I redox state (H_{red}),[12, 26, 35] the model diiron complexes invariably rely on the Fe^IFe^0 redox state for proton reduction.[32] As a result, synthetic diiron analogues require substantially higher overpotential to carry out electrocatalytic proton reduction. Second, the outer coordination sphere interactions inside the protein cavity of the natural enzyme modulate the geometry of the [2Fe2S] subsite to attain a 'rotated' conformation in which

the two iron centers are each in square pyramidal first coordination spheres but with one center inverted relative to the other. On the other hand, the catalytically active diiron model complexes generally feature the two iron centers in an eclipsed conformation.[36] While the 'rotated' geometry creates a free coordination site on the distal iron (Fe_d) of H-cluster to facilitate substrate binding, the reactive binding site of the models is between the two iron centers. Third, the natural catalytic cycle involves terminal hydride intermediates that are formed at the open coordination site on Fe_d.[13, 26] Since the synthetic analogues lack a free coordination site on one iron center, they often employ relatively inert, bridging hydride intermediates.[31, 32] Fourth, while the [2Fe2S] cluster in the natural system can bind exogenous ligands such as CO and H_2, [15, 17, 37] such reactivity is rarely observed in synthetic analogues because of the lack of the free coordination site.[33, 38, 39] The enzyme can be oxidized to $Fe^{II}Fe^{I}$ state, capable of binding H_2, but the diiron ($Fe^{I}Fe^{I}$) model complexes have limited stability under oxidative conditions.[40, 41] Fifth, according to theoretical studies, the [4Fe4S] cubane fulfills crucial redox functions that are central to the enzymatic catalytic cycle,[42, 43] but examples of diiron model complexes featuring redox-active cofactors are relatively scarce.[33, 44-46] Designing bio-inspired electrocatalysts with improved activity by incorporating some or all of these critical factors represents an important and challenging target for synthetic chemists.

Summary and scope of the dissertation

The central hypothesis of this thesis is that two essential features of the natural enzyme, the protein environment and the redox active [FeS] cofactors, are crucial for facile catalysis and therefore, model complexes should be designed to incorporate these features. In this dissertation we will describe the synthesis and electrocatalytic properties

of a number of distinct diiron models of [FeFe]-hydrogenases. The specific goals of the research presented herein were to: (1) develop synthetic methodologies for appending diiron cluster onto peptide scaffolds, (2) investigate the influence of non-innocent ligands on the electrochemical properties of the complexes, and (3) study the effect of varying the coordination geometry around iron centers.

First, we present two different synthetic strategies for incorporating two metal-binding functional groups not usually found in proteins, 1,3-dithiol and phosphines, into small peptides. These ligands have been subsequently used to anchor diiron-polycarbonyl clusters (**Chapter 2**, **3**). With the improved solubility of the complex provided by the peptide, we are able to study the electrocatalytic activities of the metallopeptide complexes in mixed aqueous solvents. The activities display an interesting trend of improved catalysis with an increasing amount of water. Second, we describe the impact of a bidentate, chelating, redox non-innocent ligand, 2,2'-bipyridyl (bpy), on the electrocatalytic properties of the diiron model $\{\mu\text{-}S(CH_2)_3S\}Fe_2(CO)_4(bpy)$, a new member of the well-known family of diiron carbonyls (**Chapter 4**). It is basic compared to related disubstituted complexes and is reduced at unexpectedly mild potentials. Third, we expand the bpy research to explore the impact of the identity of the bridging dithiolate and the bidentate, chelating N-donor ligand on the electrocatalytic properties of diiron analogues (**Chapter 5**). Two different dithiolate ligands, 1,3-propanedithiolate and 1,2-benzenedithiolate, and two N-donor ligand, 2,2'-bipyridine and 2,2'-bipyrimidine, are used for the electrochemical studies. Finally, we describe the electrocatalytic activity of pentacoordinate Fe(II) complexes related to the distal iron in [FeFe]-hydrogenase (**Chapter 6**). These complexes catalyze electrochemical proton reduction at exceptionally

mild overpotentials albeit with modest turn-over frequencies. In summary, the hydrogenase related model systems presented herein lay the foundation for developing more sophisticated systems with tailored secondary coordination sphere interactions and widen our knowledge of the utility of non-innocent ligands in building efficient molecular electrocatalysts.

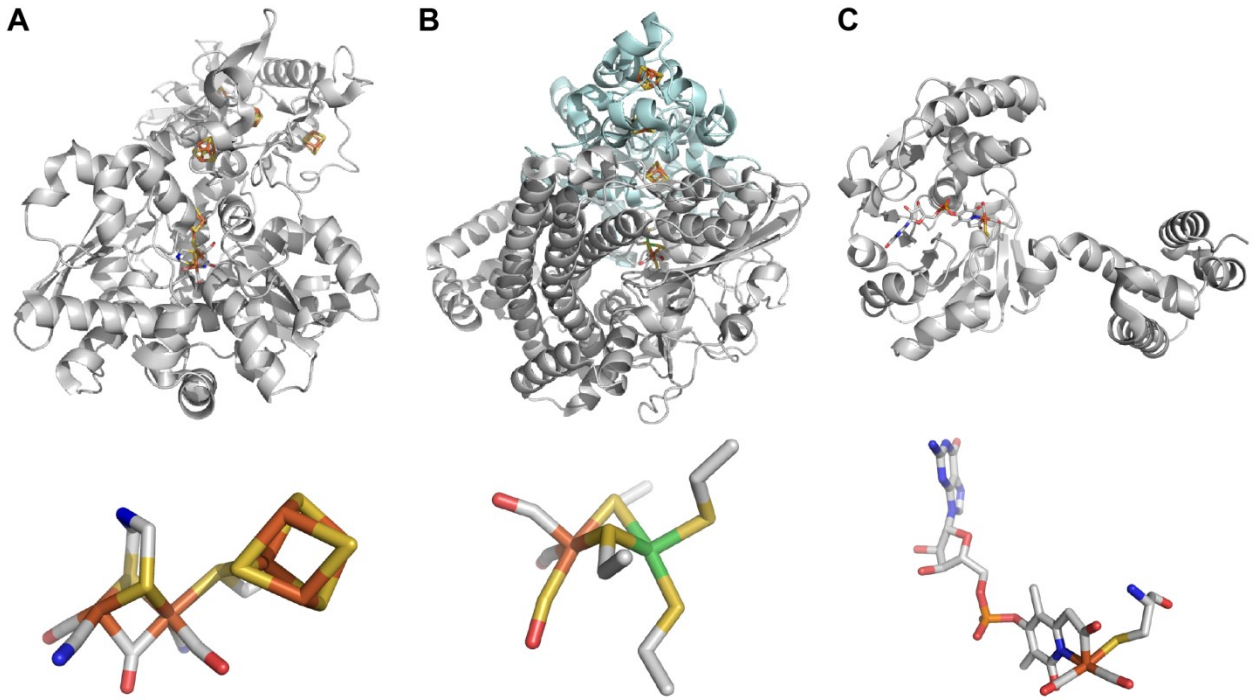

Figure 1-1. Structures of hydrogenases. X-ray crystal structures of (A) the [FeFe]-hydrogenase from *Clostridium pasteurianum* (PDB code: 3C8Y),[47] (B) the [NiFe]-hydrogenase from *Desulfovibrio vulgaris* Miyazaki F (PDB code: 1H2R),[48] and (C) the [Fe]-hydrogenase from *Methanocaldococcus jannaschii* (PDB code: 3F47).[49] The top row shows the structures of the holoenzymes and the bottom row shows the enzyme active sites. The protein structures were drawn using PyMOL. The atoms are represented as carbon (grey), nitrogen (blue), oxygen (red), sulfur (yellow), nickel (green), and iron (orange).

References

1. Cammack, R.; Frey, M.; Robson, R., *Hydrogen as a Fuel: Learning from Nature*. Talor & Francis: London & New York, 2001.

2. Happe, R. P.; Roseboom, W.; Pierik, A. J.; Albracht, S. P. J.; Bagley, K. A., *Nature* **1997,** 385, 126-126.

3. Frey, M., *ChemBioChem* **2002,** 3, 153-160.

4. Penner, S. S., *Energy* **2006,** 31, 33-43.

5. Barreto, L.; Makihira, A.; Riahi, K., *Int. J. Hydrogen Energy* **2003,** 28, 267-284.

6. Winter, M.; Brodd, R. J., *Chem. Rev.* **2004,** 104, 4245-4270.

7. Antolini, E., *Energy Environ. Sci.* **2009,** 2, 915-931.

8. Serov, A.; Kwak, C., *Appl. Catal., B* **2009,** 90, 313-320.

9. Jones, A. K.; Sillery, E.; Albracht, S. P. J.; Armstrong, F. A., *Chem. Commun.* **2002**, 866-867.

10. Madden, C.; Vaughn, M. D.; Díez-Pérez, I.; Brown, K. A.; King, P. W.; Gust, D.; Moore, A. L.; Moore, T. A., *J. Am. Chem. Soc.* **2012,** 134, 1577-1582.

11. Vignais, P. M.; Billoud, B., *Chem. Rev.* **2007,** 107, 4206-4272.

12. Lubitz, W.; Reijerse, E.; van Gastel, M., *Chem. Rev.* **2007,** 107, 4331-4365.

13. Armstrong, F. A., *Curr. Opin. Chem. Biol.* **2004,** 8, 133-140.

14. Peters, J. W.; Lanzilotta, W. N.; Lemon, B. J.; Seefeldt, L. C., *Science* **1998,** 282, 1853-1858.

15. Lemon, B. J.; Peters, J. W., *Biochemistry* **1999,** 38, 12969-12973.

16. Nicolet, Y.; Piras, C.; Legrand, P.; Hatchikian, C. E.; Fontecilla-Camps, J. C., *Structure* **1999,** 7, 13-23.

17. Bennett, B.; Lemon, B. J.; Peters, J. W., *Biochemistry* **2000,** 39, 7455-7460.

18. Silakov, A.; Wenk, B.; Reijerse, E.; Lubitz, W., *PCCP* **2009,** 11, 6592-6599.

19. Ryde, U.; Greco, C.; De Gioia, L., *J. Am. Chem. Soc.* **2010,** 132, 4512-4513.

20. Erdem, Ö. F.; Schwartz, L.; Stein, M.; Silakov, A.; Kaur-Ghumaan, S.; Huang, P.; Ott, S.; Reijerse, E. J.; Lubitz, W., *Angew. Chem. Int. Ed.* **2011,** 50, 1439-1443.

21. Berggren, G.; Adamska, A.; Lambertz, C.; Simmons, T. R.; Esselborn, J.; Atta, M.; Gambarelli, S.; Mouesca, J. M.; Reijerse, E.; Lubitz, W.; Happe, T.; Artero, V.; Fontecave, M., *Nature* **2013,** 499, 66-69.

22. Volbeda, A.; Charon, M.-H.; Piras, C.; Hatchikian, E. C.; Frey, M.; Fontecilla-Camps, J. C., *Nature* **1995,** 373, 580-587.

23. Volbeda, A.; Garcin, E.; Piras, C.; de Lacey, A. L.; Fernandez, V. M.; Hatchikian, E. C.; Frey, M.; Fontecilla-Camps, J. C., *J. Am. Chem. Soc.* **1996,** 118, 12989-12996.

24. Pierik, A. J.; Roseboom, W.; Happe, R. P.; Bagley, K. A.; Albracht, S. P. J., *J. Biol. Chem.* **1999,** 274, 3331-3337.

25. De Lacey, A. L.; FernÃ¡ndez, V. c. M.; Rousset, M.; Cammack, R., *Chem. Rev.* **2007,** 107, 4304-4330.

26. Siegbahn, P. E. M.; Tye, J. W.; Hall, M. B., *Chem. Rev.* **2007,** 107, 4414-4435.

27. Shima, S.; Pilak, O.; Vogt, S.; Schick, M.; Stagni, M. S.; Meyer-Klaucke, W.; Warkentin, E.; Thauer, R. K.; Ermler, U., *Science* **2008,** 321, 572-575.

28. Lyon, E. J.; Shima, S.; Boecher, R.; Thauer, R. K.; Grevels, F.-W.; Bill, E.; Roseboom, W.; Albracht, S. P. J., *J. Am. Chem. Soc.* **2004,** 126, 14239-14248.

29. Shima, S.; Lyon, E. J.; Thauer, R. K.; Mienert, B.; Bill, E., *J. Am. Chem. Soc.* **2005,** 127, 10430-10435.

30. Korbas, M.; Vogt, S.; Meyer-Klaucke, W.; Bill, E.; Lyon, E. J.; Thauer, R. K.; Shima, S., *J. Biol. Chem.* **2006,** 281, 30804-30813.

31. Gloaguen, F.; Rauchfuss, T. B., *Chem. Soc. Rev.* **2009,** 38, 100-108.

32. Tard, C. d.; Pickett, C. J., *Chem. Rev.* **2009,** 109, 2245-2274.

33. Camara, J. M.; Rauchfuss, T. B., *Nat Chem* **2012,** 4, 26-30.

34. Felton, G. A. N.; Mebi, C. A.; Petro, B. J.; Vannucci, A. K.; Evans, D. H.; Glass, R. S.; Lichtenberger, D. L., *J. Organomet. Chem.* **2009,** 694, 2681-2699.

35. Fontecilla-Camps, J. C.; Volbeda, A.; Cavazza, C.; Nicolet, Y., *Chem. Rev.* **2007,** 107, 4273-4303.

36. Darensbourg, M. Y.; Lyon, E. J.; Zhao, X.; Georgakaki, I. P., *Proc. Natl. Acad. Sci. USA* **2003,** 100, 3683-3688.

37. Adams, M. W. W., *Biochim. Biophys. Acta* **1990,** 1020, 115-145.

38. Olsen, M. T.; Barton, B. E.; Rauchfuss, T. B., *Inorg. Chem.* **2009,** 48, 7507-7509.

39. Camara, J. M.; Rauchfuss, T. B., *J. Am. Chem. Soc.* **2011,** 133, 8098-8101.

40. Justice, A. K.; Rauchfuss, T. B.; Wilson, S. R., *Angew. Chem. Int. Ed.* **2007,** 46, 6152-6154.

41. Liu, T.; Darensbourg, M. Y., *J. Am. Chem. Soc.* **2007,** 129, 7008-7009.

42. Schwab, D. E.; Tard, C.; Brecht, E.; Peters, J. W.; Pickett, C. J.; Szilagyi, R. K., *Chem. Commun.* **2006,** 0, 3696-3698.

43. Bruschi, M.; Greco, C.; Fantucci, P.; Gioia, L. D., *Inorg. Chem.* **2008,** 47, 6056-6071.

44. Tard, C.; Liu, X.; Ibrahim, S. K.; Bruschi, M.; Gioia, L. D.; Davies, S. C.; Yang, X.; Wang, L.-S.; Sawers, G.; Pickett, C. J., *Nature* **2005,** 433, 610-613.

45. Si, Y.; Charreteur, K.; Capon, J.-F.; Gloaguen, F.; Petillon, F. Y.; Schollhammer, P.; Talarmin, J., *J. Inorg. Biochem.* **2010,** 104, 1038-1042.

46. Roy, S.; Groy, T. L.; Jones, A. K., *Dalton Trans.* **2013,** 42, 3843-3853.

47. Pandey, A. S.; Harris, T. V.; Giles, L. J.; Peters, J. W.; Szilagyi, R. K., *J. Am. Chem. Soc.* **2008,** 130, 4533-4540.

48. Higuchi, Y.; Ogata, H.; Miki, K.; Yasuoka, N.; Yagi, T., *Structure* **1999,** 7, 549-556.

49. Hiromoto, T.; Ataka, K.; Pilak, O.; Vogt, S.; Stagni, M. S.; Meyer-Klaucke, W.; Warkentin, E.; Thauer, R. K.; Shima, S.; Ermler, U., *FEBS Lett.* **2009,** 583, 585-590.

Chapter 2

Artificial [FeFe]-hydrogenase: On resin modification of an amino acid to anchor a diiron-hexacarbonyl cluster in a peptide framework

Souvik Roy,[a,b] Sandip Shinde,[a,b] G. Alexander Hamilton[a], Hilairy E. Hartnett,[a,c] Anne K. Jones*[a,b]

[a]Department of Chemistry and Biochemistry; [b]Center for Bio-Inspired Solar Fuel Production; [c]School of Earth and Space Exploration; Arizona State University, Tempe, AZ 85287

Reproduced by permission from *Eur. J. Inorg. Chem.*, **2011**: 1050–1055

Abstract

A general method for immobilization of synthetic analogues of the [FeFe]-hydrogenase in designed peptides *via* on resin modification of an amino acid sidechain with a dithiol functional group is described. Utilizing a unique amine side chain as anchor, the dithiol unit is coupled to the peptide *via* formation of an amide. This dithiol unit precisely positions the two required sulfurs for formation of a $(\mu\text{-SRS})[Fe(CO)_3]_2$ cluster on reaction with $Fe_3(CO)_{12}$. UV-vis and FTIR spectroscopy demonstrate formation of the desired complex.

Introduction

Hydrogen is an energy currency in both biological and industrial settings, and hydrogenases are the biological catalysts for the interconversion of protons and hydrogen. This reaction is at the heart of hydrogen's usage as a fuel.[1] Unlike industrial catalysts that rely on precious metals to catalyze hydrogen activation, biology takes advantage of the earth-abundant metals nickel and iron. FTIR and X-ray crystallographic studies have shown that both [NiFe]- and [FeFe]-hydrogenases contain unusual, organometallic active sites utilizing biologically unprecedented CO and CN as intrinsic ligands.[2-9]

The structure of the active site of [FeFe]-hydrogenases (Scheme 2-1) consists of an unusual [Fe_2S_2] subunit bridged to an ordinary [4Fe4S] cubane via a single cysteinyl sulfur atom. The diiron subsite contains two features that are remarkable from a biological perspective: (1) the aforementioned diatomic ligands and (2) a dithiol organic bridging molecule that has been alternatively proposed to contain carbon, nitrogen or oxygen at its central position.[10-13] From a synthetic chemistry perspective, the active site of [FeFe]-hydrogenases has remarkable structural similarities to many known iron carbonyl compounds, and considerable progress in understanding the mechanism of this enzyme has been achieved via synthesis of relevant model compounds.[14-20]

Despite the wealth of biomimetic chemistry that has been reported, there still exist several important functional differences between synthetic model compounds and [FeFe]-hydrogenases. Model compounds cycle through the more reduced Fe(I)-Fe(0) redox state during electrocatalytic reduction of protons whereas [FeFe]-hydrogenases are believed to utilize the Fe(II)Fe(I) state.[14] Similarly, model compounds require substantial overpotentials to catalyze the reduction of protons at slower rates than can be achieved by

the enzymes. Finally, none of the [FeFe]-hydrogenase models are able to oxidize hydrogen while the enzymes are known to perform reversible catalysis.

Increasingly, attention is being focused on generation of functional [FeFe]-hydrogenase model complexes that can perform electrocatalysis or photocatalysis. In these investigations, a number of synthetic strategies have been developed for coupling relevant diiron models to electrode surfaces, redox cofactors, or photoactive centers.[21-25] In parallel, strategies for investigating the impact of second coordination sphere interactions and burial of the active site in superstructures isolated from bulk solvent are starting to emerge. [22, 26-32] On the other hand, relatively little attention has been paid to developing strategies for attachment of diiron models to amino acids[28, 33-35] or peptidic scaffolds[36, 37] - this, despite the fact, that evidence continues to build indicating that the enzyme tertiary structure plays a crucial role in tuning the properties of the active site to achieve near diffusion limited, bidirectional catalysis.

De novo designed proteins have proven an invaluable tool in the study of complex oxidoreductases and have been designed to bind a number of both naturally occurring and artificial metallocofactors.[38-43] The construction of miniaturized, peptidic systems coordinating hydrogenase-related metallocenters presents unique synthetic challenges. One approach has been utilization of the naturally occurring amino acid cysteine as an anchor for construction of a $(\mu\text{-SRS})[Fe(CO)_3]_2$ cluster.[36] This strategy has the disadvantage of relying on the correct placement of two distinct cysteines to form the desired complex. A second synthetic route involves modification of an amino acid to create an artificial amino acid ligand for the desired metal complex. In this report, we present a method to modify a peptide still attached to its resin support in order to create

an artificial derivative of a lysine bearing a propanedithiol unit. The appended sulfur sidechain posesses two sulfurs poised to anchor a covalently attached $Fe_2(SRS)(CO)_6$ unit. This approach can serve as a general method for modification of a wide range of designer synthetic peptides to probe interactions between amino acids and [FeFe]-hydrogenase small models.

Results and Discussion

Scheme 2-2 shows the general strategy for synthesis of an $Fe_2(SRS)(CO)_6$ unit appended to a dithiol modified lysine residue. First, the desired peptide is constructed via standard Fmoc/ t-Bu solid phase peptide synthesis. During synthesis, an orthogonally protected amino acid residue, in this case lysine, is introduced that serves as the site for dithiol incorporation. The dithiol unit is provided by 3-(acetylthio)-2(acetylthiomethyl)propanoic acid.[44] This propanoic acid derivative can be coupled to a primary amine to form a stable amide. After modification of the lysine, the rest of the peptide can be simultaneously deprotected and cleaved from the resin via standard trifluoroacetic acid methods and purified before incorporation of the diiron unit via reaction with $Fe_3(CO)_{12}$.

Reactions with peptides can present unique challenges relative to reactions with small, organic ligands. First, peptides are not usually soluble in the organic solvents traditionally utilized for organometallic synthesis. Second, the number and diverse composition of functional groups present in a peptide require carefully orchestrated protection/ deprotection to avoid side products. To demonstrate the efficacy of this synthetic approach, a simple variant of the N-terminal sequence of the Nickel-superoxide dismutase (SODA) from *Streptomyces coelicolor* was utilized. The

SODA peptide, ACDLPCG, binds nickel, is soluble and monomeric in aqueous solution, is spectroscopically well characterized, and retains some of the catalytic activity of the complete enzyme.[45] Three variations in this sequence were introduced. First, the two cysteine residues were exchanged for serines to eliminate competition from these thiols for interaction with iron while maintaining the approximate length and polarity of the sidechain. Second, the aspartic acid was exchanged for a lysine as an attachment point for the iron cluster. Finally, a tryptophan residue was introduced at the N-terminus to facilitate quantification of the peptide, yielding the final sequnce, WASKLPSG.

Figure 2-1 shows the analytical HPLC and Figure 2-2 the NMR spectra from (A) deprotected, unmodified peptide, (B) peptide modified with the dithiol acid, and (C) peptide modified with the diiron cluster. The HPLC traces demonstrate that with each additional modification the peptide became more hydrophobic, eluting at a higher percentage of acetonitrile. These changes in hydrophobicity facilitated efficient purification to yield high quality products as shown in the NMR spectra. The peaks of peptide modified with the dithiol acid can clearly be observed after coupling to the lysine at 1.10 (t, 2H), 2.4-2.55 (1H) and 3.0-3.15 (4H). These peaks are then shifted after incorporation of the diiron unit to overlap with the resonances of the ε-H of the lysine residue. Meanwhile, the peaks for all other protons in the peptide can be accounted for and are virtually unaffected by the modifications of the peptide (complete assignment can be found in Table 2-1). ESI-Mass spectrometry has also been utilized to demonstrate that the products have the expected composition and the iron cluster is coordinated via a single peptide monomer.

The UV-vis and FTIR spectra of $Fe_2(CO)_6$-modified peptide are shown in Figure 2-3. The UV-vis spectrum consists of three notable features: an absorption at 334 and a shoulder at 465 nm both associated with the Fe-S core, and the characteristic absorbance of the tryptophan residue at 280 nm. The ratio of the extinction coefficients of these features is similar to that observed previously for incorporation of cluster into peptide via cysteine, providing additional evidence for nearly stoichiometric incorporation of cluster in the purified product.[36] The FTIR spectrum of the $Fe_2(CO)_6$-modified peptide has three bands at 2075, 2035 and 1999 cm^{-1} arising from the coupled CO vibrational modes of the complex. These confirm the presence of the carbonyls on each iron. Furthermore, the close agreement between these values and those observed for $(\mu\text{-}S(CH_2)_3S)[Fe(CO)_3]_2$ suggests that, as expected, the iron complex is completely exposed to solution when attached to the peptide. Finally, ESI-MS data of $Fe_2(CO)_6$-modified peptide also implies the presence of the CO ligands since ions formed by loss of CO ligands [complex-CO, complex-$(CO)_3$ and complex-$(CO)_6$] could clearly be identified (Figure 2-4).

The complex $(\mu\text{-}S(CH_2)_3S)Fe_2(CO)_6$ is an unremarkable catalyst, but it can undergo substitution of the carbonyls by a number of different types of ligands such as cyanide or phosphines to form more active species.[14] Similarly, $Fe_2(CO)_6$-modified peptide is also able to undergo substitution reactions. As shown in Figure 2-3, addition of excess PMe_3 to an acetonitrile solution of the peptide, results in a uniform shifting of the frequencies of the ν(CO) bands to approximately 100 cm^{-1} lower wavenumbers (1974, 1939, and 1894). The compound $(\mu\text{-}S(CH_2)_3S)$-$[Fe(CO)_2(PMe_3)]_2$ is reported to have ν(CO) bands at 1979, 1942, and 1898 cm^{-1}.[46]

Thus, the observed data is consistent with formation of a disubstituted phosphine derivative and indicates that the cluster is accessible for ligand exchange.

Conclusions

We have demonstrated the ability to incorporate a (μ-SRS)$Fe_2(CO)_6$ model of [FeFe]-hydrogenases into a peptide via on resin construction of a modified amino acid. This synthetic scheme is general and allows covalent connection of the diiron unit to any unique primary amine. Importantly, the synthesis can be performed in water/methanol mixtures yielding a water-soluble product in high yield.

This approach provides a convenient method for constructing peptide-based models of [FeFe]-hydrogenases. Through variation of the peptide scaffold, it will be possible to construct complexes in carefully tailored cavities designed to incorporate selected aspects of the enzyme active site. The 3-(acetylthio)-2-(acetylthiomethyl)-propanoic acid unit may also be utilized as a handle to construct other sulfur-ligated metallocenters.

Experimental Section

General. All reactions were performed under an atmosphere of nitrogen. Unless otherwise specified, all chemicals were of the highest purity available from Sigma-Aldrich. Fmoc protected amino acids and peptide coupling reagents were obtained from Protein Technologies (Tucson, AZ, USA). Solvents including DMF, acetonitrile, methanol, ethyl acetate, hexanes, ether $CDCl_3$ and D_2O were obtained from Sigma Aldrich.

Instrumentation. MALDI-MS (matrix assisted laser desorption/ionization mass spectrometer) characterization of peptides was performed on a Voyager DE STR in

the Proteomics and Protein Chemistry Laboratory at Arizona State University. ESI-MS (electrospray ionization mass spectrometry) was performed using a Thermo Quantum Discovery Max triple-quadrupole mass spectrometer in the Environmental Biogeochemistry Laboratory at Arizona State University. Measurements were conducted in positive (+) and negative (–) ionization modes using a methanol:water (50:50 by volume) mobile phase at a flow rate of 10 mL min^{-1} and the following ionization conditions: spray voltage, 4000 (+, –); capillary temperature, 270 °C; sheath gas pressures, 25(+) and 15(–); auxiliary gas pressure, 2 (+, –). NMR spectra were recorded at 400 or 500 MHz (^1H) on Varian Liquid-State NMR instruments in $CDCl_3$ solutions containing 0.1% TMS (tetramethylsilane) unless otherwise mentioned. UV-vis measurements were performed on a Hewlett-Packard 8453 spectrophotometer using quartz cuvettes with a 1 cm pathlength. Peptide concentrations were determined via absorbance of the tryptophan residue (ε_{280} = 5600 $M^{-1}cm^{-1}$). FTIR spectra were recorded on a Thermo Nicolet Avatar-360 spectrometer as a dry film on a CaF_2 window. Each spectrum is an average of 1024 scans collected under nitrogen at 1 cm^{-1} resolution. The clean CaF_2 window was used as a reference.

2-Bromomethylpropenoic acid. Diethyl bis(hydroxymethyl)malonate (13 g, 0.058 mmol) was dissolved in HBr (25 mL of 48% aqueous solution, ~0.2 mol) and was heated at 120-125^oC in an oil bath for 45 min. On cooling the solution to -80 ^oC, white crystals appeared. The crystals were removed by filtration and the filtrate was heated again to 120-125^oC for 45 min. This solution was again cooled to -80 ^oC and additional crystals were filtered off. This process was repeated a third time. All the

white crystals were collected and dissolved in 30 mL dichloromethane, washed with 2x10 mL 1N HCl, dried over anhydrous $MgSO_4$ and concentrated under reduced pressure to yield a white crystalline solid (2.8 g, 29.4%). ^{1}H NMR (400 MHz): δ 6.48 (1H, s), 6.09 (1H, s), 4.17 (2H, s).

3-(acetylthio)-2-(acetylthiomethyl)propanoic acid. To a stirred suspension of 2-bromomethylpropenoic acid (2.8 g, 0.017 mol) in 50 mL water at 0 ºC was added an aqueous solution of sodium carbonate (3.1 g, 0.029 mol in 15 mL) in small portions. To the resulting mixture, thiolacetic acid (1.25 mL, 0.017 mol) was added dropwise, and the solution was stirred at 0 ºC for 2 hours. The solution was acidified with 6M HCl, and the white precipitate was extracted with ethyl acetate (3x25 mL). The EtOAc layer was dried over anhydrous $MgSO_4$ and concentrated under reduced pressure to yield a colorless oil. With this colorless oil, the reaction was repeated (as ^{1}H NMR of the oil indicated the presence of ~33% unreacted starting material, 2-bromomethylpropenoic acid) to produce pure 2-(acetylthiomethyl)acrylic acid as a colorless oil (3 g); ^{1}H NMR (400 MHz): δ 6.38 (1H, s), 6.02 (1H, s), 3.75 (2H, s), 2.32 (3H, s). To this 2-(acetylthiomethyl)acrylic acid was added thiolacetic acid (2 mL, 0.027 mol) and stirred at room temperature. After 36 hours, ^{1}H NMR spectra of the reaction mixture showed no olefinic peaks. The unreacted thiolacetic acid was removed from the reaction mixture under reduced pressure and the yellow oil like residue was purified by column chromatography on silica gel with hexane/ethyl acetate (3:1) as eluent followed by hexane/ethyl acetate (2:1) giving 3-(acetylthio)-2-(acetylthiomethyl)propanoic acid as a white solid (2.8 g, 70%). R_f = 0.2 (3:1

hexane/ethyl acetate); ^{1}H NMR (400 MHz): δ 3.19 (4H, m), 2.91 (1H, p), 2.35 (6H, s).

Peptide synthesis. The eight amino acid containing peptide (WASKLPSG) was synthesized on a Protein Technologies PS3 automated peptide synthesizer using the standard Fmoc/ t-Bu (Fmoc, 9-fluorenylmethoxycarbonyl) protection strategy and HBTU (o-Benzotriazole-*N,N,N′,N′*-tetramethyluronium hexaflurophosphate) as coupling reagent on Fmoc-Gly wang resin (Aapptec 0.54 mmole/g, 100-200 mesh) at 0.1 mmole scale.[25] Lysine with orthogonally protected side chain, Fmoc-Lys(ivDde)-OH [ivDde, 1-(4,4-dimethyl-2,6-dioxocyclohex-1-ylidene)-3-methylbutyl], was used for solid-phase peptide synthesis so that the side chain amine group of lysine can be selectively deprotected and modified. Following synthesis, the peptide was acetylated at the N-terminus [1:1 (v/v) acetic anhydride: N-methylmorpholine for 20 min, two times].

Coupling of 3-(acetylthio)-2-(acetylthiomethyl)propanoic acid to peptide and purification. Resin bound peptide (64 mg, 0.033 mmole) was treated with 2% hydrazine in DMF (10 mL) for 45 min at room temperature under nitrogen to remove the protecting group from lysine. Following deprotection, 3-(acetylthio)-2-(acetylthiomethyl)propanoic acid (35 mg, 0.15 mmole), HATU [2-(1H-7-Azabenzotriazol-1-yl)-1,1,3,3,-tetramethyluronium hexafluorophosphate methanaminium] (55 mg, 0.14 mmole) and DIEA [N,N-diisopropylethylamine] (30 μL, 0.16 mmole) dissolved in 5 mL DMF were added to the resin under nitrogen and stirred at room temperature for 30 min. This coupling reaction was repeated. The resin was then washed with DMF (5x2 mL). The thioacetal groups were reduced to

thiol by treatment with 2-3% hydrazine in DMF (10 mL) under nitrogen for 40 min. Then the peptide was simultaneously deprotected and cleaved from the resin using 95:2.5:2.5 trifluoroacetic acid (TFA): water: triisopropylsilane (TIPS) for two hours and fifteen minutes. The crude cleavage solution was filtered and the residual resin was washed with neat TFA (3x1 mL). The TFA solution of peptide was concentrated under reduced pressure to a light yellow colored liquid (~0.5-1 mL). Crude peptide was precipitated by adding cold diethyl ether (-20^{o}C). Followed by incubation with four equivalents TCEP, the crude peptide was purified by reverse phase HPLC on a Waters 600E HPLC system with photodiode array detector (3x250 mm C-18 column for analytical and PrepLC 25 mm module C-18 column for semi-preparative HPLC) using aqueous-acetonitrile gradients containing 0.1% TFA (v/v). Molecular weight of the peptide was confirmed by matrix-assisted laser desorption/ ionization time of flight (MALDI-TOF MS) mass spectrometry. $[M]^+$ Calculated = 1020.99; found = 1043.3 $[(M+Na)^+]$.

Cluster Incorporation into Peptide. Triiron dodecacarbonyl (5 mg, 0.01 mmole) in methanol (1.5 mL) and 0.16 mM aqueous solution of peptide (1 mL) were combined and refluxed for 1.5 hours resulting in a color change from green to pale red. The reaction mixture was concentrated under reduced pressure and was extracted with 3 mL water. The complex was purified by reverse phase HPLC using aqueous-acetonitrile gradients.

Substitution of carbon monoxide ligands with trimethylphosphine. Trimethylphosphine (4 μL, 0.038 mmol) was added to a 0.02 mM acetonitrile solution of peptide-[μ-$S_2Fe_2(CO)_6$] complex (1mL) under N_2 in the dark and stirred at room

temperature for 1.5 hours resulting in change in color to red. The FTIR of the crude reaction mixture showed ν(CO) bands at 1980, 1940, 1900 cm^{-1}.

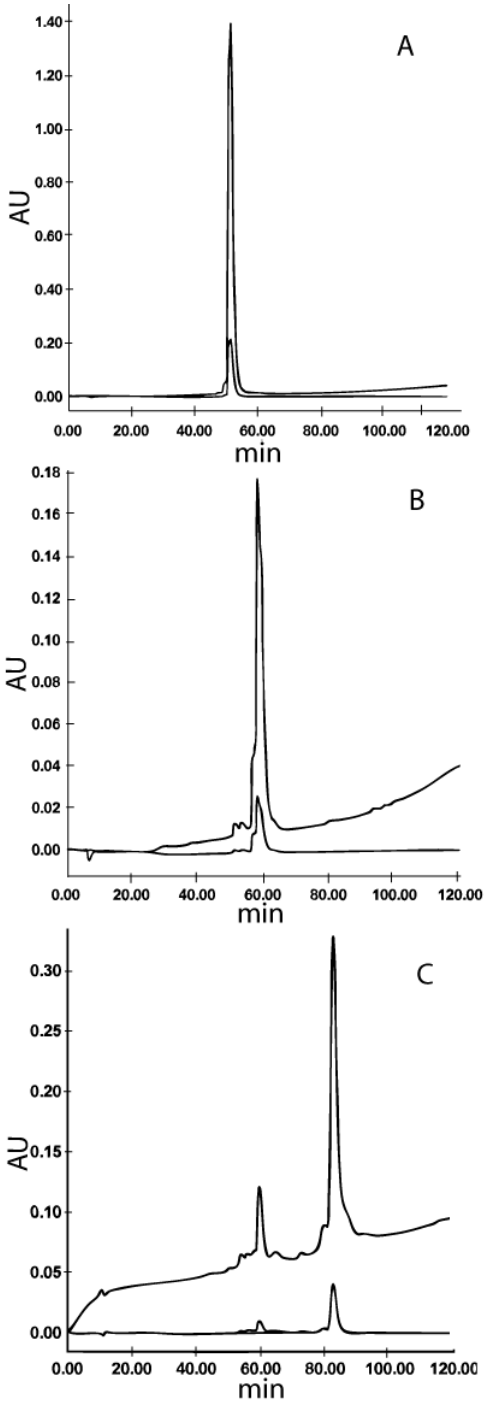

Figure 2-1. Analytical HPLC traces for unmodified peptides and dithiol-peptide diiron-hexacarbonyl complex. Analytical HPLC traces from (A) WASKLPSG, (B) peptide with dithiol side chain modification (WAS(Dt)LPSG and (C) peptide modified

with both a dithiol side chain and the $Fe_2(CO)_6$ cluster. HPLC gradient 1% acetonitrile/min; flow rate 0.25 mL/min. The higher amplitude signal in each case is absorbance at 220 nm (peptide bond) and the lower at 280 nm (tryptophan).

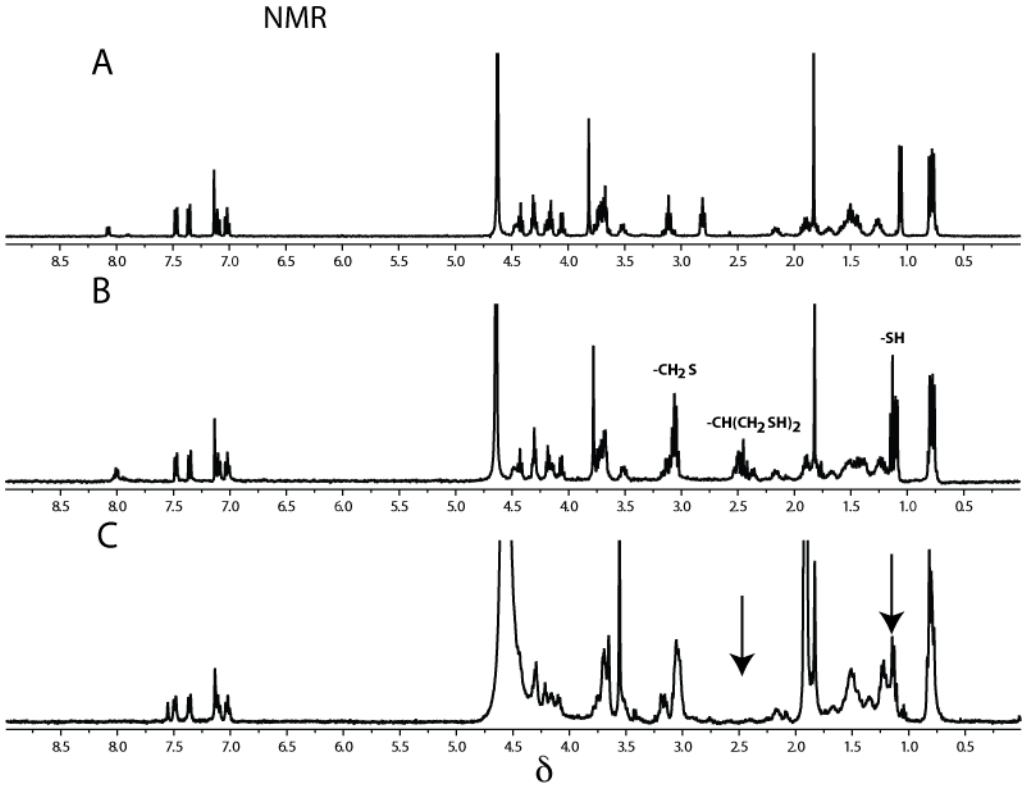

Figure 2-2. Comparative ^{1}H NMR spectra of the unmodified peptides and the dithiol-peptide diiron-hexacarbonyl complex. ^{1}H NMR spectra from (A) WASKLPSG, (B) peptide with dithiol side chain modification (WAS(Dt)LPSG and (C) both a dithiol side chain and the $Fe_2(CO)_6$ cluster. NMR spectra were obtained in D_2O.

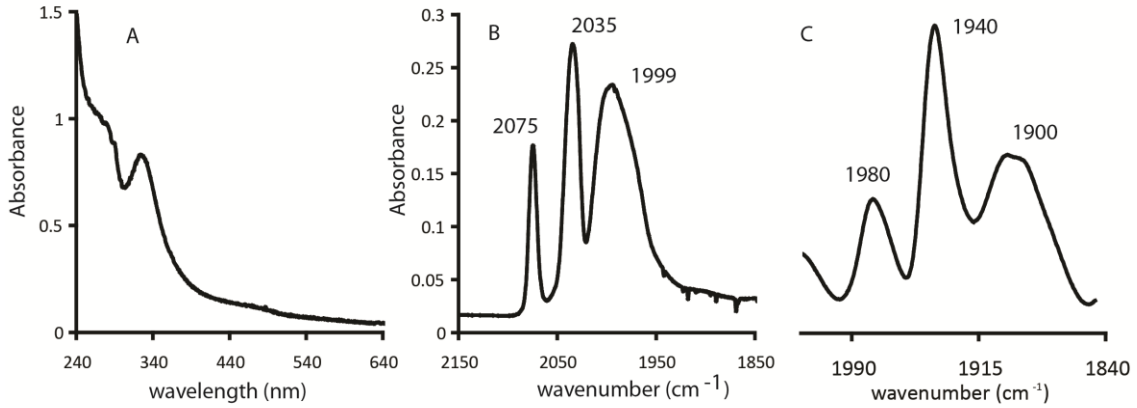

Figure 2-3. Optical and FTIR spectra of the dithiol-peptide-diiron complexes. Characterization of $Fe_2(CO)_6$ complex coordinated to dithiol modified peptide via (A) UV-vis and (B) FTIR spectroscopies and (C) FTIR spectrum of peptide-$Fe_2(CO)_4(PMe_3)_2$. UV-vis spectrum was obtained in a 1:1 mixture of water/ acetonitrile. For FTIR experiments, sample was applied to a single CaF_2 window as a methanolic solution and dried under a vacuum to form a thin film. Experiments were then performed with the film.

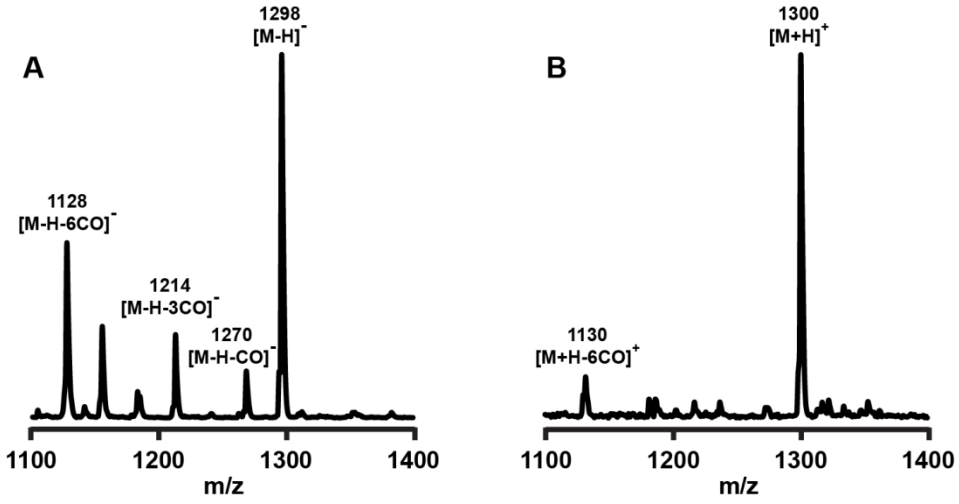

Figure 2-4. ESI-mass spectra of the dithiol-peptide diiron hexacarbonyl complex. ESI-MS spectra of peptide-[(μ-$S)_2[Fe(CO)_3]_2$] complex in (A) negative mode and (B) positive mode.

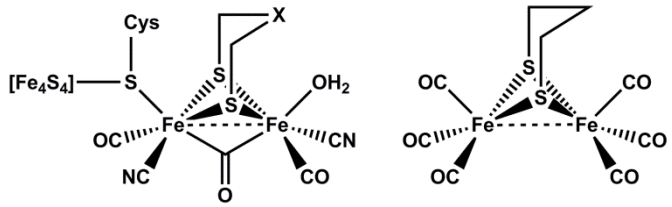

Scheme 2-1. [FeFe]-hydrogenase active site and first generation model compound utilizing a propane dithiol ligand.

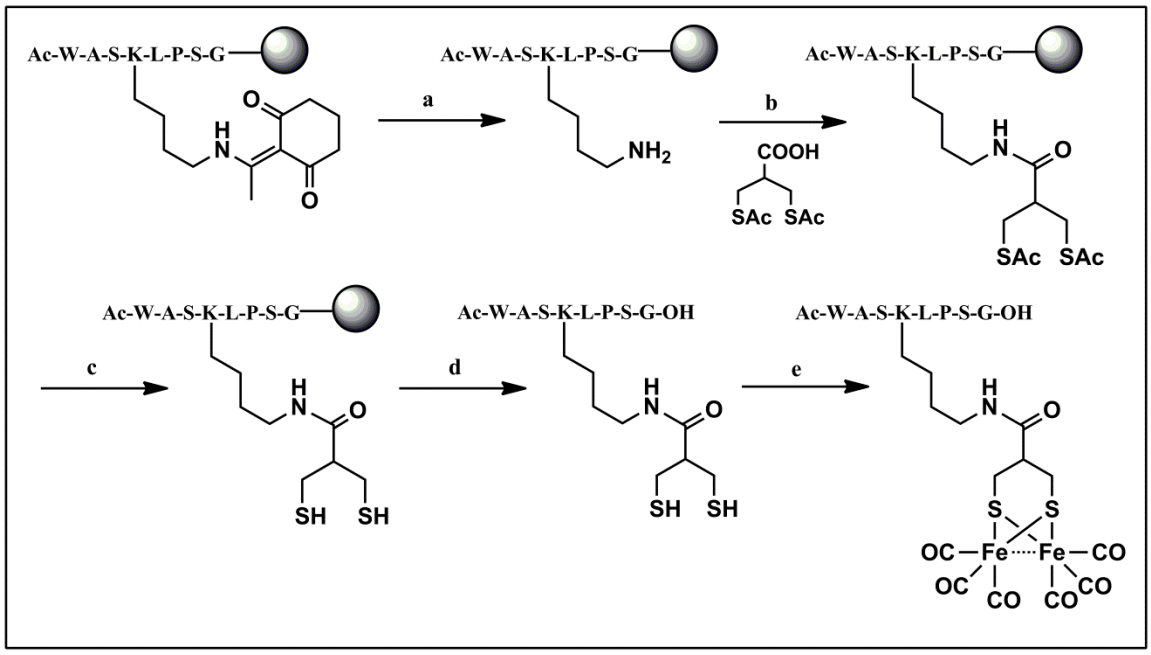

Scheme 2-2. Synthetic strategy for modification of a unique lysine with a dithiol functional unit and incorporation of an $Fe_2(CO)_6$ unit. The sphere represents the resin bead utilized for solid phase peptide synthesis. Reaction conditions: (a) 2% NH_2NH_2, DMF, Yield 100%; (b) HATU, DIEA, DMF, Yield 50%; (c) 2% NH_2NH_2, DMF, yield 100%; (d) (i) cleavage: 95% TFA, 2.5% water, 2.5% TIPS (ii) HPLC purification; (e) $Fe_3(CO)_{12}$, aq. methanol, reflux, yield 80%

Table 2-1. Chemical shifts of the amino-acid residues in ^{1}H NMR spectra of parent peptide, dithiol peptide and $Fe_2(CO)_6$-peptide complex

	Ac	**W**	**A**	**S**	**K(dt)**	**L**	**P**	**S**	**G**
$-NH_2$	1.83 (s)	7.47 (d, 1H), 7.36 (d, 1H), 7.14 (s, 1H), 7.11 (t, 1H), 7.02 (t, 1H), 4.42 (t, 1H), 3.11 (m, 2H)	4.06 (q,1H), 1.08 (d, 3H)	4.31 or 4.16 (m, 1H), 3.6-3.2 (m, 2H)	4.46 (m, 1H), 2.81 (t, 2H; εH), 1.75-1.25 (m, 6H)	4.2-4.13 (m, 1H), 1.75-1.25 (m, 3H), 0.8-0.76 (m, 6H)	4.32-4.28 (m, 1H), 3.74-3.66 (m, 1H), 3.52 (m, 1H), 2.17 (m, 1H), 1.94-1.85 (m, 3H)	4.31 or 4.16 (m, 1H), 3.6-3.2 (m, 2H)	3.82 (s, 2H)
-SH	1.82 (s)	7.48 (d, 1H), 7.36 (d, 1H), 7.14 (s, 1H), 7.11 (t, 1H), 7.02 (t, 1H), 4.43 (t, 1H), 3.14-3.02 (m, 2H)	4.06 (q, 1H), 1.08 (d, 3H)	4.3 or 4.19 (m, 1H), 3.75-3.66 (m, 2H)	4.49 (m, 1H), 2.55-2.4 (t, 2H; εH), 1.71-1.18 (m, 6H), 3.15-3 (m, 4H), 2.55-2.4 (1H, m) 1.71-1.18 (m, 2H)	4.2-4.13 (m, 1H), 1.71-1.18 (m, 3H), 0.82-0.76 (m, 6H)	4.3-4.2 (m, 1H), 3.75-3.66 (m, 1H), 3.52 (m, 1H), 2.19-2.15 (m, 1H), 1.94-1.85 (m, 3H),	4.3 or 4.19 (m, 1H), 3.6-3.2 (m, 2H)	3.78 (s, 2H)
$-S_2Fe_2(CO)_6$	1.83 (s)	7.48 (d, 1H), 7.35 (d, 1H), 7.14 (s, 1H), 7.11 (t, 1H), 7.02 (t, 1H), 4.6-4.44 (αH), 3.2-2.99 (βH)	4.1 (αH), 1.10 (d, βH)	4.3 or 4.22 (αH), 3.75-3.65 (βH)	4.6-4.44 (αH), 3.2-2.99 (εH), 1.7-1.1 (β, γ, δH), 3.2-2.99 (dithiol side chain)	4.16 (αH), 1.1-1.7 (β, γH), 0.78-0.84 (δH)	4.28-4.32 (αH), 3.8-3.5 (δH), 2.2-2.14 (βH), 1.93-1.88 (β, γH)	4.3 or 4.22 (αH), 3.75-3.65 (βH)	3.65 or 3.56 (s)

References

[1] R. Cammack, M. Frey, R. Robson, *Hydrogen as a Fuel: Learning from Nature*, Talor & Francis, London & New York, **2001**.

[2] A. Volbeda, M.-H. Charon, C. Piras, E. C. Hatchikian, M. Frey, J. C. Fontecilla-Camps, *Nature* **1995**, *373*, 580.

[3] J. C. Fontecilla-Camps, A. Volbeda, C. Cavazza, Y. Nicolet, *Chem. Rev.* **2007**, *107*, 4273.

[4] J. W. Peters, W. N. Lanzilotta, B. J. Lemon, L. C. Seefeldt, *Science* **1998**, *282*, 1853.

[5] Y. Nicolet, C. Piras, P. Legrand, C. E. Hatchikian, J. C. Fontecilla-Camps, *Structure* **1999**, *7*, 13.

[6] Y. Nicolet, A. L. de Lacey, X. Vernede, V. M. Fernandez, E. C. Hatchikian, J. C. Fontecilla-Camps, *J. Am. Chem. Soc.* **2001**, *123*, 1596.

[7] R. P. Happe, W. Roseboom, A. J. Pierik, S. P. J. Albracht, K. A. Bagley, *Nature* **1997**, *385*, 126.

[8] K. A. Bagley, E. C. Duin, W. Roseboom, S. P. J. Albracht, W. H. Woodruff, *Biochemistry* **1995**, *34*, 5527.

[9] A. J. Pierik, M. Hulstein, W. R. Hagen, S. P. J. Albracht, *Eur. J. Biochem.* **1998**, *258*, 572.

[10] A. Silakov, B. Wenk, E. Reijerse, W. Lubitz, *Phys. Chem. Chem. Phys.* **2009**, *11*, 6592.

[11] A. S. Pandey, T. V. Harris, L. J. Giles, J. W. Peters, R. K. Szilagyi, *J. Am. Chem. Soc.* **2008**, *130*, 4533.

[12] S. Zilberman, E. I. Stiefel, M. H. Cohen, R. Car, *Inorg. Chem.* **2007**, *46*, 1153.

[13] M. T. Olsen, B. E. Barton, T. B. Rauchfuss, *Inorg. Chem.* **2009**, *48*, 7507.

[14] C. d. Tard, C. J. Pickett, *Chem. Rev.* **2009**, *109*, 2245.

[15] A. Jablonskyte, J. A. Wright, C. J. Pickett, *Dalton Trans.* **2010**, *39*, 3026.

[16] C. M. Thomas, T. Liu, M. B. Hall, M. Y. Darensbourg, *Inorg. Chem.* **2008**, *47*, 7009.

[17] B. E. Barton, T. B. Rauchfuss, *Inorg. Chem.* **2008**, *47*, 2261.

[18] T. Liu, M. Y. Darensbourg, *J. Am. Chem. Soc.* **2007**, *129*, 7008.

[19] B. E. Barton, M. T. Olsen, T. B. Rauchfuss, *Curr. Opin. Biotechnol.* **2010**, *21*, 292.

[20] F. Gloaguen, T. B. Rauchfuss, *Chem. Soc. Rev.* **2009**, *38*, 100.

[21] A. M. Kluwer, R. Kapre, F. Hartl, M. Lutz, A. L. Spek, A. M. Brouwer, P. W. N. M. van Leeuwen, J. N. H. Reek, *Proc. Natl. Acad. Sci. USA* **2009**, *106*, 10460.

[22] X. Ru, X. Zeng, Z. Li, D. J. Evans, C. Zhan, Y. Tang, L. Wang, X. Liu, *J. Polym. Sci. A Polym. Chem.* **2010**, *48*, 2410.

[23] D. Streich, Y. Astuti, M. Orlandi, L. Schwartz, R. Lomoth, L. Hammarström, S. Ott, *Chem. Eur. J.* **2010**, *16*, 60.

[24] H.-Y. Wang, W.-G. Wang, G. Si, F. Wang, C.-H. Tung, L.-Z. Wu, *Langmuir* **2010**, *26*, 9766.

[25] C. Tard, X. Liu, S. K. Ibrahim, M. Bruschi, L. D. Gioia, S. C. Davies, X. Yang, L.-S. Wang, G. Sawers, C. J. Pickett, *Nature* **2005**, *433*, 610.

[26] K. N. Green, J. L. Hess, C. M. Thomas, M. Y. Darensbourg, *Dalton Trans.* **2009**, 4344.

[27] M. L. Singleton, J. H. Reibenspies, M. Y. Darensbourg, *J. Am. Chem. Soc.* **2010**, *132*, 8870.

[28] U.-P. Apfel, C. R. Kowol, Y. Halpin, F. Kloss, J. Kuebel, H. Goerls, J. G. Vos, B. K. Keppler, E. Morera, G. Lucente, W. Weigand, *J. Inorg. Biochem.* **2009**, *103*, 1236.

[29] A. D. Wilson, R. K. Shoemaker, A. Miedaner, J. T. Muckerman, D. L. DuBois, M. R. DuBois, *Proc. Natl. Acad. Sci. USA* **2007**, *104*, 6951.

[30] M. R. DuBois, D. L. DuBois, *Chem. Soc. Rev.* **2009**, *38*, 62.

[31] S. Ezzaher, J.-F. Capon, F. Gloaguen, F. Y. Petillon, P. Schollhammer, J. Talarmin, N. Kervarec, *Inorg. Chem.* **2009**, *48*, 2.

[32] S. Ezzaher, A. Gogoll, C. Bruhn, S. Ott, *Chem. Commun.* **2010**, *46*, 5775.

[33] L.-C. Song, J. Yan, Y.-L. Li, D.-F. Wang, Q.-M. Hu, *Inorg. Chem.* **2009**, *48*, 11376.

[34] C. He, M. Wang, X. Zhang, Z. Wang, C. Chen, J. Liu, B. Åkermark, L. Sun, *Angew. Chem. Int. Ed.* **2004**, *43*, 3571.

[35] X. de Hatten, E. Bothe, K. Merz, I. Huc, N. Metzler-Nolte, *Eur. J. Inorg. Chem.* **2008**, *2008*, 4530.

[36] A. K. Jones, B. R. Lichtenstein, A. Dutta, G. Gordon, P. L. Dutton, *J. Am. Chem. Soc.* **2007**, *129*, 14844.

[37] U.-P. Apfel, M. Rudolph, C. Apfel, C. Robl, D. Langenegger, D. Hoyer, B. Jaun, M.-O. Ebert, T. Alpermann, D. Seebach, W. Weigand, *Dalton Trans.* **2010**, *39*, 3065.

[38] R. T. M. de Rosales, M. Faiella, E. Farquhar, L. Que, Jr., C. Andreozzi, V. Pavone, O. Maglio, F. Nastri, A. Lombardi, *J. Biol. Inorg. Chem.* **2010**, *15*, 717.

[39] J. G. Saven, *Curr. Opin. Colloid Interf. Sci.* **2010**, *15*, 13.

[40] J. L. R. Anderson, R. L. Koder, C. C. Moser, P. L. Dutton, *Biochem. Soc. Trans.* **2008**, *36*, 1106.

[41] M. Faiella, C. Andreozzi, R. T. M. de Rosales, V. Pavone, O. Maglio, F. Nastri, W. F. DeGrado, A. Lombardi, *Nat. Chem. Biol.* **2009**, *5*, 882.

[42] A. F. A. Peacock, O. Iranzo, V. L. Pecoraro, *Dalton Trans.* **2009**, 2271.

[43] V. Nanda, R. L. Koder, *Nat. Chem.* **2010**, *2*, 15.

[44] R. Singh, G. M. Whitesides, *J. Am. Chem. Soc.* **1990**, *112*, 1190.

[45] J. Shearer, L. M. Long, *Inorg. Chem.* **2006**, *45*, 2358.

[46] X. Zhao, I. P. Georgakaki, M. L. Miller, J. C. Yarbrough, M. Y. Darensbourg, *J. Am. Chem. Soc.* **2001**, *123*, 9710.

Chapter 3

Biomimetic peptide-based models of [FeFe] Hydrogenases: Utilization of phosphine containing peptides

Souvik Roy[†§], Thuy-Ai Nguyen[†], Anne K. Jones[†§]*

[†]Department of Chemistry and Biochemistry; [§]Center for Bio-Inspired Solar Fuel Production; Arizona State University, Tempe, AZ 85287

Abstract

Two synthetic strategies for incorporating diiron analogues of [FeFe]-hydrogenases into short peptides *via* phosphine functional groups are described. First, utilizing a unique amine side chain of lysine as an anchor, phosphine carboxylic acids were coupled to resin-bound peptides *via* formation of an amide linkage to create phosphine derivatives of lysine. Second, we developed a general procedure for the synthesis of artificial phosphine containing amino acids that can be directly incorporated into peptides *via* solution phase peptide synthesis. Three amino acids with different phosphine substitution (-PPh_2, -P^iPr_2, -PEt_2) were synthesized and incorporated into small peptides. Five distinct mono-phosphine substituted diiron model complexes were prepared by reaction of the phosphine-peptides with diiron hexacarbonyl precursors, either (μ-pdt)$Fe_2(CO)_6$ or (μ-bdt)$Fe_2(CO)_6$ (pdt = propane-1,2-dithiolate, bdt = benzene-1,2-dithiolate). The formation of the complexes was confirmed by UV/Vis, FTIR and ^{31}P NMR spectroscopy. Furthermore, electrocatalytic reduction of protons from acetic acid in acetonitrile and water-acetonitrile mixtures (up to 40% water) showed that addition of water significantly improved the catalytic efficiency of these complexes by lowering the overpotential and enhancing the catalytic current.

Introduction

Hydrogenases, the biological catalyst for the reversible reduction of proton to molecular hydrogen, employ earth-abundant base metals, either iron or nickel and iron, to carry out this transformation under mild conditions.[1-4] The utility of this reaction for developing technologies to produce sustainable solar fuels has engendered widespread interest in [FeFe]-hydrogenases, the most efficient biological system for producing hydrogen. X-ray crystallographic studies revealed that the structure of the active site of [FeFe]-hydrogenase, known as the H-cluster, consists of a [2Fe] subsite at which substrate binding and catalytic reaction occurs, and a covalently connected [4Fe4S] cubane which serves as a conduit for the transfer of electrons to/from the protein surface.[5, 6] The H-cluster is connected to the protein through a single cysteinyl thiolate which also connects the [4Fe4S] cubane and [2Fe] subsite. The [2Fe] subunit features CO and CN^- as terminal diatomic ligands and a biologically unusual non-proteinaceous dithiolate that bridges the two iron centers.

From a synthetic perspective, the [2Fe] subunit is reminiscent of the well known organoiron complex $[\{\mu\text{-}S(CH_2)_3S\}\{Fe(CO)_3\}_2]$ which serves as a convenient starting point for building a multitude of sophisticated biomimetic diiron analogues.[7] Although many of these bio-inspired organometallic models show moderate electrocatalytic proton reduction activity, none of them catalyzes hydrogen production with the same exquisite combination of high turnover frequency and low activation energy as the enzymes.[8, 9] Moreover, the hydrophobic nature of these diiron dithiolate clusters renders most of them soluble only in organic solvents. They are therefore unsuitable for applications in fuel cells based on aqueous solvents and their activity in such a setting cannot be evaluated.

In recent years, as the importance of the protein environment for the catalytic activity of hydrogenases and other metalloenzymes has become increasingly clear, more attention has been focused on incorporating the diiron cluster into supramolecular constructs to investigate the impact of secondary coordination sphere interactions on chemical properties.[10-16] While diiron models generally feature the two iron centers in an "eclipsed" conformation, in the natural system, the outer coordination sphere interactions constrain the coordination geometry of the catalytic site to attain a more catalytically active "rotated" form that leaves one iron center (distal iron, Fe_d) with an open coordination site.[17, 18] Recently, Berggren *et al*. have reported reconstitution of a fully functional [FeFe]-hydrogenase from a model diiron complex with limited catalytic activity and the apo-enzyme. This clearly demonstrates the key role played by the protein matrix in modulating the coordination geometry of the [2Fe] subunit to facilitate efficient, bidirectional catalysis.[19]

De novo designed proteins and peptides that can bind natural and artificial metallocofactors are proving to be a powerful technique for understanding the function of metalloenzymes, and realizing the roles of metallocenters within protein scaffolds.[20-22] The construction of small artificial peptides binding diiron models serves to bridge the ground between natural metalloenzymes and organometallic analogues and presents an appealing opportunity to introduce secondary coordination sphere interactions into model systems. Synthetic methods have been developed to incorporate thiolate bridged diiron hexacarbonyl clusters into suitably designed peptides *via* both natural cysteine and artificial dithiol groups.[23-25] However, these hexacarbonyl [FeFe]-hydrogenase models are less electron rich and thus, poorer catalysts than pentacarbonyl complexes in

which one terminal ligand is replaced by a stronger σ-donor like a phosphine. Furthermore, these peptide-based models offer little opportunity for improving their catalytic efficiency through ligand substitution because awkward solvent mixtures are required to simultaneously solubilize peptide and substituting ligand resulting in relatively low yields.

Phosphines have been widely employed in models as a surrogate of the CN^- ligand found in the natural system due to their strong electron donating ability.[26, 27] Thus, construction of phosphine-functionalized peptides represents a tantalizing route to build peptide-based diiron models with better electrocatalytic properties. Moreover, phosphino-peptides offer the possibility of synthesizing a wide range of ligands through variation of the peptide sequence as well as the substituents on the phosphines. In this report, we describe two general methods for introducing a phosphine functionality into small peptides. The first approach is to modify the side chain amine of a lysine in a resin-bound peptide generating a phosphine containing peptide. The second method directly incorporates an appropriately protected artificial phosphine amino acid *via* solution phase peptide synthesis. To demonstrate the efficiency of the second synthetic approach, three different amino acids were prepared using the method developed by Gilbertson and co-workers: *N*-Boc-3-(diethylphosphorothioyl)alanine (Boc-Epa-OH), *N*-Boc-3-(diisopropylphosphorothioyl)alanine (Boc-Ipa-OH), and *N*-Boc-3-(diphenylphosphorothioyl)alanine (Boc-Ppa-OH).[28, 29] Four distinct diiron-peptide complexes were synthesized using these phosphine amino acids, and the influence of the peptide ligands on the hydrophilicity, redox properties and electrocatalytic activities of coordinated diiron carbonyl complexes were explored in

acetonitrile and acetonitrile/water mixtures. Notably, the complexes display favorable energetics towards electrocatalytic proton reduction from acetic acid in the presence of water.

Results and Discussion

Synthesis of metallopeptides.

Two different synthetic strategies were utilized to construct phosphine functionalized artificial peptides for can binding dithiolate bridged diiron-polycarbonyl clusters through coordination of the phosphine. The first method is analogous to that used for thiol substitution previously.[25] Using a unique amine side chain of lysine as an anchor, a resin-bound peptide was modified *via* formation of an amide with a phosphine functionalized carboxylic acid to create an artificial derivative of lysine bearing a phosphine unit. Second, several phosphine-containing amino acids, amenable to both solid-phase and solution-phase peptide synthesis, were synthesized and directly incorporated into small peptides. Phosphines are known to substitute a CO ligand from the diironhexacarbonyl complexes $[(\mu\text{-}S_2)Fe_2(CO)_6]$ in the presence of a decarbonylating agent such as trimethylamine-N-oxide (Me_3NO) to produce mono-substituted diiron complexes.[30-32] We show below that the phosphine-containing peptides undergo the same reaction under similar conditions to yield analogous diiron complexes in peptide scaffolds.

On-resin modification of lysine. Scheme 3-1 shows the general method for modifying the resin-bound peptide to introduce a phosphine functionality and the subsequent incorporation of a diiron cluster. The peptide sequence utilized (WASKLPSG) is a simple variant of the N-terminal sequence of nickel-superoxide dismutase (SODA) from

Streptomyces coelicolor.[33] Previously, this sequence was employed to create an artificial 1,3-dithiol peptide which could bind a diiron-hexacarbonyl cluster.[25] Herein, we exploit a similar strategy to construct water a soluble, phosphine-substituted diiron cluster attached to a peptide. First, the desired eight residue peptide was synthesized via standard solid-phase peptide synthesis using the Fmoc/t-Bu strategy. Lysine with an orthogonally protected amine group was used for selective modification with diphenylphosphinopropionic acid to generate the iron binding site. Subsequent cleavage of the phosphine-peptide WASK(-PPh_2)LPSG (**1a**) from the resin and reaction with the diiron hexacarbonyl precursor [(μ-pdt)$Fe_2(CO)_6$; pdt = propane-1,3-dithiolate] produced the desired metallopeptide (μ-pdt)[Fe-$(CO)_3$][$Fe(CO)_2${WASK(PPh_2)LPSG}] (**1**). However, moderate sensitivity of the phosphines to aerial oxidation reduced the overall yield of the process. To prevent the loss of phosphine-peptide during synthesis and purification, a new approach in which the free phosphine was replaced by a sulfur-protected phosphine synthon {3-(diphenylphosphorothioyl) propanoic acid} was used for peptide modification (Scheme 3-1). After cleavage of the peptide from the resin, the phosphine sulfide was reduced by Raney nickel to produce the free phosphine-peptide [WASK(-PPh_2)LPSG] which was immediately used, without further purification, for the reaction with (μ-pdt)$Fe_2(CO)_6$. Nonetheless, use of sulfur protected phosphine did not lead to significant improvement in the overall yield of the process due to the inefficiency of the desulfurization step.

The product metallopeptide was purified *via* HPLC and a range of spectroscopic techniques were used to confirm the presence of the desired cluster. The UV-vis spectrum of the complex in water consists of three prominent features: an intense charge transfer

band at 349 nm and a weak d-d transition at 470-480 nm both of which are associated with the [Fe_2S_2] core, and a strong π-π* transition in the range 250-280 nm originating from the diphenylphosphine and tryptophan residues. The IR spectrum of the complex contains three characteristic bands at 2042, 1980, and 1924 cm^{-1} corresponding to the C-O stretching modes, similar to those observed for analogous monosubstituted organometallic diiron models.[32, 34] Furthermore, the ^{31}P NMR spectrum of the complex shows a single resonance at 55.4 ppm, confirming formation of a unique complex with a Fe-P bond. Finally, ESI-MS of the metallopeptide also indicates the presence of $Fe_2(CO)_5$ cluster, because in addition to the molecular ion peak, signals attributable to the sequential loss of CO ligands were observed.

Artificial amino acids. The necessity of including an orthogonally protected amino acid in the peptide sequence and carefully designed selective protection/deprotection steps limits the range of phosphines that can be employed using the synthetic scheme described above. Therefore, a second synthetic route in which an artificial phosphine amino acid is directly incorporated during solid-phase peptide synthesis was developed. This second method has the added benefit that the side chain of the phosphine bearing amino acid is necessarily shorter and more stable since the amide functionality is no longer necessary. Since less rotamers are available, a more compact metal binding site with lesser solvent accessibility can be envisioned. To demonstrate the utility of this strategy, three different phosphine amino acids were synthesized and embedded into the tripeptide sequence, Val-Xpa-Leu in which Xpa represents the phosphine amino acid.

The phosphine amino acids were synthesized by the method developed by Gilbertson *et al*. starting from enantiomerically pure *N*-Boc-protected 3-iodo-alanine

methyl ester [Boc-Ala(I)-OMe].[29, 35, 36] Metalation of the iodo-amino acid with activated zinc, followed by metalation with copper, produced a reactive zinc/copper-iodo intermediate. Reaction of this intermediate with a chlorodialkylphosphine or chlorodiarylphosphine provided the phosphino derivative which was then protected as phosphine sulfide by reaction with elemental sulfur. Ester hydrolysis produced the *N*-Boc and sulfide protected phosphine amino acid in good yield. For the purposes of this study, three amino acids with different phosphine substituents were synthesized: *N*-Boc-3-(diethylphosphorothioyl)alanine (Boc-Epa-OH), *N*-Boc-3-(diisopropylphosphorothioyl)-alanine (Boc-Ipa-OH), and *N*-Boc-3-(diphenylphosphorothioyl)alanine (Boc-Ppa-OH).

Three distinct tripeptides, Val-Ppa-Leu, Val-Ipa-Leu, and Val-Epa-Leu, were synthesized by solution-phase peptide synthesis (Scheme 3-2). The valine and leucine were chosen for their hydrophobic side chains to allow large-scale chromatographic purification of the tripeptides on a normal-phase silica column. The *N*- and *C*-termini of the peptides were protected as acetyl and methyl ester, respectively. Treatment of purified tripeptide with Raney nickel converted the phosphine sulfide to free phosphine.[28] Reduction of the phosphine sulfide to phosphine was monitored by ^{31}P NMR and/or MALDI-TOF mass spectrometry. Notably, ^{31}P NMR revealed that desulfurization by Raney nickel also caused racemization at the α-carbon of the phosphine amino acid resulting in diasteromeric peptides. Phosphine peptides were metalated by reaction with (μ-pdt)$Fe_2(CO)_6$ or (μ-bdt)$Fe_2(CO)_6$ (bdt = benzene-1,2-dithiolate) in CH_3CN/CH_2Cl_2 in the presence of Me_3NO to produce phosphine-substituted diiron-peptide complexes as red solids in good yields. Four distinct complexes were prepared. Three complexes contain 1,3-propanedithiolate (pdt) as the dithiol ligand bridging the irons with variation of the

substituents on the phosphine as the only difference between the complexes: [(Val-Epa-Leu)-{(μ-pdt)$Fe_2(CO)_5$}] (**2**), [(Val-Ipa-Leu)-{(μ-pdt)$Fe_2(CO)_5$}] (**3**), and [(Val-Ppa-Leu)-{(μ-pdt)$Fe_2(CO)_5$}] (**4**). A fourth complex, [(Val-Ppa-Leu)-{(μ-bdt)$Fe_2(CO)_5$}] (**5**), was synthesized using Val-Ppa-Leu as the ligand and benzene-1,2-dithiolate (bdt) bridged diiron hexacarbonyl [(μ-bdt)$Fe_2(CO)_6$] as the metallo-precursor.

Spectroscopic Characterization.

Despite numerous attempts, crystals of X-ray quality were not obtained for the diiron-peptide complexes. Thus, the compounds were characterized *via* a combination of spectroscopic and electrochemical methods. The spectroscopic data recorded for complexes **1-5** are summarized in Table 3-1. As shown in Figure 3-1, the UV-vis spectra of the complexes in acetonitrile consist of a characteristic Fe-S charge transfer band (CT) in the 340–370 nm region and a weak shoulder at *ca.*470 nm. Changing the substituents on the phosphine from phenyl to isopropyl or ethyl but utilizing the same bridging ligand had little influence on the UV-vis spectra of the complexes (**2** , **3**, and **4**) apart from the slight shift in the wavelength of the metal centered charge transfer band. On the other hand, comparing the UV-vis spectra of **4** and **5** revealed that replacing pdt by bdt, predictably, resulted in significant changes in the wavelength and intensity of the charge transfer transition. While the intensities of this charge transfer band are similar for **2**, **3**, and **4**, the extinction coefficient for **5** is considerably higher (Table 3-1).

The FTIR spectra of the complexes in acetonitrile show characteristic three-band patterns in the C-O stretching region originating from the monosubstituted (μ-S_2)$Fe_2(CO)_5$ assembly. The stretching frequencies of the carbonyls are a proxy for the electron density on the iron centers. As shown in Table 3-1, replacing aromatic groups on

the phosphine with more electron donating alkyl groups (isopropyl or ethyl) resulted in a slight shift of the CO stretching frequencies by 5–6 cm^{-1} to lower wavenumbers. The poorer donor ability of bdt compared to pdt is reflected in the stretching frequencies of **4** and **5**. The ν(CO) bands of the latter are shifted by an average of 9 cm^{-1} to higher frequencies relative to **4**.

Electrochemical studies

Electrochemical studies in acetonitrile. The electrochemical properties of the complexes were investigated by cyclic voltammetry in acetonitrile under argon. The complexes show electrochemical responses similar to those reported for analogous monosubstituted diiron compounds.[8] Cyclic voltammograms of the pdt complexes, **2**, **3** and **4**, display an irreversible wave corresponding to $Fe^{I}Fe^{I}$ / $Fe^{I}Fe^{0}$ reduction and an irreversible wave corresponding to $Fe^{I}Fe^{I}$ / $Fe^{I}Fe^{II}$ oxidation (Figure 3-2 and Table 3-2). In contrast, for complex **5**, the $Fe^{I}Fe^{I}$ / $Fe^{I}Fe^{II}$ oxidation is irreversible, but the $Fe^{I}Fe^{I}$ / $Fe^{I}Fe^{0}$ couple is partially-reversible (i_p^{ox}/i_p^{red} = 0.47). The cyclic voltammogram of **5** also exhibits a second oxidative feature at approximately -1.29 V. This feature did not appear when the reductive scan was stopped prior to the $Fe^{I}Fe^{I}$ / $Fe^{I}Fe^{0}$ reduction suggesting an EC process in which the $Fe^{I}Fe^{0}$ species undergoes a chemical change that allows it to be re-oxidized at a new potential. The peak potentials (E_p), both the reductive and oxidative, correlate well with the donating abilities of the phosphines and the thiolates. Their trends are the same as these established from the ν(CO) of the complexes. Among the pdt bridged complexes, the diphenylphosphino complex **4** is reduced at a less reducing potential (-1.82 V) and oxidized at a more oxidizing potential (+0.31 V) than the dialkylphosphino complexes **2** and **3**. Notably, changing the bridging thiolate from pdt to

bdt has a more pronounced influence on the electronic properties of the diiron core as demonstrated by the 200 mV and 160 mV shift of the $Fe^{I}Fe^{I}$ / $Fe^{I}Fe^{0}$ and $Fe^{I}Fe^{II}$ / $Fe^{I}Fe^{I}$ couples, respectively, in **5** compared to **4**. The electrochemical differences are more pronounced when cyclic voltammograms in the presence of acetic acid (vide infra), added as a source of protons to study electrocatalytic proton reduction, are compared.

The ability of the monosubstituted [(μ-SR_1S)$Fe_2(CO)_5L$] (L = phosphine peptide) complexes to electrocatalyze proton reduction from a weak acid was investigated in acetonitrile. For the complexes with a pdt bridge, **2**, **3**, and **4**, sequential addition of AcOH resulted in increased reductive current corresponding to production of hydrogen. Notably, this catalytic current is not observed at the $Fe^{I}Fe^{I}$ / $Fe^{I}Fe^{0}$ reduction potential of the (*ca.* -1.8 to -1.9 V dependent on complex). Instead, catalytic current is observed at a lower potential in the range -2.1 to -2.2 V. This observation is consistent with electrochemical studies previously reported for less electron rich analogues.[37-39] Similarly, upon addition of AcOH, the bdt complex **5** also displays catalytic current at *ca.* -2.08 V, a potential well beyond its reduction peak at -1.62 V. However, complex **5** is more a efficient electrocatalyst than the other complexes as demonstrated by the greater catalytic current it produces under similar experimental conditions. Finally, while **5** exhibits a shift of the potential at which half of catalytic current is observed to more reducing values with increasing acid concentration, no clear trend is observed for **2**, **3**, and **4**.

Electrochemistry in acetonitrile/water mixtures. The improved water solubility of the diiron-peptide complexes relative to analogous phosphine complexes reported in the literature allowed electrochemical investigation in mixed acetonitrile-water solvents.

Cyclic voltammograms of complexes **3**, **4**, and **5** were obtained in 3:1 and 3:2 CH_3CN/H_2O (Figure 3-4). The redox potentials determined from these experiments are summarized in Table 3-2. Since the diethylphosphino complex (**2)** and the diisopropylphosphino complex (**3**) were already shown to have similar electronic properties, only the electrochemistry of **3** was studied in mixed solvents. With an increasing amount of water, the reductive wave associated with each of the Fe^IFe^I/Fe^IFe^0 couples of **3-5** is shifted to less reducing potentials. The shifts observed for the Fe^IFe^I/Fe^IFe^0 couple on changing the solvent from neat CH_3CN to 3:2 CH_3CN/H_2O are 160, 100 and 150 mV for **3**, **4**, and **5**, respectively. Similar shifts were observed when electrochemical measurements of analogous diiron complexes with hydrophilic phosphine ligands, included to improve water solubility, were performed in mixed acetonitrile/water solvents.[40, 41] However, the $Fe^{II}Fe^I/Fe^IFe^I$ oxidation of complexes **3-5** was less affected by the addition of water as indicated by nearly unaltered oxidation potentials. These results suggest that the presence of water can selectively tune the potential required for the reduction of the diiron core without impacting all electrochemical properties.

The electrocatalytic activity of complexes **3-5** using AcOH as proton source was investigated in CH_3CN/H_2O mixtures (Figures 3-5 and 3-6). For complexes **3** and **4** there are notable changes in the intensities and positions of the catalytic waves when mixed aqueous solvents are used. Unlike the electrocatalysis in acetonitrile, in CH_3CN/H_2O mixtures, cyclic voltammograms of complexes **3** and **4** display catalytic electrochemical responses with onset at the Fe^IFe^I/Fe^IFe^0 reduction potential. This suggests that the basicity of the reduced complexes ($\mathbf{3}^-$ and $\mathbf{4}^-$) and the acidity of AcOH is modulated by

water such that $\mathbf{3}^-$ and $\mathbf{4}^-$ can catalyze proton reduction at considerably less reducing potentials than in neat acetonitrile. Furthermore, in the presence of 40% water, increasing the concentration of AcOH from 10 mM to 50 mM resulted in 19-fold or 21-fold enhancement of peak current for complex **3** or **4**, respectively. In contrast, only 9-fold or 7-fold current increase was observed for the same complexes in neat acetonitrile. On the other hand, although the onset of catalysis by $\mathbf{5}^-$ also shifts to less reducing potentials with the addition of water, it is still significantly more negative than the $\mathbf{5/5}^-$ reduction. Notably, all of complexes **3-5** exhibit a negative shift for the catalytic wave with increasing concentration of AcOH. To quantify these trends, the catalytic peak current was determined as function of the number of equivalents of acetic acid (Figure 3-7). Addition of water resulted in noticeable improvement in the catalytic activities of **3** and **4** as demonstrated by the steeper slope of the current response in the presence of water. On the other hand, the catalytic current observed for complex **5** is largely unaffected by the addition of water. These results suggest that although the electrocatalytic activity of some diiron models can be significantly increased by adding water, the trend does not hold even for all sets of closely related complexes.

Conclusion

In summary, we have demonstrated the synthesis of peptide models of [FeFe]-hydrogenase utilizing phosphine-peptides. Two general synthetic schemes are shown that have been successfully employed to introduce phosphine functional groups into peptides and to covalently anchor a $(\mu\text{-SRS})\{Fe(CO)_3\}\{Fe(CO)_2(PR_2R')\}$ cluster through the phosphine. This approach offers major advantages over other methods reported for building peptide-based diiron complexes: (1) the phosphine amino acids are

directly incorporated into designated peptide sequences, (2) Electron rich stable diiron complexes are prepared in only one step with peptide as reagent resulting in better yields than if two peptide modifying steps are employed, and (3) the synthesis of a diverse array of complexes can be achieved through variation of the artificial amino acid. Importantly, utilization of peptide ligands significantly increased the polarity of the complexes allowing electrochemical studies in partially aqueous solvents. The presence of water has a significant influence on the electrochemical properties of the complexes as demonstrated by the shift of the reduction potential of the $Fe^{I}Fe^{I}/Fe^{I}Fe^{0}$ couple towards less reducing potential and increased catalytic current. Thus the synthetic approach described here provides convenient access to monosubstituted diiron-peptide model complexes and opens the door for the design of more sophisticated peptides with tailored outer coordination sphere interactions.

Materials and methods

All reactions were carried out under an atmosphere of dry nitrogen using standard Schlenk and vacuum line techniques unless otherwise mentioned. All anhydrous solvents were purchased from Sigma-Aldrich and deuterated solvents from Cambridge Isotope Laboratories. Fmoc protected amino acids and peptide coupling reagents were obtained from Protein Technologies. Compounds 3-(diphenylphosphino)-propionic acid,[42] *N*-Boc-3-iodo-alanine methyl ester,[43] *N*-Boc-3-(diphenylphosphinothioyl)-alanine (Boc-Ppa-OH),[29, 44] (μ-pdt)$Fe_2(CO)_6$,[45] and (μ-bdt)$Fe_2(CO)_6$ [46] were synthesized according to the literature procedures. The other *N*-Boc protected phosphine-sulfide amino acids (Boc-Epa-OH and Boc-Ipa-OH) were analogously synthesized by slight

modification of the literature method.[44] All other starting materials were commercially available and used as obtained.

^{1}H, ^{13}C and ^{31}P NMR spectra were recorded at room temperature on a Varian Liquid-State NMR spectrometer (400 or 500 MHz for ^{1}H). NMR chemical shifts are quoted in ppm; spectra were referenced to tetramethylsilane for ^{1}H and ^{13}C NMR. The ^{31}P NMR spectra were referenced to external phosphoric acid at 0 ppm. Splitting patterns are designated as follows: s, singlet; d, doublet; t, triplet; m, multiplet; br, broad singlet; dd, doublet of doublet; td, triplet of doublet. FTIR spectra were recorded on a Bruker Vertex 70 spectrophotometer using a stainless steel sealed liquid spectrophotometer cell with CaF_2 windows. UV-vis measurements were performed on a Hewlett-Packard 8453 spectrophotometer using quartz cuvettes with a 1 cm pathlength. MALDI-MS (matrix assisted laser desorption/ionization mass spectrometry) characterization of peptides was performed on a Voyager DE STR instrument using α-cyano-4-hydroxycinnamic acid as matrix. ESI-MS of the metallopeptides with molecular weights above 1200 was performed using a Thermo Quantum Discovery Max triple-quadrupole mass spectrometer. Measurements were conducted in positive (+) and negative (–) ionization modes using a methanol/water (50:50 by volume) mobile phase at a flow rate of 10 mL min^{-1}. Mass spectra of metallopeptides with lower molecular weight was recorded on a JEOL LCmate instrument using atmospheric-pressure chemical ionization (APCI) technique in positive mode. HPLC purification of peptides was performed on a Waters 600E HPLC system with a photodiode array detector. For analytical HPLC, 3×50 mm C-18 column was used, and PrepLC 25 mm module C-18 column was used for semi-preparative HPLC.

3-(diphenylphosphinothioyl)propionic acid. 3-(diphenylphosphino)propionic acid (2.5 g, 9.7 mmol) and sulfur (0.316 g, 9.8 mmol) were suspended in toluene (17.5 mL) and refluxed under nitrogen for two hours. The reaction mixture was cooled to room temperature and the toluene was removed under reduced pressure to yield pure 3-(diphenylphosphorothioyl)propionic acid as slightly yellowish solid(2.8 g, 99%). ^{1}H NMR (400 MHz, $CDCl_3$): δ = 7.83 (m, 4H), 7.5 (m, 6H), 2.73 (m, 4H); ^{31}P {^{1}H} NMR (161.9 MHz, $CDCl_3$): δ = 41.86.

***N*-Boc-3-(diethylphosphinothioyl)-alanine methyl ester (Boc-Epa-OMe).** The *N*-Boc phosphine sulfide methyl ester was synthesized from *N*-Boc-3-iodo-alanine methyl ester. The general synthetic procedure is described in reference [44]. Yield 63%.^{1}H NMR (400 MHz, $CDCl_3$): δ = 5.68 (d, 1H), 4.55-4.64 (m, 1H), 3.76 (s, 3H), 2.52-2.64 (m, 2H), 2.02 (m, 4H), 1.42 (s, 9H), 1.14-1.24 (m, 6H); ^{31}P {^{1}H} NMR (161.9 MHz, $CDCl_3$): δ = 52.80. R_f = 0.3 (35% EtOAc/hexane).

***N*-Boc-3-(diisopropylphosphinothioyl)-alanine methyl ester (Boc-Ipa-OMe).** Same procedure as above. Yield 69%. ^{1}H NMR (400 MHz, $CDCl_3$): δ = 5.86 (d, 1H), 4.61-4.52 (m, 1H), 3.75 (s, 3H), 2.38-2.46 (m, 2H), 2.13 (m, 2H), 1.43 (s, 9H), 1.15-1.24 (m, 12H); ^{31}P {^{1}H} NMR (161.9 MHz, $CDCl_3$): δ = 64.74. R_f = 0.45 (40% EtOAc/hexane).

***N*-Boc-3-(diethylphosphinothioyl)-alanine (Boc-Epa-OH).** Hydrolysis of the *N*-Boc phosphine sulfide methyl ester by LiOH followed by acidification produced the *N*-Boc phosphine sulfide amino acid.[44] Yield 82%. ^{1}H NMR (400 MHz, $CDCl_3$): δ = 9.54 (br, 1H), 5.87 (d, 1H), 4.58-4.64 (m, 1H), 2.51 (m, 1H), 2.39 (m, 1H), 1.84-1.99 (m, 4H), 1.43 (s, 9H), 1.13-1.22 (m, 6H); ^{13}C{^{1}H} NMR (100 MHz, $CDCl_3$): δ = 174.6 (s), 155.6 (s), 80.8 (s), 50 (s), 29.9 (d, J_{C-P} = 45 Hz), 24.7 (d, J_{C-P} = 51 Hz), 24.3 (d,

$J_{C\text{-}P}$ = 51 Hz), 6.26 (d, $J_{C\text{-}P}$ = 5 Hz); $^{31}P\{^{1}H\}$ NMR (161.9 MHz, $CDCl_3$): δ = 51.55. R_f = 0.13 (1:1 EtOAc/hexane)

***N*-Boc-3-(diisopropylphosphinothioyl)-alanine (Boc-Ipa-OH).** Same procedure as above. Yield 69%. ^{1}H NMR (400 MHz, $CDCl_3$): δ = 9.21 (br, 1H), 5.95 (d, 1H), 4.56-4.62 (m, 1H), 2.42 (m, 1H), 2.32 (m, 1H), 2.09-2.21 (m, 2H), 1.42 (s, 9H), 1.15-1.27 (m, 12H); $^{13}C\{^{1}H\}$ NMR (100 MHz, $CDCl_3$): δ = 171.1 (s), 155.4 (s), 80.6 (s), 50.4 (s), 28.7 (d, $J_{C\text{-}P}$ = 49 Hz), 28.3 (d, $J_{C\text{-}P}$ = 49 Hz), 25.5 (d, $J_{C\text{-}P}$ = 48 Hz), 16.1 (m), 15.8 (m); $^{31}P\{^{1}H\}$ NMR (161.9 MHz, $CDCl_3$): δ = 65.14. R_f = 0.2 (1:1 EtOAc/hexane).

Solid phase peptide synthesis. The eight amino acid containing peptide (WASKLPSG) was synthesized on a Protein Technologies PS3 automated peptide synthesizer using the standard Fmoc/*t*Bu protection strategy and HBTU as coupling reagent on Fmoc-Gly wang resin (Aapptec 0.54 mmol/g, 100–200 mesh) at 0.1 mmol scale. Following synthesis, the peptide was acetylated at the N-terminus by treating the resin bound peptide with 1:1 (v/v) acetic anhydride: N-methylmorpholine in DMF for 30 min.

On-resin modification of peptide. Resin bound peptide (0.05 mmol) was treated with 2% hydrazine (v/v) in DMF (10 mL) for 1 h under nitrogen at room temperature. The resin beads were then thoroughly washed with DMF. The resin beads were then treated with the solution of 3-(diphenylphosphino)propionic acid or 3-(diphenylphosphinothioyl)propionic acid (0.15 mmol), HATU (54 mg, 0.14 mmol), and DIEA (30 μL, 0.16 mmol) in 8 mL DMF for 45 min. The coupling was repeated to ensure complete reaction. The resin was then washed with DMF (4×2 mL) and dichloromethane (5×2 mL) followed by cleavage of peptide using 95:2.5:2.5 TFA/water/TIPS (v/v) for two hours (TFA = trifluoroacetic acid, TIPS = triisopropylsilane). The TFA solution of

the peptide was concentrated under reduced pressure. The peptide was purified by reverse phase HPLC using aqueous acetonitrile gradients containing 0.1% TFA (v/v).

Peptide WASK{-$COC_2H_4PPh_2$}LPSG, 1a. $^{31}P\{^1H\}$ NMR (161.9 MHz, CD_3CN): δ = -14.4; R_t = 60 min (HPLC gradient 1% acetonitrile/min); MALDI-TOF MS: m/z = 1149.8 $(M+Na)^+$.

Peptide WASK{-$COC_2H_4P(S)Ph_2$}LPSG. $^{31}P\{^1H\}$ NMR (161.9 MHz, CD_3CN): δ = 43.08; R_t = 54 min (HPLC gradient 1% acetonitrile/min); MALDI-TOF MS: m/z = 1181.6 $(M+Na)^+$.

Solution phase peptide synthesis. *N*-Boc protected phosphino amino acid (1 equiv), leucine methyl ester hydrochloride (1 equiv), and PyBOP (1.5 equiv) were dissolved in CH_2Cl_2 under nitrogen and cooled to 0°C. DIEA (3 equiv) was added and the reaction mix was allowed to warm up to room temperature. After stirring at room temperature for 40 min, the reaction mixture was washed with 1M HCl, saturated $NaHCO_3$, and brine. The CH_2Cl_2 solution was dried over $MgSO_4$, filtered, concentrated under reduced pressure and purified over silica using hexane/ethyl acetate as eluent. The N-Boc methyl ester protected dipeptide was treated with 1:1 TFA/CH_2Cl_2 until complete removal of Boc as indicated by TLC. The reaction mixture was then concentrated under reduced pressure, dissolved in toluene and concentrated. The last step was continued until white solid was obtained. Then the solid was dissolved in CH_2Cl_2 and concentrated followed by drying under vacuum for 12 h. The TFA salt of the dipeptide, N-acetyl valine (1 equiv.), and PyBOP (1.5 equiv.) was dissolved in CH_2Cl_2, cooled to 0°C and DIEA (3 equiv.) was added. After stirring at room temperature for 40 min, the reaction mixture was washed

with 1M HCl, saturated $NaHCO_3$ and brine. The CH_2Cl_2 layer was dried, concentrated and purified over silica using 2% methanol/ethyl acetate as eluent.

Ac-Val-Epa-Leu-OMe, 2a. ^{1}H NMR (400 MHz, $CDCl_3$): δ = 7.98 (d, 1H), 7.82 (d, 1H), 6.06 (m, 1H), 4.89 (m, 1H), 4.44 (m, 1H), 4.12-4.22 (m, 1H), 3.69 (s, 3H), 2.1-2.5 (m, 3H), 2.06 (s, 3H), 1.7-1.94 (m, 6H), 1.37 (m, 1H), 1.11-1.21 (m, 6H), 0.89 -0.95 (m, 12H); $^{31}P\{^1H\}$ NMR (161.9 MHz, $CDCl_3$): δ = 52.00 (major isomer 92%), 51.98 (minor diastereomer 8%); R_f = 0.2 (EtOAc); MALDI-TOF MS: m/z = 500.31 $(M+Na)^+$. The two diastereomeric tripeptides could not be separated because of their nearly identical polarity.

Ac-Val-Ipa-Leu-OMe, 3a. ^{1}H NMR (400 MHz, $CDCl_3$): δ = 7.94 (d, 1H), 7.85 (d, 1H), 6.04 (m, 1H), 4.88 (m, 1H), 4.45 (m, 1H), 4.28 (m, 1H), 3.72 (s, 3H), 2.42-2.48 (m, 1H), 2.29-2.35 (m, 2H), 2.22-2.26 (m, 1H), 2.11-2.17(m, 1H) 2.09 (s, 3H), 1.78 (m, 1H), 1.63-1.71 (m, 2H) 1.19-1.31 (m, 12H), 0.92-1 (m, 12H); $^{31}P\{^1H\}$ NMR (161.9 MHz, $CDCl_3$): δ = 64.98. R_f = 0.22 (EtOAc). MALDI-TOF MS: m/z = 528.36 $(M+Na)^+$.

Ac-Val-Ppa-Leu-OMe, 4a. ^{1}H NMR (400 MHz, CD_2Cl_2): δ = 7.83 (m, 4H), 7.75 (d, 1H), 7.49 (m, 6H), 7.10 (d, 1H), 5.98 (d, 1H), 4.69-4.79 (m, 1H), 4.21 (m, 1H), 4.07 (m, 1H), 3.64 (s, 3H), 2.09 (m, 1H), 2.06 (s, 3H), 1.97 (m, 1H), 1.52-1.54 (m, 3H), 0.81-0.90 (m, 12 H); $^{31}P\{^1H\}$ NMR (161.9 MHz, CD_2Cl_2): δ = 40.35. R_f = 0.1 (2:1 EtOAc/hexane). MALDI-TOF MS: m/z = 595.8 $(M+Na)^+$.

Preparation of 1a by desulfurization of WASK{-$COC_2H_4P(S)Ph_2$}LPSG. Raney nickel slurry (800 mg) was transferred to a Schlenk flask and washed with degassed methanol until the washings were clear. Then the Raney nickel was washed with degassed CH_3CN (3×5 mL). The peptide (29 μmol) in 4:1 CH_3CN/water (v/v, 10 mL)

was added to the Raney nickel and stirred at room temperature for 2 h. Completion of desulfurization was confirmed by MALDI-TOF MS. The Raney nickel was allowed to settle and the reaction mixture was filtered into a Schlenk flask under an argon atmosphere. The Raney nickel was rinsed with 5×5 mL CH_3CN and filtered into the Schlenk flask. The CH_3CN solution was concentrated under reduced pressure and lyophilized overnight to obtain phosphine-peptide (**1a**) as white powder that was immediately used for the cluster incorporation.

Synthesis of 1 from 1a. The phosphine-peptide **1a** (3 μmol) was dissolved in CH_3CN (5 mL). In a separate flask (μ-pdt)$Fe_2(CO)_6$ (4 mg) and trimethylamine-N-oxide (2 mg) were dissolved in CH_3CN (1 mL) and stirred in the dark for 10 min. This solution was transferred to the peptide solution *via* cannula. After stirring for two hours in the dark, the solvent was removed under reduced pressure, and the product metallopeptide (**1**) was purified *via* reverse phase HPLC. Yield 15%. $^{31}P\{^1H\}$ NMR (161.9 MHz, 10% D_2O/CD_3CN): δ = 55.43. IR (KBr, cm^{-1}): ν(CO) = 2044, 1981, 1958, 1925. ESI-MS: (EI^+) m/z = 1458.5 $(M+H-CO)^+$; (EI^-) m/z = 1456.4 $(M-H-CO)^-$, 1373.6 $(M-H-4CO)^-$. R_t = 76 min (HPLC gradient 1% acetonitrile/min).

Desulfurization of tripeptides (2a, 3a, 4a) by Raney nickel. To a slurry of Raney nickel (washed with MeOH and CH_3CN) was added a solution of tripeptide (0.25 mmol) in CH_3CN (15 mL). The reaction mixture was stirred at 45-55°C under argon until complete reduction of the phosphine sulfide as indicated by either ^{31}P NMR or MALDI. The Raney nickel was allowed to settle, and the supernatant was filtered under argon. The filtrate was concentrated under reduced pressure and lyophilized overnight. The

tripeptide with free phosphine was immediately used for the reaction with diiron hexacarbonyl precursor.

Reduction of 2a. Reaction condition: 2 h at 25°C, then 1 h at 44°C. MALDI-TOF MS: m/z = 446.37 $(M+H)^+$.

Reduction of 3a. Reaction condition: 4 h at 48°C. $^{31}P\{^1H\}$ NMR (161.9 MHz, $CDCl_3$): δ = -4.06.

Reduction of 3a. Reaction condition: 4 h at 55°C. $^{31}P\{^1H\}$ NMR (161.9 MHz, $CDCl_3$): δ = -23.34.

General procedure for cluster incorporation into tripeptide. A solution of $(\mu\text{-}SR_1S)Fe_2(CO)_6$ (0.3 mmol) in CH_3CN (3 mL) was added dropwise to a CH_2Cl_2 (2 mL) solution of $Me_3NO.2H_2O$ (0.3 mmol) at room temperature. After stirring the reaction mixture in the dark for 10 min, a CH_2Cl_2 (10 mL) solution of the phosphine-peptide (0.2 mmol) was added dropwise. After 3 h, the solvent was removed under reduced pressure, and the residue was purified by silica gel chromatography with 2% $MeOH/CH_2Cl_2$ to produce the peptide-diiron complex as red powder.

(Val-Epa-Leu)-{(μ-pdt)$Fe_2(CO)_5$}, 2. Yield 77%. ^1H NMR (400 MHz, CD_2Cl_2): δ = 6.78 (d, 1H), 6.63 (d, 1H), 5.98 (d, 1H), 4.93 (m, 1H), 4.47 (m, 1H), 4.18 (m, 1H), 3.69 (s, 3H), 2.56 (m, 1H), 2.27 (m, 3H), 2.10 (m, 1H), 1.99 (s, 3H), 1.72-1.88 (m, 6H) 1.56-1.60 (m, 5H), 1.23-1.26 (m, 6H), 0.90-0.94 (m, 12H); ^{31}P NMR (161.9 MHz, CD_2Cl_2): δ = 54.78 (major isomer 78%), 54.95 (minor diastereomer 22%); IR (CH_2Cl_2, cm^{-1}): ν(CO) = 2040, 1981, 1966, 1921; R_f = 0.5 (EtOAc); MS ($APCI^+$): m/z = 804.1117 (calculated 804.1139).

(Val-Ipa-Leu)-{(μ-pdt)$Fe_2(CO)_5$}, 3. Yield 80%. ^{1}H NMR (400 MHz, CD_2Cl_2): δ = 6.85 (d, 1H), 6.63 (d, 1H), 5.95 (d, 1H), 4.98 (m, 1H), 4.47 (m, 1H), 4.03-4.18 (m, 1H), 3.67 (s, 3H), 2.23 (m, 1H), 2.24 (m, 4H), 2.00 (m, 5H), 1.55-1.68 (m, 7H), 1.26-1.35 (m, 12H), 0.89-0.98 (m, 12H); ^{31}P NMR (161.9 MHz, CD_2Cl_2): δ = 70.15 (major isomer 60%), 69.75 (minor diastereomer 40%); IR (CH_2Cl_2, cm^{-1}): ν(CO) = 2043, 1979, 1960, 1919; R_f = 0.6 (EtOAc); MS (APCI$^+$): m/z = 832.1449 (calculated 832.1452).

(Val-Ppa-Leu)-{(μ-pdt)$Fe_2(CO)_5$}, 4. Yield 87%. ^{1}H NMR (400 MHz, CD_2Cl_2): δ = 7.62-7.76 (m, 4H), 7.41-7.51 (m, 6H), 6.56 (d, 1H), 5.77 (d, 1H), 5.52 (d, 1H), 4.74 (m, 1H), 4.36 (m, 1H), 3.75 (m, 1H), 3.69 (s, 3H), 2.83-3.30 (m, 3H), 1.93 (s, 3H), 1.85 (m, 3H), 1.50-1.58 (m, 6H), 0.85-0.88 (m, 6H), 0.73-0.80 (m, 6H); ^{31}P NMR (161.9 MHz, CD_2Cl_2): δ = 55.30 (major isomer 70%), 55.91 (minor diastereomer, 30%); IR (CH_2Cl_2, cm^{-1}): ν(CO) = 2046, 1984, 1961, 1928; R_f = 0.3 (2% MeOH/CH_2Cl_2); MS (APCI$^+$): m/z = 900.1159 (calculated 900.1139).

(Val-Ppa-Leu)-{(μ-bdt)$Fe_2(CO)_5$}, 5. Yield 84%. ^{1}H NMR (400 MHz, CD_2Cl_2): δ = 7.65 (m, 2H), 7.47-7.53 (m, 4H), 7.32-7.4 (m, 2H), 7.24-7.27 (4H), 6.94 (d, 1H), 6.54 (d, 1H), 6.48 (td, 1H), 6.39 (m, 1H), 4.84 (m, 1H), 4.41 (m, 1H), 3.73 (s, 3H), 3.7 (m, 1H), 2.73 (m, 2H), 1.94 (s, 3H), 1.49-1.60 (m, 4H), 0.86-0.90 (m, 6H), 0.72-0.77 (m, 6H); ^{31}P NMR (161.9 MHz, CD_2Cl_2): δ = 51.25; IR (CH_2Cl_2, cm^{-1}): ν(CO) = 2053, 1994, 1937; R_f = 0.37 (2% MeOH/CH_2Cl_2); MS (APCI$^+$): m/z = 934.0973 (calculated 934.0983).

Electrochemistry. Electrochemical measurements were made using a CHI 1200A electrochemical analyzer under an atmosphere of argon. A conventional three-electrode cell was used for recording cyclic voltammograms. The working electrode was a 3 mm diameter glassy carbon disk polished with 1 mm and 0.3 mm deagglomerated alpha

alumina, successively, and sonicated for 15 min in ultrapure water prior to use. The Ag/Ag^+ reference electrode was prepared by immersing a silver wire anodized with AgCl in an CH_3CN solution of 0.1 M $[NBu_4][PF_6]$. A platinum wire was used as counter electrode. For the electrochemical studies in pure CH_3CN, a 0.1 M solution of $[NBu_4][PF_6]$ was used as supporting electrolyte. Mixtures of 0.1 M $[NBu_4][PF_6]$ in CH_3CN and 0.1 M KCl in water were used for the mixed solvent experiments. Deaeration of the solutions was performed by bubbling argon through the solution for 15 min after which an atmosphere of argon was maintained during the course of electrochemical measurements. All potentials are reported relative to the ferrocene couple (Fc^+/Fc) as reference. Concentrations of the complexes were determined spectrophotometrically based on the extinction coefficients of the Fe-S charge transfer bands in the range 342-365 nm.

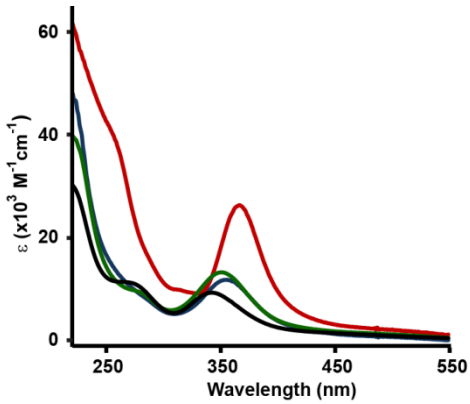

Figure 3-1. Optical spectra of the phosphine-peptide substituted diiron complexes. UV-vis spectra of **2** (black), **3** (green), **4** (blue), and **5** (red) in acetonitrile. Spectra were obtained from solutions of approximately 0.1 mM complex.

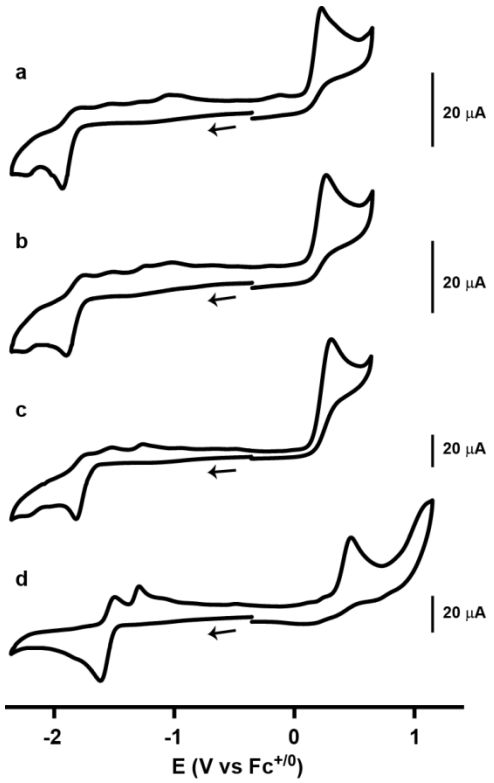

Figure 3-2. Cyclic voltammograms of the phosphine-substituted diiron-peptide complexes in acetonitrile. Cyclic voltammograms of (a) **2** (0.88 mM), (b) **3** (0.69 mM), (c) **4** (1.39 mM), and (d) **5** (1 mM) in acetonitrile with 0.1 M $[NBu_4][PF_6]$ at a scan rate 0.2 Vs^{-1}. Arrows mark the starting potential and scan direction.

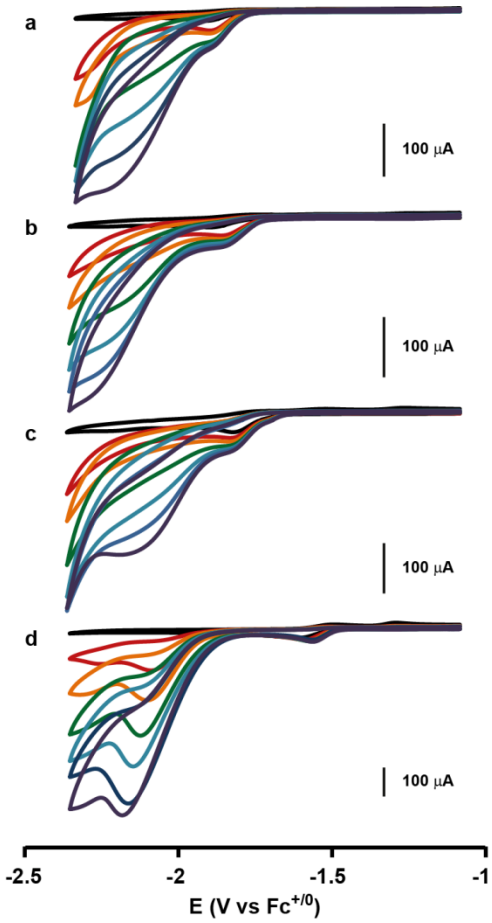

Figure 3-3. Electrocatalytic proton reduction from AcOH in acetonitrile. Cyclic voltammograms of (a) **2** (0.88 mM), (b) **3** (0.69 mM), (c) **4** (1.39 mM), and (d) **5** in acetonitrile with various concentrations of acetic acid. The acid concentrations used are 5, 10, 20, 30, 40, and 50 mM. Reductive current increases with increasing acid concentration. Other experimental conditions are as described in Figure 3-2.

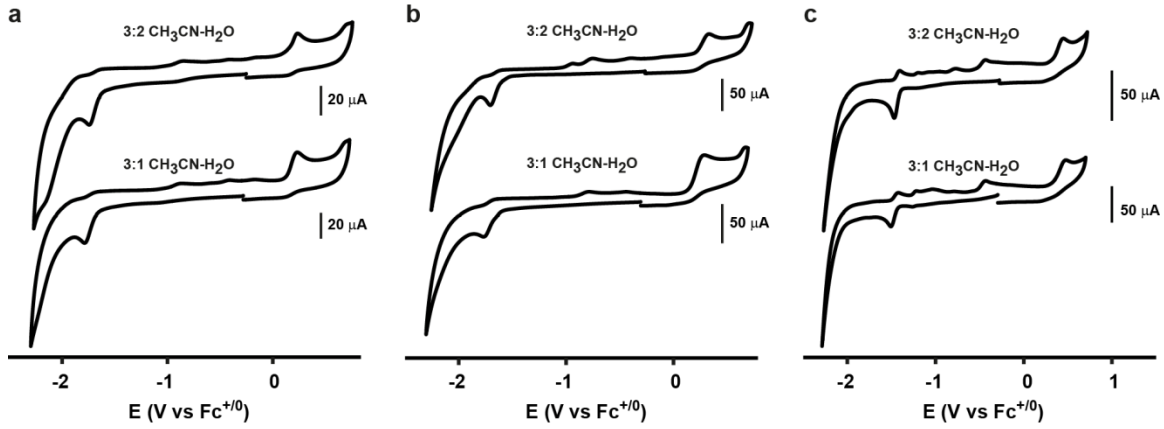

Figure 3-4. Cyclic voltammograms of the phosphine-peptide substituted diiron complexes in acetonitrile/water mixtures. Cyclic voltammograms of (a) **3**, (b) **4**, and (c) **5** in 3:2 acetonitrile-water (top) and 3:1 acetonitrile-water (bottom) at a potential scan rate of 0.2 Vs^{-1}. Cyclic voltammograms in neat acetonitrile are shown in Figure 3-2. In acetonitrile, 0.1 M $[NBu_4][PF_6]$ is used as supporting electrolyte. Similarly, 0.1 M KCl is used as supporting electrolyte in water. Solvent mixtures include both electrolytes at the concentration formed by mixing. Concentrations of the complexes: (i) 3:1 CH_3CN/H_2O: **3** (0.63 mM), **4** (1.06 mM), and **5** (0.86 mM); (ii) 3:2 CH_3CN/H_2O: **3** (0.64 mM), **4** (1.25 mM), and **5** (0.72 mM).

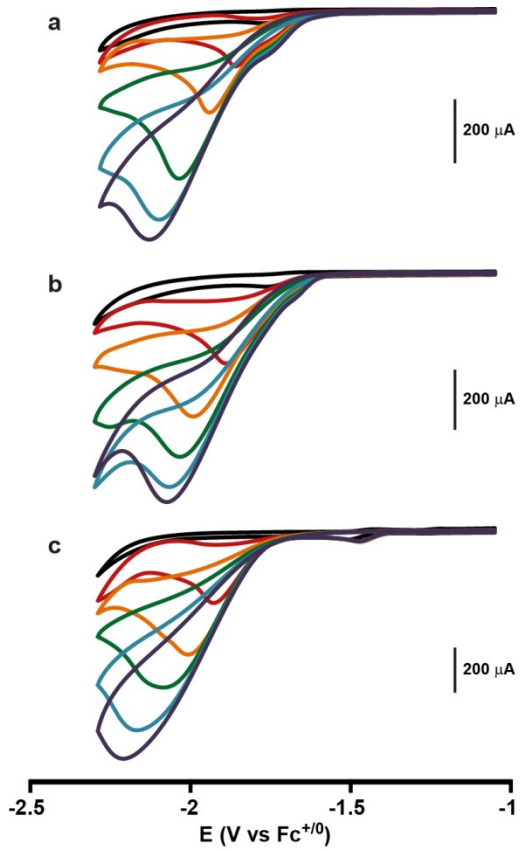

Figure 3-5. Electrocatalytic proton reduction from AcOH in 3:1 acetonitrile/water. Cyclic voltammograms of (a) **3** (0.63 mM), (b) **4** (1.06 mM), and (c) **5** (0.86 mM) in 3:1 acetonitrile-water with various concentrations of acetic acid. The acid concentrations used are 5, 10, 20, 30, 40, and 50 mM. Other experimental conditions are as described in Figure 3-4.

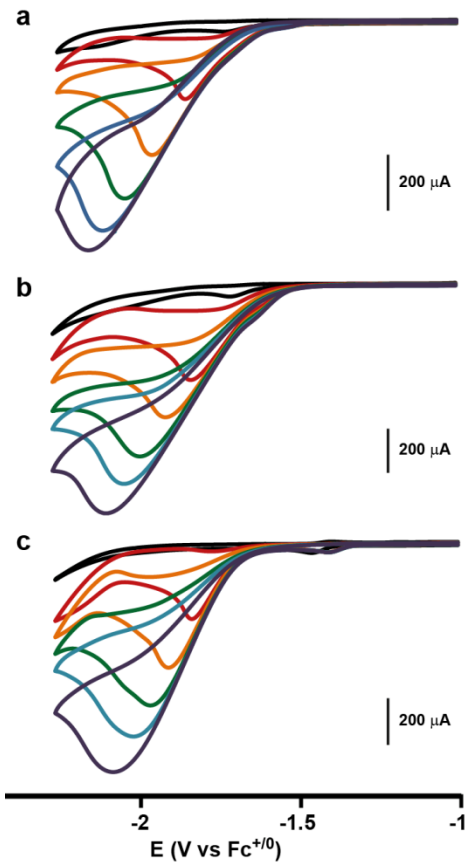

Figure 3-6. Electrocatalytic proton reduction from AcOH in 3:2 acetonitrile/water. Cyclic voltammograms of (a) **3** (0.64 mM), (b) **4** (1.25 mM), and (c) **5** (0.72 mM) in 3:2 acetonitrile-water with various concentrations of acetic acid. The acid concentrations used are 5, 10, 20, 30, 40, and 50 mM. Other experimental conditions are as described in Figure 3-4.

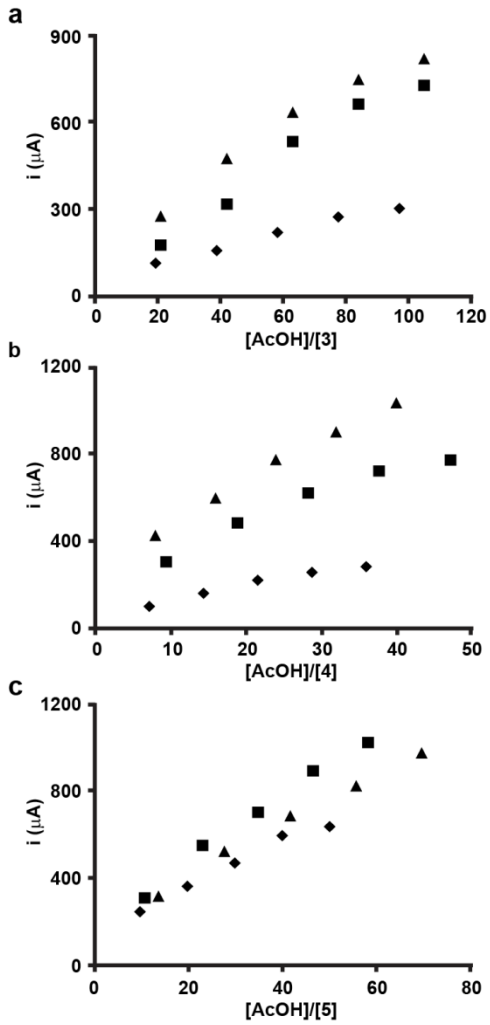

Figure 3-7. Plots of catalytic peak current *vs.* [AcOH] for mixed acetonitrile/water (3:1 and 3:2) solvents. Dependence of the catalytic peak current (i_{cat}) on equivalents of acetic acid added for (a) **3**, (b) **4**, and (c) **5** in acetonitrile (♦), 3:1 acetonitrile-water (■), and 3:2 acetonitrile-water (▲). The values of i_{cat} were calculated using Figure 3-3, 3-5 and 3-6.

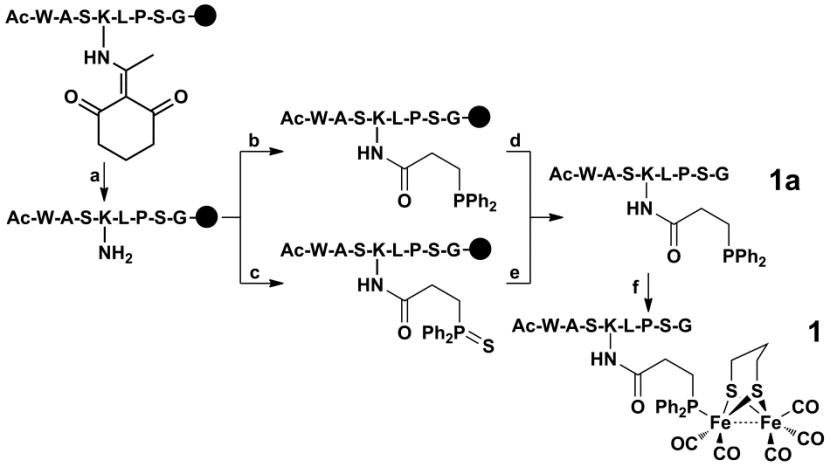

Scheme 3-1. Synthetic scheme for on-resin modification of the lysine residue of an eight amino acid peptide to incorporate a phosphine functional group and subsequent reaction with diiron-hexacarbonyl to produce the [(μ-pdt){$Fe(CO)_3$}{peptide-$Fe(CO)_2$}] complex (**1**). The solid circle represents the resin bead. Reaction conditions: (a) 2% N_2H_4, DMF; (b) $Ph_2PC_2H_4COOH$, HATU, DIEA, DMF; (c) $Ph_2P(S)C_2H_4COOH$, HATU, DIEA, DMF; (d) 95% TFA, 2.5% water, 2.5% TIPS; (e) (i) 95% TFA, 2.5% water, 2.5% TIPS, (ii) Raney nickel, aq. CH_3CN; (f) (μ-pdt)$Fe_2(CO)_6$, Me_3NO, aq. CH_3CN.

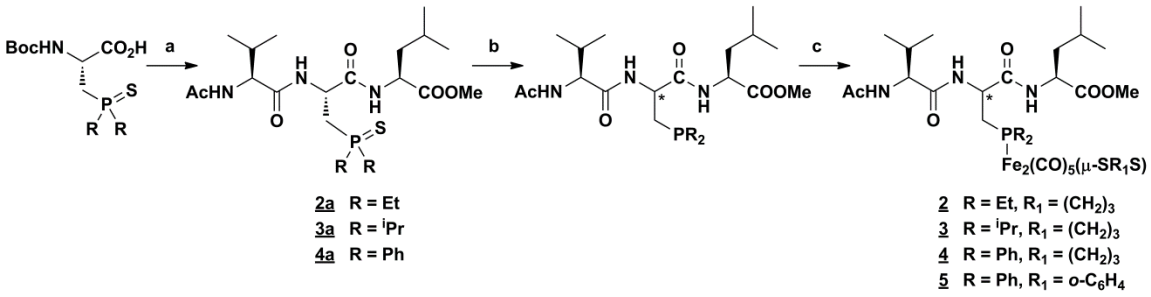

Scheme 3-2. Synthetic scheme for diiron-tripeptide complexes utilizing artificial *N*-Boc phosphine sulfide amino acids. Reaction conditions: (a) (i) H-Leu-OMe.HCl, PyBOP, DIEA, CH_2Cl_2, (ii) Ac-Val-OH, PyBOP, DIEA, CH_2Cl_2; (b) Raney nickel, CH_3CN, heat (* racemization occurred during reduction); (c) (μ-SR_1S)$Fe_2(CO)_6$, Me_3NO, CH_3CN.

Table 3-1. UV-vis absorbance for the Fe-S charge transfer band and IR stretching frequencies in the ν(CO) region data for complexes **1-5**

Complex	λ_{max}, nm (ε, $M^{-1}cm^{-1}$)	ν (CO), cm^{-1}
1[a]	350	2044 (s), 1981 (s), 1958 (sh.), 1925 (w)
2	342 (9300)	2040 (s), 1981 (vs), 1966 (sh.), 1921 (w)
3	351 (13250)	2043 (s), 1979 (vs), 1960 (sh.), 1919 (w)
4	354 (12050)	2046 (s), 1984 (s), 1961 (sh.), 1928 (w)
5	365 (25700)	2053 (s), 1994 (s), 1937 (w)

[a] Extinction coefficient was not determined

Table 3-2. Electrochemical data for **2-5** in acetonitrile and acetonitrile/water mixed solvents

Complex	E_{pc} ($Fe^{I}Fe^{I}/Fe^{I}Fe^{0}$), V			E_{pa} ($Fe^{II}Fe^{I}/Fe^{I}Fe^{I}$), V		
	CH_3CN	3:1 CH_3CN/H_2O	3:2 CH_3CN/H_2O	CH_3CN	3:1 CH_3CN/H_2O	3:2 CH_3CN/H_2O
2	-1.93	ND[a]	ND	+0.22	ND	ND
3	-1.90	-1.78	-1.74	+0.26	+0.22	+0.22
4	-1.82	-1.77	-1.72	+0.31	+0.29	+0.32
5	-1.62	-1.51	-1.47	+0.47	+0.48	+0.46

[a] ND = not determined.

References

1. Fontecilla-Camps JC, Volbeda A, Cavazza C, Nicolet Y (2007) Chem. Rev. 107:4273-4303 DOI 10.1021/cr050195z
2. Adams MWW, Stiefel EI (1998) Science 282:1842-1843 DOI 10.1126/science.282.5395.1842
3. Cammack R (1999) Nature 397:214-215 DOI 10.1038/16601
4. Frey M (2002) ChemBioChem 3:153-160 DOI 10.1002/1439-7633(20020301)3:2/3<153::aid-cbic153>3.0.co;2-b
5. Peters JW, Lanzilotta WN, Lemon BJ, Seefeldt LC (1998) Science 282:1853-1858 DOI 10.1126/science.282.5395.1853
6. Nicolet Y, Piras C, Legrand P, Hatchikian CE, Fontecilla-Camps JC (1999) Structure 7:13-23 DOI 10.1016/s0969-2126(99)80005-7
7. Evans DJ, Pickett CJ (2003) Chem. Soc. Rev. 32:268-275 DOI 10.1039/b201317g
8. Felton GAN, Mebi CA, Petro BJ, Vannucci AK, Evans DH, Glass RS, Lichtenberger DL (2009) J. Organomet. Chem. 694:2681-2699 DOI 10.1016/j.jorganchem.2009.03.017
9. Tard C, Pickett CJ (2009) Chem. Rev. 109:2245-2274 DOI 10.1021/cr800542q
10. Singleton ML, Reibenspies JH, Darensbourg MY (2010) J. Am. Chem. Soc. 132:8870-8871 DOI 10.1021/ja103774j
11. Frederix PWJM, Kania R, Wright JA, Lamprou DA, Ulijn RV, Pickett CJ, Hunt NT (2012) Dalton Trans. 41:13112-13119 DOI 10.1039/c2dt30307h
12. Li Y, Zhong W, Qian G, Xiao Z, Liu X (2013) Appl. Organomet. Chem. 27:253-260 DOI 10.1002/aoc.2979

13. Shaw WJ (2012) Catalysis Reviews-Science and Engineering 54:489-550 DOI 10.1080/01614940.2012.679453

14. Sano Y, Onoda A, Hayashi T (2012) J. Inorg. Biochem. 108:159-162 DOI http://dx.doi.org/10.1016/j.jinorgbio.2011.07.010

15. Sano Y, Onoda A, Hayashi T (2011) Chem. Commun. 47:8229-8231 DOI 10.1039/c1cc11157d

16. Green KN, Hess JL, Thomas CM, Darensbourg MY (2009) Dalton Trans.:4344-4350 DOI 10.1039/b823152d

17. Darensbourg MY, Lyon EJ, Zhao X, Georgakaki IP (2003) Proc. Natl. Acad. Sci. U.S.A. 100:3683-3688 DOI 10.1073/pnas.0536955100

18. Bethel RD, Darensbourg MY (2013) Nature 499:40-41

19. Berggren G, Adamska A, Lambertz C, Simmons TR, Esselborn J, Atta M, Gambarelli S, Mouesca JM, Reijerse E, Lubitz W, Happe T, Artero V, Fontecave M (2013) Nature 499:66-69

20. Nanda V, Koder RL (2010) Nat Chem 2:15-24

21. Wallar BJ, Lipscomb JD (1996) Chem. Rev. 96:2625-2658 DOI 10.1021/cr9500489

22. Faiella M, Andreozzi C, de Rosales RTM, Pavone V, Maglio O, Nastri F, DeGrado WF, Lombardi A (2009) Nat Chem Biol 5:882-884

23. Jones AK, Lichtenstein BR, Dutta A, Gordon G, Dutton PL (2007) J. Am. Chem. Soc. 129:14844-14845 DOI 10.1021/ja075116a

24. Apfel U-P, Rudolph M, Apfel C, Robl C, Langenegger D, Hoyer D, Jaun B, Ebert M-O, Alpermann T, Seebach D, Weigand W (2010) Dalton Trans. 39:3065-3071 DOI 10.1039/b921299j

25. Roy S, Shinde S, Hamilton GA, Hartnett HE, Jones AK (2011) Eur. J. Inorg. Chem. 2011:1050-1055 DOI 10.1002/ejic.201000979

26. Gloaguen Fdr, Lawrence JD, Rauchfuss TB (2001) J. Am. Chem. Soc. 123:9476-9477 DOI 10.1021/ja016516f

27. Chong DS, Georgakaki IP, Mejia-Rodriguez R, Samabria-Chinchilla J, Soriaga MP, Darensbourg MY (2003) Dalton Trans.:4158-4163 DOI 10.1039/b304283a

28. Gilbertson SR, Chen GH, McLoughlin M (1994) J. Am. Chem. Soc. 116:4481-4482 DOI 10.1021/ja00089a049

29. Agarkov A, Greenfield S, Xie D, Pawlick R, Starkey G, Gilbertson SR (2006) Biopolymers 84:48-73 DOI 10.1002/bip.20395

30. Li P, Wang M, He C, Li G, Liu X, Chen C, Åkermark B, Sun L (2005) Eur. J. Inorg. Chem. 2005:2506-2513 DOI 10.1002/ejic.200400947

31. Gao W, Liu J, Åkermark B, Sun L (2007) J. Organomet. Chem. 692:1579-1583 DOI http://dx.doi.org/10.1016/j.jorganchem.2006.12.009

32. Song L-C, Wang H-T, Ge J-H, Mei S-Z, Gao J, Wang L-X, Gai B, Zhao L-Q, Yan J, Wang Y-Z (2008) Organometallics 27:1409-1416 DOI 10.1021/om700956e

33. Shearer J, Long LM (2006) Inorg. Chem. 45:2358-2360 DOI 10.1021/ic0514344

34. Tard Cd, Pickett CJ (2009) Chem. Rev. 109:2245-2274 DOI 10.1021/cr800542q

35. Gilbertson SR, Collibee SE, Agarkov A (2000) J. Am. Chem. Soc. 122:6522-6523 DOI 10.1021/ja992306f

36. Agarkov A, Greenfield SJ, Ohishi T, Collibee SE, Gilbertson SR (2004) J. Org. Chem. 69:8077-8085 DOI 10.1021/jo049103g

37. Capon J-F, Ezzaher S, Gloaguen F, Petillon FY, Schollhammer P, Talarmin J, Davin TJ, McGrady JE, Muir KW (2007) New J. Chem. 31:2052-2064 DOI 10.1039/b709273c

38. Capon J-F, Gloaguen F, Petillon FY, Schollhammer P, Talarmin J (2009) Coord. Chem. Rev. 253:1476-1494 DOI 10.1016/j.ccr.2008.10.020

39. Surawatanawong P, Tye JW, Darensbourg MY, Hall MB (2010) Dalton Trans. 39:3093-3104 DOI 10.1039/b925262b

40. Mejia-Rodriguez R, Chong DS, Reibenspies JH, Soriaga MP, Darensbourg MY (2004) J. Am. Chem. Soc. 126:12004-12014 DOI 10.1021/ja039394v

41. Na Y, Wang M, Jin K, Zhang R, Sun L (2006) J. Organomet. Chem. 691:5045-5051 DOI http://dx.doi.org/10.1016/j.jorganchem.2006.08.082

42. Tsvetkov EN, Bondarenko NA, Malakhova IG, Kabachnik MI (1986) Synthesis 1986:198-208 DOI 10.1055/s-1986-31510

43. van Zutphen S, Margarit VJ, Mora G, Le Floch P (2007) Tetrahedron Lett. 48:2857-2859 DOI http://dx.doi.org/10.1016/j.tetlet.2007.02.102

44. Greenfield SJ, Agarkov A, Gilbertson SR (2003) Org. Lett. 5:3069-3072 DOI 10.1021/ol035097j

45. Lyon EJ, Georgakaki IP, Reibenspies JH, Darensbourg MY (1999) Angew. Chem. Int. Ed. 38:3178-3180 DOI 10.1002/(sici)1521-3773(19991102)38:21<3178::aid-anie3178>3.3.co;2-w

46. Zhao J, Wei Z, Zeng X, Liu X (2012) Dalton Trans. 41:11125-11133 DOI 10.1039/c2dt31083j

Chapter 4

Biomimetic model for [FeFe]-hydrogenase: Asymmetrically disubstituted diiron model complex with a redox-active 2,2'-bipyridyl ligand

Souvik Roy,[a,b] Thomas L. Groy,[a] and Anne K. Jones*[a,b]

[a]Department of Chemistry and Biochemistry; [b]Center for Bio-Inspired Solar Fuel Production; Arizona State University, Tempe, AZ 85287

Reproduced by permission of The Royal Society of Chemistry

Dalton Trans., 2013, **42**, 3843-3853

Abstract

[FeFe]-hydrogenases feature a unique active site in which the primary catalytic unit is directly coordinated via a bridging cysteine thiolate to a secondary, redox active [4Fe4S] unit. The goal of this study was to evaluate the impact of a bidentate, redox non-innocent ligand on the electrocatalytic properties of the (μ-$S(CH_2)_3S)Fe_2(CO)_4L_2$ family of [FeFe]-hydrogenase models as a proxy for the iron-sulfur cluster. Reaction of the redox non-innocent ligand 2,2'-bipyridyl (bpy) with (μ-$S(CH_2)_3S)Fe_2(CO)_6$ leads to substitution of two carbonyls to form the asymmetric complex (μ-$S(CH_2)_3S)Fe_2(CO)_4(\kappa^2$-bpy) (**1**) which was structurally characterized by single crystal X-ray diffraction. This complex can be protonated by $HBF_4.OEt_2$ to form a bridging hydride. Furthermore, electrochemical investigation shows that, at slow scan rates, the complex undergoes a two electron reduction at -2.06 V vs. Fc^+/Fc that likely involves reduction of both the bpy ligand and the metal. Electrocatalytic reduction of protons is observed in the presence of three distinct acids of varying strengths: $HBF_4.OEt_2$, AcOH, and *p*-TsOH. The catalytic mechanism depends on the strength of the acid.

Introduction

Hydrogenases are the enzymes that catalyze the oxidation of hydrogen to protons and electrons as well as the reverse, reduction of protons to hydrogen.[1-4] This reaction is important to carbon neutral fuel production, and much research is focused on developing robust, renewable catalysts. Since hydrogenases rely only on earth abundant first row transition metals at their active sites, they have served as a source of inspiration for much work in this area.[5-7] As shown in Figure 4-1, structural studies have shown that the active site of [FeFe]-hydrogenases, often referred to as the H-cluster, consists of a diiron catalytic subsite bridged via a single cysteinyl thiolate to a redox active [4Fe4S] cluster.[8-13] The diiron subsite is a [2Fe2S] unit in which the irons are linked via a bridging organic dithiolate ligand. The remainder of the coordination sphere of each iron is occupied by the biologically uncommon π-acceptor ligands CO and CN^-.

Organometallic complexes of the type $[(\mu\text{-}SR)_2Fe_2(CO)_6]$ and their derivatives in which one or more carbonyl ligands are substituted by σ-donor ligands such as phosphines or *N*-heterocyclic carbenes have proven to be both structural and functional models of [FeFe]-hydrogenases.[14-16] However, several significant differences from the enzymes have limited the catalytic abilities of these complexes. First, although the enzymes utilize the Fe(II)Fe(I) redox state of the H-cluster for proton reduction, electrocatalysis via model compounds almost invariably relies on the Fe(I)Fe(0) state.[7] The result is that model complexes require considerable overpotential to initiate proton reduction catalysis. Second, while the enzyme features an inverted geometry around one of the metal centers allowing ligand binding at an

exposed terminal position, the model complexes are most stable in the relatively inert eclipsed conformation.[17] Third, theoretical work has indicated that electron density is delocalized throughout all six irons of the H-cluster and the redox active [4Fe4S] cubane is crucial in the catalytic cycle of the enzyme,[18, 19] but few models have incorporated either an iron-sulfur cluster or a redox-active ligand.[20-23]

Theoretical studies have suggested that asymmetrically substituted complexes with strong donor ligands should favor a rotated geometry and thus facilitate proton reduction catalysis.[24] To this end, chelating ligands such as diphosphines, phenanthroline, or carbenes have proven useful in controlling and modulating the properties of [FeFe]-hydrogenase model compounds. [25-32] For example, formation of short-lived terminal hydrides upon protonation has been detected for complexes with chelating ligands of the form (μ-SRS)$Fe_2(CO)_4$(LL) (LL=chelating ligand).[33, 34] This indicates that these compounds can attain a rotated geometry and accommodate an external ligand, albeit fleetingly. Although seldom used in hydrogenase models, redox active ligands have proven useful in modulating catalytic properties at a metallocenter as a function of the redox state of the ligand in other chemical contexts.[35, 36]

To explore the effects of a chelating, redox non-innocent ligand, we have synthesized (μ-S$(CH_2)_3$S)$Fe_2(CO)_4(\kappa^2$-bpy), in which bpy is the weakly π-accepting 2,2'-bipyridyl ligand. In this paper, we describe the electronic properties of this complex as well as its electrochemical behavior under both oxidizing and reducing conditions. Importantly, the first reductive event is a two electron process that likely involves both metal and ligand reduction. Comparison to other model complexes suggests avenues for producing better electrocatalysts for proton reduction.

Results and Discussion

Synthesis and Characterization of [(μ-pdt)$Fe_2(CO)_4(\kappa^2$-bpy)], 1. 2,2′-bipyridyl (bpy) was chosen as a ligand for substitution of carbonyls because it is both redox non-innocent and weakly π-accepting. The complex, [(μ-pdt)$Fe_2(CO)_4(\kappa^2$-bpy)] (**1**), was synthesized from the hexacarbonyl precursor in 60% yield via substitution of two CO ligands by 2,2′-bipyridyl in refluxing toluene (pdt = 1,3-propanedithiol). Purification of the resulting solution via silica chromatography resulted in isolation of the product as moderately air-stable, dark green crystals. The molecular structure of **1** was determined by X-ray diffraction analysis of a single crystal obtained by slow diffusion of hexane into a dichloromethane solution of **1**. The crystal structure of **1** is shown in Figure 4-2, and selected bond lengths and bond angles are listed in Table 4-1. The bond angles indicate that, as reported previously for analogous diiron(I) pdt complexes, the coordination geometry around both iron centers is distorted square pyramidal.[7, 37, 38] However, the structure is asymmetric with binding of κ^2-(2,2′-bpy) to only one of the irons in a basal-basal conformation. The two Fe units, $Fe(CO)_3$ and Fe(CO)(2,2′-bpy), are eclipsed and are connected by an Fe–Fe bond and a 1,3-propanedithiolate bridge. The Fe–Fe bond (2.5623(4) Å) is longer than the corresponding bond of the parent hexacarbonyl complex (2.5103(11) Å)[39] but similar to the corresponding bond in reduced DdH hydrogenase (2.55 Å).[40] On the other hand, the Fe–Fe bond is shorter than that determined in related compounds containing basal-basal diphosphine or bis-carbene, such as [(μ-pdt)$Fe_2(CO)_4(\kappa^2$-LL)] (LL = 1,2-bis(dimethylphosphino)ethane, 2.6038(5) Å;[27] LL = 1,1-bis(diphenylphosphino)methane, 2.5879(7) Å;[41] LL = $(PPh_2)_2N(^iPr)$, 2.6236(4)

Å; LL = $(PPh_2)_2N$(allyl), 2.6042(4) Å);[42] LL = I_{Me}-CH_2-I_{Me} , 2.5774(6) Å (I_{Me} = 1-methylimidazol-2-ylidene); and LL = I_{Me}-C_2H_4-I_{Me}, 2.6253(4) Å).[34] The coordination of 2,2′-bpy induces a slight asymmetry of the Fe_2S_2 skeleton which is reflected by shorter Fe-S bonds to the Fe(CO)(2,2′-bpy) moiety. Furthermore, the weak π-accepting ability of 2,2′-bpy leads to a shortening of the adjacent Fe-CO_{ax} [Fe(1)-C(11) 1.755(2) Å] bond compared to the Fe-CO_{ax} [Fe(2)-C(13) 1.813(2) Å] and Fe-CO_{ba} [Fe(2)-C(12) 1.778(2) Å, Fe(2)-C(14) 1.779(2) Å] bonds on the $Fe(CO)_3$ moiety (*ax* and *ba* denote axial and basal positions, respectively).

1 was characterized by UV-vis, FTIR and NMR spectroscopies. As shown in Figure 4-3, IR spectra of **1** in dichloromethane or acetonitrile consist of three characteristic bands at 2007, 1937 and 1896 cm^{-1}, similar to those observed for the analogous 1,10-phenanthroline substituted complex.[26] Relative to the hexacarbonyl precursor, the ν_{CO} bands are *ca.* 70 cm^{-1} lower in energy. This shift is greater than that of bis-phosphine analogues[25, 27, 33, 43] and only slightly less than bis-(N-heterocyclic carbene) analogues.[34] This suggests that the weak accepting ability of the 2,2′-bpy ligand results in electron rich diiron core with the basicity of the diiron center comparable to that of bis-(*N*-heterocyclic carbene) analogues. We note also that five strong bands at 2002, 1993, 1935, 1920, and 1882 cm^{-1} are observed in the carbonyl region when the spectrum is obtained from a KBr pellet of **1**. The difference suggests that **1** may be fluxional in solution or pellet preparation may have resulted in modification of crystal packing.

The positions of the resonances of the 2,2′-bpy ligand in the ^1H and ^{13}C NMR spectra can be compared to those of the free ligand to describe qualitatively the

electronic impact of bonding interactions between the Fe and the 2,2′-bpy. The ^{1}H NMR spectrum of **1** in CD_2Cl_2 includes four resonances (two doublets and two triplets) in the aromatic region, indicating symmetrical coordination of 2,2′-bpy (Figure 4-4). As listed in Table 4-2, it is interesting to note that, relative to the free ligand, the chemical shifts for the 2,2′-bpy H(5), H(4), and H(3) protons are all shifted upfield. On the other hand, H(6) is shifted downfield. The ^{13}C NMR spectrum shows a similar pattern in the chemical shifts of the ring carbons with the exception of C(5) which is shifted slightly downfield. Effectively, π-backdonation from the metal to the empty π^* (LUMO) of the ligand causes all of the 2,2′-bpy carbons, except C(6) and C(5), to become more electron rich upon coordination to the iron center. From the NMR resonances, we conclude this back-donation is particularly prominent at position 3 of the ring [$\Delta\delta(^{1}H)$ = -0.4 and $\Delta\delta(^{13}C)$ = -2.91]. As expected since the C(6)-2p orbital does not contribute to the LUMO, C(6) and H(6) resonances are shifted slightly downfield.[44]

The presence of a 2,2′-bpy or other diimine ligands on a low spin iron complex usually leads to three absorption bands in the UV-vis spectrum: an intense ligand-centered π-π^* band in the high energy UV region, weak metal-centered d-d transitions in the visible region, and metal-to-ligand-charge-transfer (MLCT) bands.[45] As shown in Figure 4-5, the UV-vis spectrum of **1** in acetonitrile consists of a series of absorptions at 298, 342, 391, 519, 613, and 685 nm. The highest energy band is likely attributable to the bpy $\pi-\pi^*$ transition. The weaker, lower energy bands are thought to arise from Fe^{I}-CO charge-transfer and $Fe^{I}(d\pi)$-bpy(π^*) interactions.[46]

Protonation of 1. The reaction of **1** in acetonitrile at room temperature (298 K) with excess $HBF_4.OEt_2$ resulted in a change of the color of the solution from deep green to light brown. The course of the reaction was monitored by IR spectroscopy. As shown in Figure 4-3, upon addition of acid three new bands in the ν_{CO} region at 2098, 2044, and 1970 cm^{-1} appeared with a concomitant decrease of the bands associated with **1**. The reaction was complete, *i.e.* the spectrum associated with starting material disappeared, within six minutes. The carbonyl stretching frequencies shifted by an average of 92 cm^{-1} to higher wavenumbers; this shift is consistent with protonation of the Fe-Fe bond of **1** to form a bridging hydride species.[26, 27, 34] Corroborating evidence was obtained through NMR experiments. Addition of three equivalents of $HBF_4.OEt_2$ to a solution of **1** in CD_2Cl_2 at room temperature resulted in formation of a singlet at -9.01 ppm in the ^1H NMR spectrum (Figure 4-6). This suggests formation of a bridging hydride species, $\mathbf{[1H]^+}$, under these conditions. Although, the protonated species was stable up to one hour in solution, attempts to isolate the product $\mathbf{[1H][BF_4]}$ for structural analysis were unsuccessful. Comparison of the UV-vis spectra of **1** and $\mathbf{[1H]^+}$ (Figure 4-5) shows bleaching of the MLCT bands in the visible region upon protonation of **1**. This can be explained by a decrease of electron density on the iron centers upon binding the proton.

Oxidation of 1 to 1^+. The electrochemical properties of **1** were investigated by cyclic voltammetry to evaluate the effect of the redox non-innocent 2,2′-bpy ligand on the diiron cluster. As shown in Figure 4-7A, cyclic voltammograms of **1** in CH_2Cl_2 under oxidizing conditions reveal a partially reversible (i_p^c/i_p^a= 0.62 at 0.1 V s^{-1}) oxidation at $E_{1/2}$= -0.25 V (all potentials are reported relative to Fc^+/Fc measured under the same experimental conditions). By analogy to other electrochemical studies, this is likely the

$Fe^{II}Fe^{I}/Fe^{I}Fe^{I}$ couple. It is interesting to note that at faster scan rates, 0.8 V s^{-1}, the process becomes more reversible (i_p^c/i_p^a= 0.9) suggesting that an EC process is occurring with a slower chemical step that does not have time to occur on shorter timescales. Loss of a CO ligand, although not common for complexes with bidentate chelating ligands, has been shown to occur under oxidizing conditions for a number of diiron carbonyl complexes.[47, 48] Thus, we hypothesized that loss of CO was the chemical step, and experiments were also undertaken in the presence of CO. As shown in Figure 4-7B, under an atmosphere of CO, complete reversibility of the redox couple was maintained even at scan rates as low as 0.05 V s^{-1} (i_p^c/i_p^a= 0.88, 0.9, and 0.94 at 0.05, 0.2, and 0.8 V s^{-1} respectively). Thus it is likely that oxidation under an inert atmosphere leads to loss of CO. Although loss of CO is known for many iron carbonyl compounds, it was not observed for either [(μ-pdt)$Fe_2(CO)_4$(dppe)] or [(μ-pdt)$Fe_2(CO)_4(I_{Me}$-CH_2-$I_{Me})$], analogous complexes including bidentate chelating ligands.[30, 31] In the case of the dppe derivative, oxidation led to binding of an additional CO which was detected by a new oxidation peak in the voltammogram.[31] On the other hand, cyclic voltammograms of [(μ-pdt)$Fe_2(CO)_4(I_{Me}$-CH_2-$I_{Me})$] were identical under N_2 and CO suggesting no reaction occurs between $[(\mu\text{-pdt})Fe_2(CO)_4(I_{Me}\text{-}CH_2\text{-}I_{Me})]^+$ and CO.[31] Thus the electrochemical behavior of **1** under oxidative conditions is significantly different from both the dppe and I_{Me}-CH_2-I_{Me} analogues. $\mathbf{1}^+$ is likely less stable than the other two cationic compounds and loses CO very readily.

Reaction of $\mathbf{1}^+$ with $P(OMe)_3$. Both experimental and theoretical studies have shown that diiron complexes analogous to **1** with a chelating ligand [(μ-SRS)$Fe_2(CO)_4(\kappa^2$-LL)] undergo a change in geometry upon oxidation in which one of the iron centers

adopts an inverted pyramidal structure, creating an open coordination site for external ligand binding.[24, 49] Thus the oxidized compound is often more reactive towards formation of adducts or substitution reactions than the neutral parent compound. To explore the reactivity of $\mathbf{1}^+$, we have undertaken electrochemical experiments in the presence of $P(OMe)_3$. Experiments were carried out under CO to minimize the undesired loss of CO.

As shown in Figure 4-8, the oxidation of **1** in CH_2Cl_2 at room temperature in the presence of $P(OMe)_3$ was partially reversible with a new reduction occurring at -1.06 V. This suggests a coupled EC process in which, after the initial oxidation, the phosphite is coordinated by $\mathbf{1}^+$. Substitution of a carbonyl by $P(OMe)_3$ typically leads to a negative shift of reduction potential of 0.310-0.375 V.[30] The negative shift of 0.8 V in the reduction potential of $\mathbf{1}^+$ is consistent with increased electron density around the metal attributable to the coordination of two phosphite ligands to the diiron center. Using cyclic voltammetry at faster scan rates (ν = 0.8 V s^{-1}), two different reductive events were observed at E_p = -0.76 and -1.06 V. This suggests that the reaction between $\mathbf{1}^+$ and $P(OMe)_3$ may produce two species. The reduction at -0.76 V may be attributable to a complex containing a single $P(OMe)_3$ ligand and whereas that at -1.06 V likely possesses two $P(OMe)_3$ ligands. In further support of this hypothesis, we note that even at faster scan rates, addition of excess $P(OMe)_3$, which should thermodynamically favor formation of a more substituted product, led to an increase in the reductive peak current at E_p = -1.06 V (Figure 6, bottom panel). Taken together, these results suggest the species at E_p = -0.76 V forms first and that at -1.06 V is formed later or in the presence of more ligand. Chemical synthesis of the phosphite

substituted cationic complex by addition of $P(OMe)_3$ to a solution of $\mathbf{1}^+$ (produced by addition of 1 equivalent of $FcBF_4$ at -42°C) was unsuccessful due to the extreme sensitivity of the oxidized product to air and temperature.

The cationic complex $[1\text{-}P(OMe)_3]^+$ likely formed in these experiments could be either an adduct $[(\mu\text{-pdt})Fe_2(CO)_4(\kappa^2\text{-bpy})(P(OMe)_3)]^+$ or a $P(OMe)_3$/CO substitution product $[(\mu\text{-pdt})Fe_2(CO)_3(\kappa^2\text{-bpy})(P(OMe)_3)]^+$. Formation of CO substituted complex (E_p = -0.76 V) seems more likely since the experiments in CH_2Cl_2 demonstrated that $\mathbf{1}^+$ is prone to loss of CO. Similarly, we anticipate that the complex with a reduction at -1.06 V is likely the disubstituted cation, $[(pdt)Fe_2(CO)_2(\kappa^2\text{-bpy})(P(OMe)_3)_2]^+$. Similar results have been reported for the dppe complex $[(\mu\text{-pdt})Fe_2(CO)_4(\kappa^2\text{-dppe})]^+$.[30] The $P(OMe)_3$ substituted cationic bis-carbene complex $[Fe_2(CO)_3(P(OMe)_3)(\kappa^2\text{-}I_{Me}\text{-}CH_2\text{-}I_{Me})(\mu\text{-pdt})]^+$ has been reported to undergo disproportionation to form a disubstituted dication and the neutral unsubstituted complex.[31] However, there is no evidence that $[\mathbf{1}+P(OMe)_3]^+$ disproportionates. If the dication were to form, it is expected that it would have a much less negative reduction potential. The relative ease of losing CO from oxidized forms of **1** may explain why they do not undergo disproportionation.

Reduction of 1. Cyclic voltammograms of **1** in acetonitrile under an inert atmosphere show a reduction at E_p^{red} = -2.06 V which was completely irreversible at scan rates lower than 1 V s^{-1} (Figure 4-9). At faster scan rates (1-10 V s^{-1}), the reduction became quasi-reversible (i_p^c/i_p^a= 1.84 (Ar) and 4.67 (CO) at 4 V s^{-1}; i_p^c/i_p^a= 2.42 (Ar) and 5.85 (CO) at 2 V s^{-1}) under both Ar and CO. The reduction is likely an EC process, but this demonstrates that loss of CO is not the chemical step. Additionally, the chemical step

following reduction must be reasonably slow. Controlled-potential coulometry demonstrated that the reduction at -2.06 V is a two electron process (Figure 4-10). Moreover, at scan rates faster than 1 V s^{-1}, the reductive peak begins to split into two reductive features, separated by 0.25 V, indicating that the process is not concerted. This behavior has been observed previously for several diiron complexes with *N*-heterocyclic carbene ligands.[50-52] Since substituted iron carbonyl complexes in this family are not usually observed to form an Fe^0Fe^0 state, we hypothesize that only one of the reductions occurs at a metal center forming an Fe^IFe^0 species.[30, 31, 50, 51] The other likely corresponds to the bpy^0/bpy^{1-} couple. This assignment is consistent with the reduction potential of the bpy ligand alone, -2.63 V in CH_3CN, assuming that coordination of the ligand by removing electron density will shift its reduction potential to more positive values.[53] The presence of two small oxidation peaks at E_p = -1.53, and -1.19 V suggests that the reduction may be followed by a chemical reaction(s) resulting in multiple products that are reoxidized at different potentials.

Electrocatalytic proton reduction activity of 1. The electrocatalytic proton reduction activity of **1** was investigated in CH_3CN in the presence of three distinct proton sources: a strong acid ($HBF_4.OEt_2$), a weak acid (AcOH) and an acid of intermediate strength (*p*-TsOH).

As shown in Figure 4-11, sequential addition of AcOH from 1.4 mM to 42 mM (1-30 equiv), shows a 12-fold enhancement of peak current at -2.06 V with little impact on the rest of the voltammogram. This is characteristic of electrocatalytic H_2 evolution.[54-56] The catalytic efficiency (C.E.) of **1** in AcOH was calculated using the method defined by Felton and coworkers,[15]

$$\text{C. E.} = \frac{i_{cat}/i_d}{C_{HA}/C_{cat}}$$

(i_{cat} = catalytic current, i_d = current for reduction of catalyst in absence of acid, C_{HA} = concentration of acid, C_{cat} = concentration of catalyst). The value of C.E. of **1** varies in the range 0.44 to 0.25, decreasing with increasing acid concentration. The overpotential for the process, defined as the difference between the standard potential for reduction of the acid and the half-wave potential for catalytic proton reduction, was 0.68 V.[56, 57] The shift of the catalysis to less reducing potentials as acid concentration increases is consistent with a proton coupled electrochemical process. On the basis of these experimental results and previous reports on similar complexes, it is reasonable to propose an EECC mechanism such as that depicted in Figure 4-12 to account for the electrocatalysis by **1** in AcOH.[52, 55, 58, 59] First, **1** undergoes a two-electron reduction with one metal-centered reduction and one ligand-based reduction producing the electron rich dianion $\mathbf{1}^{2-}$. Then the dianion accepts two protons. The catalyst is regenerated following reductive elemination of hydrogen.

In the presence of HBF_4, cyclic voltammograms of **1** exhibit two new reduction peaks at -1.33 and -1.69 V in addition to the peak at -2.06 V observed in weak acid (Figure 4-13A). All three peaks grow at a similar rate with increasing acid concentration indicating electrocatalytic proton reduction occurs. The electrocatalytic behavior of **1** in *p*-TsOH is similar to that observed in HBF_4 with three different catalytic processes as shown in Figure 4-13B. However, the first two reduction events at less negative potential are poorly separated and appear as a broad peak at *ca.* -1.4 to -1.7 V. The current for the second reduction increases at a faster rate than the first

reductive current with increasing concentration of *p*-TsOH, when the acid is not present in large excess. This experimental observation suggests that the strength of the acid plays an important role in controlling the mechanism of electrocatalytic proton reduction (direct reduction of HBF_4 and *p*-TsOH on the glassy carbon electrode in absence of **1** are shown in Figure 4-14).

The Fe–Fe bond of a sufficiently basic model diiron compound can be protonated by HBF_4 to form bridging hydride species which are reduced at potentials from 0.75 to 1.08 V more positive than the parent compound.[15] The 2,2′-bpy ligand of **1** should make it basic enough to be protonated by HBF_4 at the Fe^IFe^I level leading to formation of the bridging hydride species, $\mathbf{1\mu H^+}$. The electrocatalysis at -1.33 V, 0.74 V more positive than the catalysis in HOAc, is expected to arise from this species via an ECEC mechanism as shown in pathway A of Figure 4-15. First, $\mathbf{1\mu H^+}$ is reduced to **1μH**, followed by protonation to produce $\mathbf{1–2H^+}$. Then it accepts another electron to form the neutral complex **1–2H** which gets further protonated followed by evolution of hydrogen and regeneration of $\mathbf{1\mu H^+}$. However, this pathway cannot account for the catalytic reduction of protons observed at -1.7 V. Instead, based on similar electrochemistry observed for $[(\mu\text{-pdt})Fe_2(CO)_4(\kappa^2\text{-dppe})(\mu\text{-H})]^+$,[60] we propose that the active electrocatalytic species for the second process is **1μH** and the mechanism for the catalysis is probably CEEC, as shown in Figure 4-15 (pathway B). The catalytic current arises from the reduction of **1–2H** to $\mathbf{1–2H^-}$ which occurs at -1.7 V. Protonation of $\mathbf{1–2H^-}$ followed by release of hydrogen regenerates the active species **1μH**. Electrocatalysis observed in presence of *p*-TsOH also supports such a CEEC

mechanism. The catalytic current for the second process at -1.7 V increases faster than the first process for *p*-TsOH when concentration of acid is low (1-4 equivalent). It suggests that protonation and reduction of **1–2H** compete with each other, and the reduction is dominant when *p*-TsOH rather than HBF_4 is used. HBF_4, being a stronger acid, tends to favor pathway A by protonating **1–2H**. Moreover, when excess *p*-TsOH (> 4 equivalent) is present, the acidity of the solution is sufficiently high that pathway A becomes more prominent than pathway B.

Conclusions

Our studies have focused on the impact of incorporating a redox non-innocent, bidentate chelating ligand on the electronic and catalytic properties of dithiolate-bridged diiron models. In comparison to the parent hexacarbonyl complex, substitution of two of the CO ligands by 2,2′-bpy leads to a negative shift of the Fe^IFe^I/Fe^IFe^0 reduction potential by 0.4 V and an average shift of the ν_{CO} of 70 cm^{-1} to lower energy (to 2007, 1937, and 1896 cm^{-1}). Both of these properties can be explained by the weaker π-accepting propensity of the 2,2'-bpy ligand. In essence, increased electron density at the iron makes it more difficult to reduce the metal complex, resulting in a shift of the reduction potential. Furthermore, the extra electron density is, in large part, accommodated by increased density in the orbitals with largely CO π* character, decreasing the energies of the CO vibrations. In fact, for complexes in this family, there is usually a correlation between the average value of ν(CO) and the reduction potential of the complex. In the case of **1**, however, this strong correlation does not seem to hold. Although the CO vibrational frequencies of **1** are similar to those of bidentate ligand substituted complexes such as bis-phosphine

or *N*-heterocyclic carbene containing complexes (for example, 1996, 1920 and 1872 cm^{-1} for [(μ-pdt)$Fe_2(CO)_4(\kappa^2$-(I_{Me}-CH_2-I_{Me}))]), the reduction potentials are not aligned. The reduction potential of **1** is closer to what would be expected for a monosubstituted complex such as [[(μ-pdt)$Fe_2(CO)_5(PMe_3)$] (-1.94 V) than either the analogous 1,2-bis(diphenylphosphino)ethane complex (E_p^{red} = -2.33 V) or the I_{Me}-CH_2-I_{Me} substituted complex (E_p^{red}= -2.42 V).[9a, 9c, 10, 17, 29] In essence, the reduction potential of **1** is 300-400 mV higher than might be expected based on its FTIR frequencies and comparisons to related compounds. The physical mechanisms by which the FTIR frequencies of **1** are shifted more dramatically than the reduction potential are unclear. It could be a result of either the π-acidity or redox non-innocence of the ligand. With that in mind, it is interesting to note that **1** undergoes both ligand and metal centered reductions at similar potentials. The physical mechanism not withstanding, the result is an exciting one because it suggests that **1** should be relatively basic and nonetheless reduced at relatively mild potentials. These are exactly the properties desired in a good proton reduction electrocatalyst, and indeed **1** is able to reduce protons supplied by the relatively weak acid HOAc as well as stronger acids. This stands in contrast to [$Fe_2(CO)_4$(bma)(μ-pdt)] {bma=2,3-bis (diphenylphosphino) maleic anhydride}, a related complex incorporating a chelating, redox active ligand that has no detectable proton reduction activity. In short, by decoupling to some extent basicity and redox potential, utilization of redox non-innocent ligands with reduction potentials similar to those of the iron may allow us to develop catalysts that operate both at high efficiency and with little overpotential.

Experimental Section

General procedures. All reactions were carried out at room temperature under an atmosphere of nitrogen using standard Schlenk and vacuum-line techniques unless otherwise noted. Anhydrous dichloromethane, toluene and acetonitrile were obtained from Sigma-Aldrich and deuterated solvents from Cambridge Isotope Laboratories. (μ-$S(CH_2)_3S)Fe_2(CO)_6$ was synthesized according to literature method;[13] all other starting materials were obtained commercially and used without further purification.

Synthesis of (μ-pdt)$Fe_2(CO)_4(\kappa^2$-bpy), (1). (μ-pdt)$Fe_2(CO)_6$ (410 mg, 1.06 mmol) and 2,2′-bipyridyl (337 mg, 2.15 mmol) were dissolved in toluene (20 mL) and the solution was heated to reflux under nitrogen until the evolution of carbon monoxide stopped (12 hours). The reaction mixture was concentrated under reduced pressure, and the residue was purified via column chromatography on silica gel using dichloromethane/hexane as eluent. The dark green band was collected and dried under vaccum. The dark green solid was thoroughly washed with hexane to remove any unreacted (μ-pdt)$Fe_2(CO)_6$ Single crystals for X-ray diffraction were grown via slow diffusion of hexane into a CH_2Cl_2 solution of the compound at -20°C. Yield: 290 mg (60%). IR (KBr pellet, cm^{-1}): 2002 (s), 1993 (sh), 1935 (s), 1920 (s), 1882 (vs). IR (CH_2Cl_2, cm^{-1}): 2007 (vs), 1937 (s), 1896 (m). ^1H NMR (400 MHz, CD_2Cl_2): δ = 8.73 (d, 2H, bpy, $C_{(6)}$-H), 8.03 (d, 2H, bpy, $C_{(3)}$-H), 7.74 (tr, 2H, bpy, $C_{(4)}$-H), 7.23 (tr, 2H, bpy, $C_{(5)}$-H), 2.05 (m, 3H, pdt), 1.88 (tr, 2H, pdt), 1.31 (m, 1H, pdt). ^{13}C {^1H} NMR (100 MHz, CD_2Cl_2): δ = 216.9 (CO), 213.6 (CO), 155.9 (bpy, $C_{(2)}$), 151 (bpy, $C_{(6)}$), 133.8 (bpy, $C_{(3)}$), 122.7 (bpy, $C_{(4)}$), 121.3 (bpy, $C_{(5)}$), 29.6 (pdt), 23.9 (pdt). Anal. Calcd for $C_{17}H_{14}N_2Fe_2O_4S_2$: C, 42.00; H, 2.90; N, 5.76. Found: C, 41.90; H, 3.15; N,

5.65.

Protonation of 1. To a solution of **1** (12 mg, 0.024 mmol) in anhydrous acetonitrile (6 mL), $HBF_4.OEt_2$ (7 μL, 0.051 mmol, 2.13 equivalent) was added at room temperature under argon. The FTIR spectrum of the solution was monitored as a function of time. IR (CH_3CN, cm^{-1}), t = 0 min (before addition of acid): 2006 (vs), 1935 (s), 1895 (m); t = 2 min (after addition of acid): 2094 (m), 2079 (sh), 2036 (m), 2015 (sh), 2006 (s), 1966 (m), 1935 (m), 1895 (m); t = 8 min: 2094 (vs), 2044 (s), 1975 (sh).

To a solution of **1** (5.2 mg, 0.011 mmol) in CD_2Cl_2 (0.75 mL) in an NMR tube, $HBF_4.OEt_2$ (5 μL, 0.036 mmol, 3.27 equivalent) was added at room temperature. The solution changed color from green to reddish brown. The ^1H NMR spectrum of the clear solution was recorded. ^1H NMR (400 MHz, CD_2Cl_2): δ = 8.8–7.4 (m, 8H, bpy), -9.04 (s, 1H, Fe–H–Fe), {1,3-propanedithiolate peaks were masked by the diethyl ether signals}.

X-Ray Crystallography. The crystal was mounted on the end of a thin glass fiber using Apiezon type N grease and optically centered. Cell parameter measurements and single-crystal diffraction data collection were performed at low temperature (123 K) with a Bruker Smart APEX diffractometer using graphite monochromated Mo Kα radiation (λ = 0.71073 Å) in the ω–φ scanning mode. The structure was solved by direct methods and refined by full-matrix least-squares on F^2. The following is the list of the programs used: data collection, Bruker Instrument Service v2010.9.0.0; cell refinement and data reduction, SAINT V7.68A; structure solution and refinement, SHELXS-97; molecular graphics, XShell v6.3.1; preparation of material for

publication, Bruker APEX2 v2010.9-1.[30] Details of crystal data and parameters for data collection and refinement are listed in Table 3.

Electrochemistry. Electrochemical measurements were conducted using a PG-STAT 128N Autolab electrochemical analyzer. All cyclic voltammograms were recorded in a conventional three-electrode-cell under inert atmosphere at room temperature. The working electrode was a 3 mm diameter glassy carbon disk polished with 1 μm and 0.3 μm deagglomerated alpha alumina, successively, and sonicated for 15 min in ultrapure water prior to use. The supporting electrolyte was [^{n}Bu$_4$N][PF$_6$] (0.1 M in acetonitrile or dichloromethane, as mentioned). The Ag/Ag$^+$ reference electrode was prepared by immersing a silver wire anodized with AgCl in an CH_3CN or CH_2Cl_2 solution of 0.1 M [^{n}Bu$_4$N][PF$_6$]. A platinum wire was used as counter electrode. For studies under argon and carbon monoxide, deaeration of the solutions was performed by bubbling argon or carbon monoxide through the solution (15 min) and then maintaining an atmosphere of Ar or CO over the solution during the course of electrochemical measurements. All other electrochemical experiments were carried out under nitrogen in a glovebox. All potentials are reported relative to the Fc/Fc$^+$ couple as reference (Fc = ferrocene). The concentration of iron complex in solution was determined spectrophotometrically based on $\varepsilon_{613} = 3500\ M^{-1}\ cm^{-1}$.

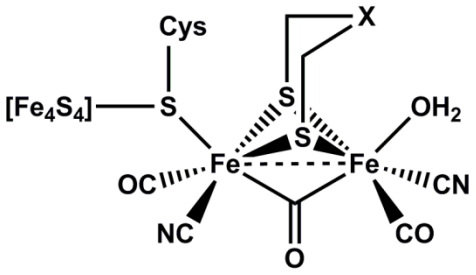

Figure 4-1. Structure of the active site of [FeFe]-hydrogenase. [FeFe]-hydrogenase active site (H-cluster).

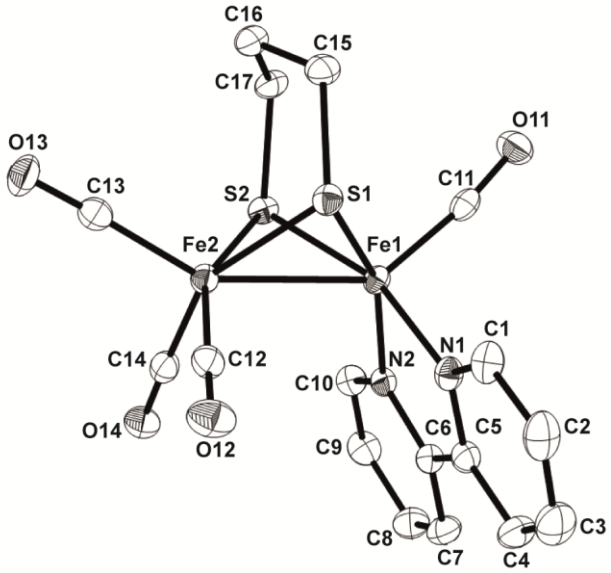

Figure 4-2. X-ray crystal structure of 1. Molecular structure of (μ-pdt)$Fe_2(CO)_4(\kappa^2$-bpy) with thermal ellipsoids drawn at 50% probability level. Hydrogen atoms have been omitted for clarity.

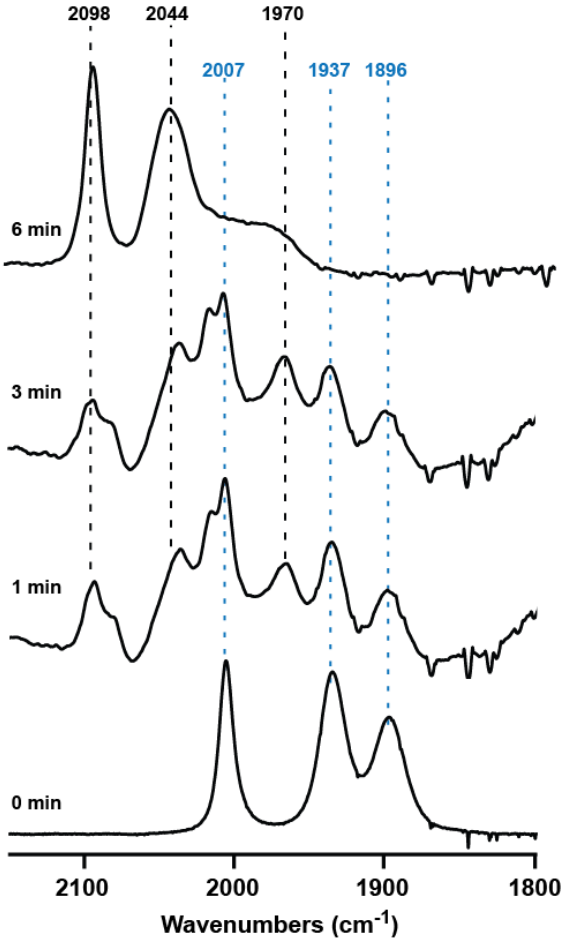

Figure 4-3. FTIR spectra of 1 in the presence of $HBF_4.OEt_2$. FTIR spectra as a function of time for **1** upon addition of 3 equivalents HBF_4 in acetonitrile solution.

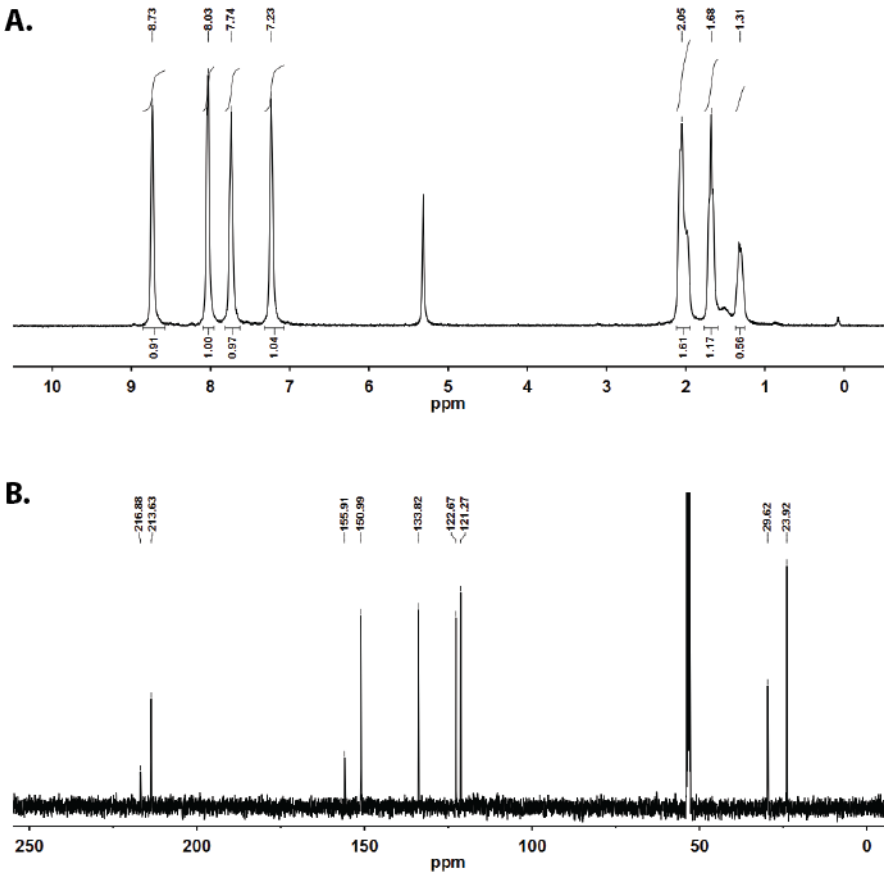

Figure 4-4. ^{1}H and ^{13}C NMR spectra of 1. (A) ^{1}H NMR spectrum and (B) ^{13}C NMR spectrum of **1** in CD_2Cl_2.

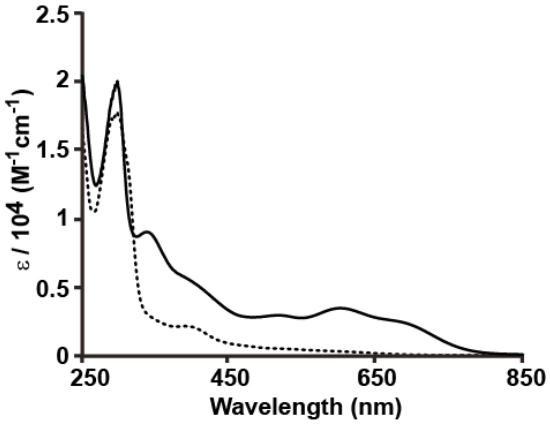

Figure 4-5. Optical spectra of 1 in the presence of $HBF_4.OEt_2$. UV-vis spectra of **1** (solid line) and [**1**H][BF_4] (dotted line) in acetonitrile at room temperature. Spectra were obtained from solutions of approximately 0.1 mM compound.

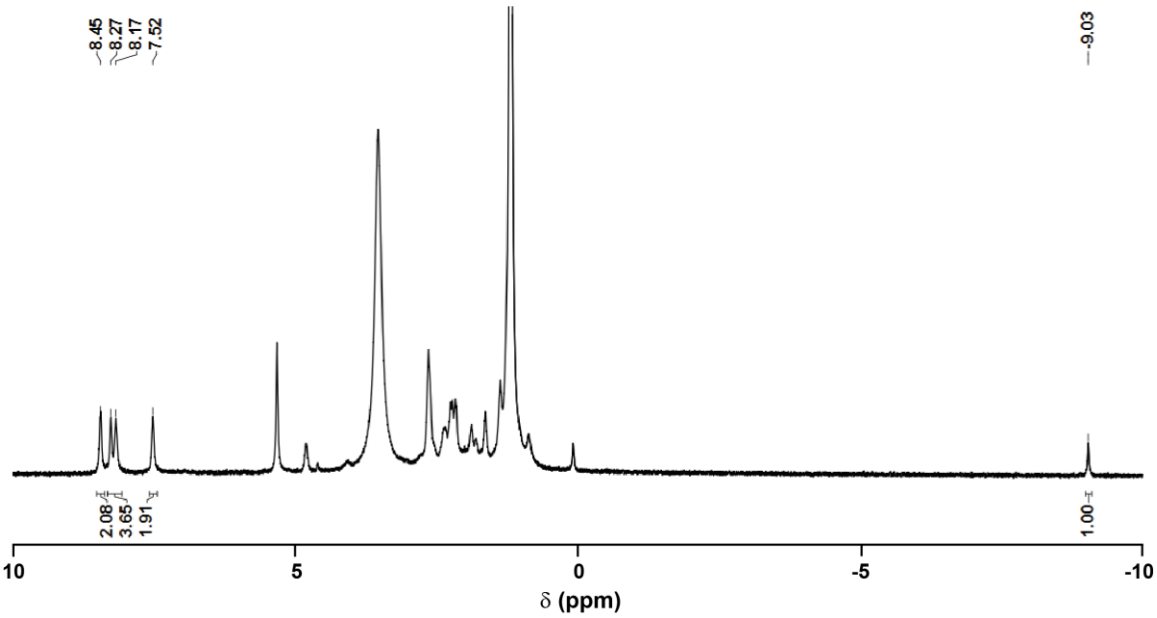

Figure 4-6. ^{1}H NMR spectrum of 1 in the presence of $HBF_4.OEt_2$. ^{1}H NMR of **1** (10 mM) in CD_2Cl_2 in presence of 3 equivalents of $HBF_4.OEt_2$.

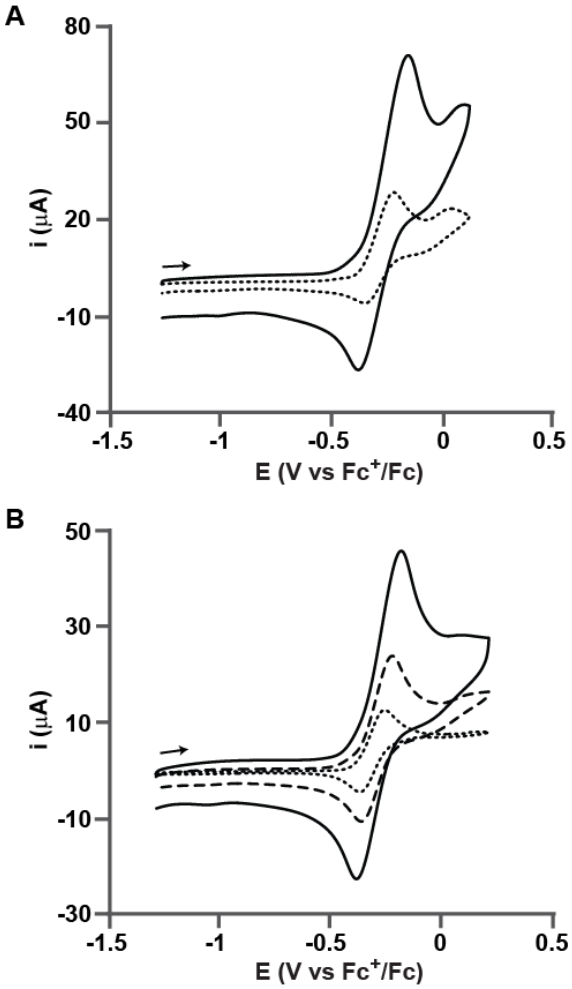

Figure 4-7. Cyclic voltammograms of 1 under argon and CO atmosphere. Cyclic voltammograms of **1** (1.1 mM) in dichloromethane, (A) under nitrogen at scan rates of 0.8 V s^{-1} (solid line) and 0.1 V s^{-1} (dotted line), (B) under CO at scan rates of 0.8 V s^{-1} (solid line), 0.2 V s^{-1} (dashed line), and 0.05 V s^{-1} (dotted line).

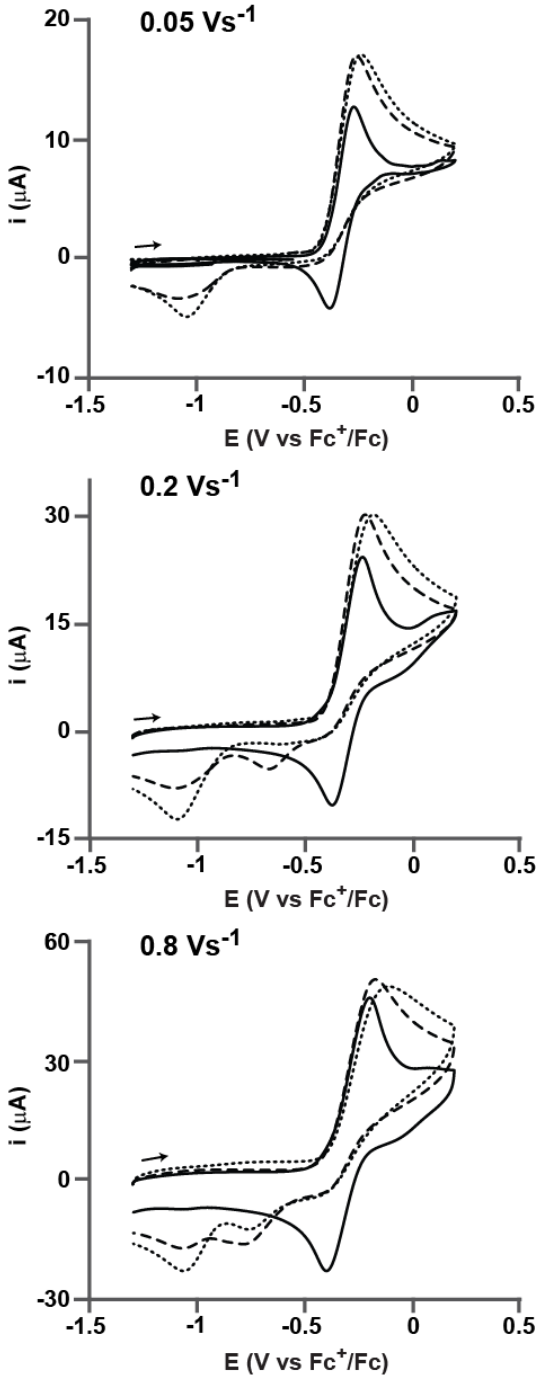

Figure 4-8. Cyclic voltammograms of 1 in the presence of $P(OMe)_3$. Cyclic voltammograms of **1** (1.1 mM) in dichloromethane in the presence of 1-2 equivalent of $P(OMe)_3$ under an atmosphere of CO. Solid lines are without addition of phosphine.

Dashed lines include 1 equivalent of $P(OMe)_3$ and dotted lines include 2 equivalents of $P(OMe)_3$.

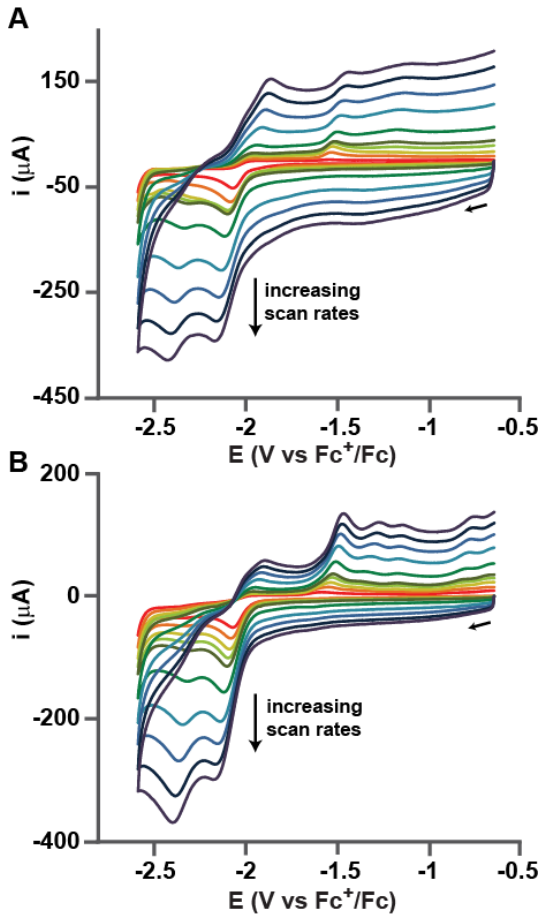

Figure 4-9. Cyclic voltammograms of 1 at different potential-scan rates. Cyclic voltammograms of **1** in acetonitrile under (A) argon (0.75 mM of 1) and (B) CO (0.68 mM of **1**). Potential scan rates shown are 0.2, 0.4, 0.6, 0.8, 1, 2, 4, 6, 8, 10 Vs^{-1}.

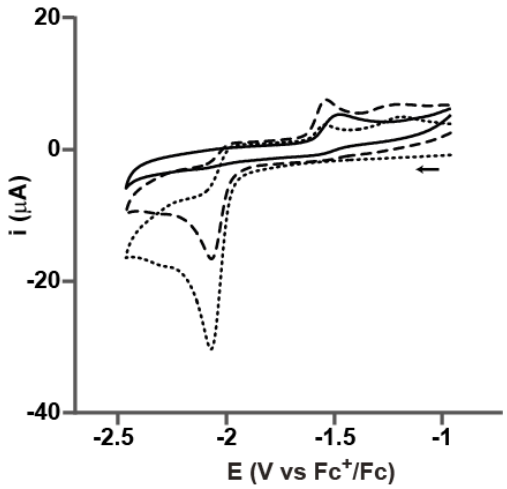

Figure 4-10. Bulk electrolysis of 1. Cyclic voltammograms of **1** in an acetonitrile solution before bulk electrolysis (dotted line), after passage of 1 F mol^{-1} charge (dashed line), and after passage of 2.4 F mol^{-1} charge (solid line).

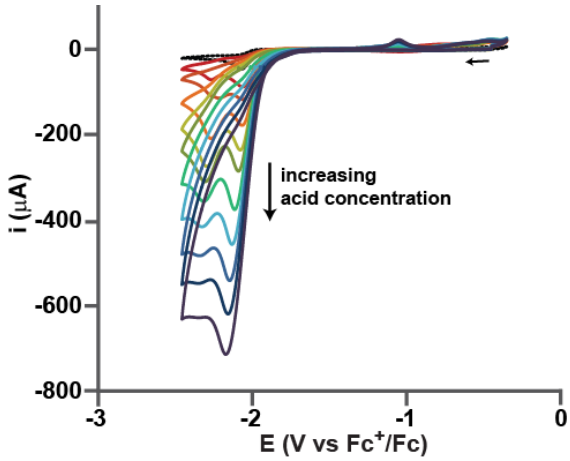

Figure 4-11. Electrocatalytic proton reduction from AcOH by 1. Cyclic voltammograms of **1** (1.4 mM) with various concentrations of acetic acid in acetonitrile. Acid concentrations are 0, 1.4, 2.8, 5.6, 8.4, 11.2, 16.8, 22.4, 28, 33.6, 42 mM.

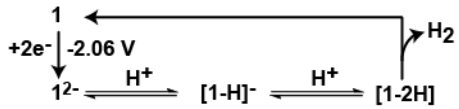

Figure 4-12. Proposed mechanism for electrocatalytic proton reduction from AcOH. Proposed EECC mechanism for H_2 production from acetic acid by **1**.

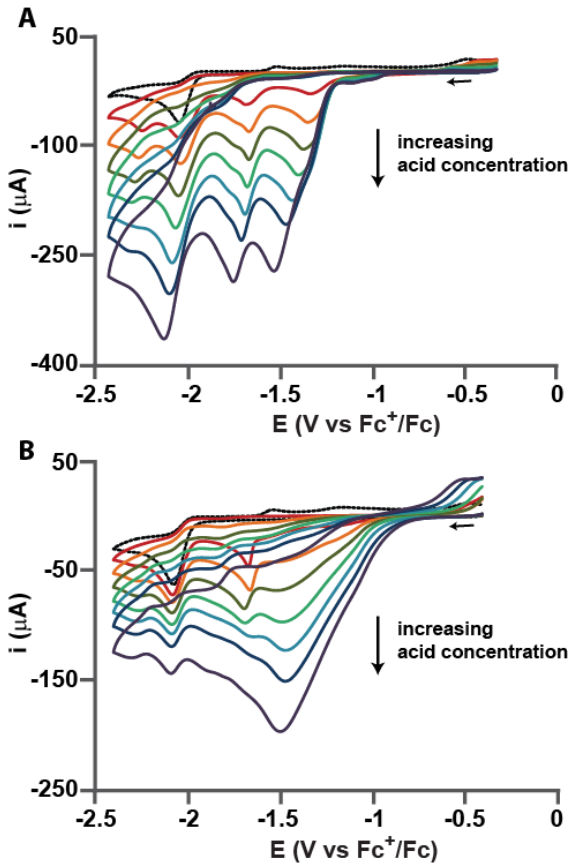

Figure 4-13. Electrocatalytic proton reduction from HBF_4 and *p*-TsOH by 1. Cyclic voltammograms of (A) **1** (1.36 mM) with HBF_4 in acetonitrile (acid concentrations are 1.4, 2.7, 4.1, 5.4, 6.8, 8.2, 11 mM) and (B) **1** (0.90 mM) with *p*-TsOH in acetonitrile (acid concentrations are 1.1, 2.2, 3.3, 4.3, 5.4, 6.5, 8.6 mM).

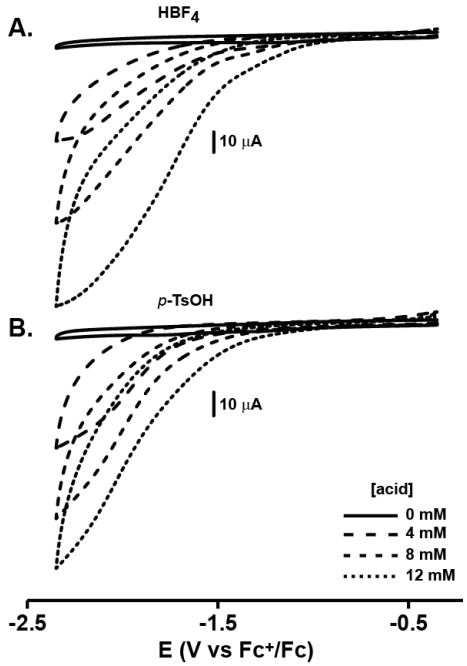

Figure 4-14. Direct reduction of HBF_4 and *p*-TsOH at the electrode. Cyclic voltammograms of (A) HBF_4 and (B) *p*-TsOH in acetonitrile solution (0.1 M *n*-Bu_4NPF_6) in absence of **1** with a glassy carbon electrode at scan rate of 0.2 Vs^{-1}.

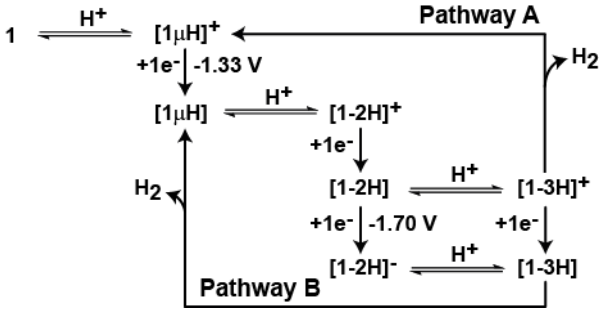

Figure 4-15. Proposed mechanism for electrocatalytic proton reduction from HBF_4 and *p*-TsOH by 1. Proposed mechanism for electrocatalytic proton reduction by **1** in presence of strong acids.

Table 4-1. Selected bond lengths (Å) and bond angles (°) for **1**.

Bond lengths			
Fe(1)-S(1)	2.2081(5)	Fe(1)-N(2)	1.9901(15)
Fe(1)-S(2)	2.2151(5)	Fe(2)-C(12)	1.778(2)
Fe(2)-S(1)	2.2703(5)	Fe(2)-C(13)	1.813(2)
Fe(2)-S(2)	2.2766(5)	Fe(2)-C(14)	1.779(2)
Fe(1)-Fe(2)	2.5623(4)	N(1)-C(5)	1.360(2)
Fe(1)-C(11)	1.755(2)	N(2)-C(6)	1.461(2)
Fe(1)-N(1)	1.9819(15)	C(5)-C(6)	1.363(3)
Bond angles			
S(1)-Fe(1)-S(2)	85.958(19)	S(2)-Fe(2)-Fe(1)	54.097(14)
S(1)-Fe(1)-Fe(2)	56.250(14)	Fe(1)-S(1)-Fe(2)	69.784(16)
S(2)-Fe(1)-Fe(2)	56.354(15)	Fe(1)-S(2)-Fe(2)	69.549(17)
S(1)-Fe(2)-S(2)	83.087(18)	N(1)-Fe(1)-N(2)	80.81(6)
S(1)-Fe(2)-Fe(1)	53.966(15)	C(12)-Fe(2)-C(14)	91.84(8)

Table 4-2. ^{1}H and ^{13}C chemical shifts of 2,2′-bipyridyl.

Position	**δ (^{1}H)**		**δ (^{13}C)**	
	2,2′-bpy	**Complex 1**	**2,2′-bpy**	**Complex 1**
2	-	-	156.04	155.91
3	8.43	8.03	136.73	133.82
4	7.82	7.74	123.64	122.67
5	7.31	7.23	120.71	121.27
6	8.65	8.73	149.06	150.99

Table 4-3. Crystallographic experimental data for **1**.

Parameter	1
Empirical formula	$C_{17}H_{14}Fe_2N_2O_4S_2$
Formula weight	486.12
Temperature (K)	123(2)
Wavelength (Å)	0.71073
Z	8
Crystal system	Monoclinic
Space group	*C* 1 2/*c* 1
a (Å)	31.260(3)
b (Å)	7.5532(7)
c (Å)	17.5720(17)
α (°)	90
β (°)	118.7770(10)
γ (°)	90
Volume (Å^3)	3636.6(6)
μ (mm^{-1})	1.852
Density (g cm^{-3})	1.776
Goodness-of-fit	1.034
R_1, wR_2 [$I > 2\sigma(I)$]	0.0214, 0.0528
R_1, wR_2 (all data)	0.0237, 0.0542

References

1. Adams, M. W. W.; Stiefel, E. I., *Science* **1998,** 282, 1842-1843.

2. Cammack, R., *Nature* **1999,** 397, 214-215.

3. Frey, M., *Chembiochem* **2002,** 3, 153-160.

4. Evans, D. J.; Pickett, C. J., *Chem. Soc. Rev.* **2003,** 32, 268-275.

5. Gloaguen, F.; Rauchfuss, T. B., *Chem. Soc. Rev.* **2009,** 38, 100-108.

6. Heinekey, D. M., *J. Organomet. Chem.* **2009,** 694, 2671-2680.

7. Tard, C.; Pickett, C. J., *Chem. Rev.* **2009,** 109, 2245-2274.

8. Pierik, A. J.; Hulstein, M.; Hagen, W. R.; Albracht, S. P. J., *Eur. J. Biochem.* **1998,** 258, 572-578.

9. Lemon, B. J.; Peters, J. W., *Biochemistry* **1999,** 38, 12969-12973.

10. Nicolet, Y.; Piras, C.; Legrand, P.; Hatchikian, C. E.; Fontecilla-Camps, J. C., *Structure* **1999,** 7, 13-23.

11. Peters, J. W.; Lanzilotta, W. N.; Lemon, B. J.; Seefeldt, L. C., *Science* **1998,** 282, 1853-1858.

12. De Lacey, A. L.; Stadler, C.; Cavazza, C.; Hatchikian, E. C.; Fernandez, V. M., *J. Am. Chem. Soc.* **2000,** 122, 11232-11233.

13. Chen, Z. J.; Lemon, B. J.; Huang, S.; Swartz, D. J.; Peters, J. W.; Bagley, K. A., *Biochemistry* **2002,** 41, 2036-2043.

14. Capon, J.-F.; Gloaguen, F.; Petillon, F. Y.; Schollhammer, P.; Talarmin, J., *Coord. Chem. Rev.* **2009,** 253, 1476-1494.

15. Felton, G. A. N.; Mebi, C. A.; Petro, B. J.; Vannucci, A. K.; Evans, D. H.; Glass, R. S.; Lichtenberger, D. L., *J. Organomet. Chem.* **2009,** 694, 2681-2699.

16. Tschierlei, S.; Ott, S.; Lomoth, R., *Energy Environ. Sci.* **2011,** 4, 2340-2352.

17. Darensbourg, M. Y.; Lyon, E. J.; Zhao, X.; Georgakaki, I. P., *Proc. Natl. Acad. Sci. U.S.A.* **2003,** 100, 3683-3688.

18. Schwab, D. E.; Tard, C.; Brecht, E.; Peters, J. W.; Pickett, C. J.; Szilagyi, R. K., *Chem. Commun.* **2006**, 3696-3698.

19. Bruschi, M.; Greco, C.; Fantucci, P.; De Gioia, L., *Inorg. Chem.* **2008,** 47, 6056-6071.

20. Si, Y.; Charreteur, K.; Capon, J.-F.; Gloaguen, F.; Petillon, F. Y.; Schollhammer, P.; Talarmin, J., *J. Inorg. Biochem.* **2010,** 104, 1038-1042.

21. Camara, J. M.; Rauchfuss, T. B., *Nature Chemistry* **2012,** 4, 26-30.

22. Tard, C.; Liu, X. M.; Ibrahim, S. K.; Bruschi, M.; De Gioia, L.; Davies, S. C.; Yang, X.; Wang, L. S.; Sawers, G.; Pickett, C. J., *Nature* **2005,** 433, 610-613.

23. Liu, Y.-C.; Lee, C.-H.; Lee, G.-H.; Chiang, M.-H., *Eur. J. Inorg. Chem.* **2011**, 1155-1162.

24. Tye, J. W.; Darensbourg, M. Y.; Hall, M. B., *Inorg. Chem.* **2006,** 45, 1552-1559.

25. Justice, A. K.; Zampella, G.; De Gioia, L.; Rauchfuss, T. B.; van der Vlugt, J. I.; Wilson, S. R., *Inorg. Chem.* **2007,** 46, 1655-1664.

26. Orain, P.-Y.; Capon, J.-F.; Kervarec, N.; Gloaguen, F.; Petillon, F.; Pichon, R.; Schollhammer, P.; Talarmin, J., *Dalton Transactions* **2007**, 3754-3756.

27. Ezzaher, S.; Capon, J.-F.; Gloaguen, F.; Kervarec, N.; Petillon, F. Y.; Pichon, R.; Schollhammer, P.; Talarmin, J., *Comptes Rendus Chimie* **2008,** 11, 906-914.

28. Ezzaher, S.; Orain, P.-Y.; Capon, J.-F.; Gloaguen, F.; Petillon, F. Y.; Roisnel, T.; Schollhammer, P.; Talarmin, J., *Chem. Commun.* **2008**, 2547-2549.

29. Ezzaher, S.; Capon, J.-F.; Gloaguen, F.; Petillon, F. Y.; Schollhammer, P.; Talarmin, J.; Kervarec, N., *Inorg. Chem.* **2009,** 48, 2-4.

30. Chouffai, D.; Zampella, G.; Capon, J.-F.; De Gioia, L.; Gloaguen, F.; Petillon, F. Y.; Schollhammer, P.; Talarmin, J., *Inorg. Chem.* **2011,** 50, 12575-12585.

31. Chouffai, D.; Zampella, G.; Capon, J.-F.; De Gioia, L.; Le Goff, A.; Petillon, F. Y.; Schollhammer, P.; Talarmin, J., *Organometallics* **2012,** 31, 1082-1091.

32. Capon, J.-F.; Gloaguen, F.; Petillon, F. Y.; Schollhammer, P.; Talarmin, J., *Eur. J. Inorg. Chem.* **2008**, 4671-4681.

33. Ezzaher, S.; Capon, J.-F.; Gloaguen, F.; Petillon, F. Y.; Schollhammer, P.; Talarmin, J., *Inorg. Chem.* **2007,** 46, 3426-3428.

34. Morvan, D.; Capon, J.-F.; Gloaguen, F.; Le Goff, A.; Marchivie, M.; Michaud, F.; Schollhammer, P.; Talarmin, J.; Yaouanc, J.-J.; Pichon, R.; Kervarec, N., *Organometallics* **2007,** 26, 2042-2052.

35. Allgeier, A. M.; Mirkin, C. A., *Angew. Chem. Int. Ed.* **1998,** 37, 894-908.

36. Ringenberg, M. R.; Kokatam, S. L.; Heiden, Z. M.; Rauchfuss, T. B., *J. Am. Chem. Soc.* **2008,** 130, 788-789.

37. Capon, J. F.; Gloaguen, F.; Schollhammer, P.; Talarmin, J., *Coord. Chem. Rev.* **2005,** 249, 1664-1676.

38. Rauchfuss, T. B., *Inorg. Chem.* **2004,** 43, 14-26.

39. Lyon, E. J.; Georgakaki, I. P.; Reibenspies, J. H.; Darensbourg, M. Y., *Angew. Chem. Int. Ed.* **1999,** 38, 3178-3180.

40. Nicolet, Y.; de Lacey, A. L.; Vernede, X.; Fernandez, V. M.; Hatchikian, E. C.; Fontecilla-Camps, J. C., *J. Am. Chem. Soc.* **2001,** 123, 1596-1601.

41. Adam, F. I.; Hogarth, G.; Richards, I., *J. Organomet. Chem.* **2007,** 692, 3957-3968.

42. Adam, F. I.; Hogarth, G.; Richards, I.; Sanchez, B. E., *Dalton Transactions* **2007**, 2495-2498.

43. Adam, F. I.; Hogarth, G.; Kabir, S. E.; Richards, D., *Comptes Rendus Chimie* **2008,** 11, 890-905.

44. Irwin, M.; Jenkins, R. K.; Denning, M. S.; Kraemer, T.; Grandjean, F.; Long, G. J.; Herchel, R.; McGrady, J. E.; Goicoechea, J. M., *Inorg. Chem.* **2010,** 49, 6160-6171.

45. Palmer, R. A.; Piper, T. S., *Inorg. Chem.* **1966,** 5, 864-&.

46. Braterman, P. S.; Song, J. I.; Peacock, R. D., *Inorg. Chem.* **1992,** 31, 555-559.

47. Razavet, M.; Borg, S. J.; George, S. J.; Best, S. P.; Fairhurst, S. A.; Pickett, C. J., *Chem. Commun.* **2002**, 700-701.

48. Gloaguen, F.; Lawrence, J. D.; Schmidt, M.; Wilson, S. R.; Rauchfuss, T. B., *J. Am. Chem. Soc.* **2001,** 123, 12518-12527.

49. Justice, A. K.; Rauchfuss, T. B.; Wilson, S. R., *Angew. Chem. Int. Ed.* **2007,** 46, 6152-6154.

50. Tye, J. W.; Lee, J.; Wang, H. W.; Mejia-Rodriguez, R.; Reibenspies, J. H.; Hall, M. B.; Darensbourg, M. Y., *Inorg. Chem.* **2005,** 44, 5550-5552.

51. Capon, J.-F.; Ezzaher, S.; Gloaguen, F.; Petillon, F. Y.; Schollhammer, P.; Talarmin, J.; Davin, T. J.; McGrady, J. E.; Muir, K. W., *New J. Chem.* **2007,** 31, 2052-2064.

52. Song, L.-C.; Luo, X.; Wang, Y.-Z.; Gai, B.; Hu, Q.-M., *J. Organomet. Chem.* **2009,** 694, 103-112.

53. Tokel-Takvoryan, N. E.; Hemingway, R. E.; Bard, A. J., *J. Am. Chem. Soc.* **1973,** 95, 6582-6589.

54. Felton, G. A. N.; Vannucci, A. K.; Chen, J.; Lockett, L. T.; Okumura, N.; Petro, B. J.; Zakai, U. I.; Evans, D. H.; Glass, R. S.; Lichtenberger, D. L., *J. Am. Chem. Soc.* **2007,** 129, 12521-12530.

55. Mejia-Rodriguez, R.; Chong, D. S.; Reibenspies, J. H.; Soriaga, M. P.; Darensbourg, M. Y., *J. Am. Chem. Soc.* **2004,** 126, 12004-12014.

56. Felton, G. A. N.; Glass, R. S.; Lichtenberger, D. L.; Evans, D. H., *Inorg. Chem.* **2006,** 45, 9181-9184.

57. Fourmond, V.; Jacques, P.-A.; Fontecave, M.; Artero, V., *Inorg. Chem.* **2010,** 49, 10338-10347.

58. Gloaguen, F.; Lawrence, J. D.; Rauchfuss, T. B., *J. Am. Chem. Soc.* **2001,** 123, 9476-9477.

59. Chong, D. S.; Georgakaki, I. P.; Mejia-Rodriguez, R.; Samabria-Chinchilla, J.; Soriaga, M. P.; Darensbourg, M. Y., *Dalton Transactions* **2003**, 4158-4163.

60. Ezzaher, S.; Capon, J.-F.; Dumontet, N.; Gloaguen, F.; Petillon, F. Y.; Schollhammer, P.; Talarmin, J., *J. Electroanal. Chem.* **2009,** 626, 161-170.

Chapter 5

Synthesis and electrocatalytic activity of [FeFe]-H_2ase model complexes with non-innocent chelating nitrogen-donor ligands

Souvik Roy,[a,b] John Collins,[a] Thomas L. Groy, [a] Anne K. Jones* [a,b]

[a]Department of Chemistry and Biochemistry; [b]Center for Bio-Inspired Solar Fuel Production; Arizona State University, Tempe, AZ 85287

Abstract

To evaluate the impact of redox non-innocent ligands on a well-known class of [FeFe]-hydrogenase models, three new asymmetrically disubstituted diiron complexes of the general formula (μ-SRS){Fe(CO)$_3$}{Fe(CO)(N-N)} [SRS = propane-1,3-dithiolate (pdt) or benzene-1,2-dithiolate (bdt), and N-N = 2,2'-bipyridine (bpy) or 2,2'-bipyrimidine (bpym)] have been synthesized from their parent hexacarbonyls by ligand substitution, and characterized. The new complexes (μ-pdt)Fe$_2$(CO)$_4$(κ^2-bpym) (**2**), (μ-bdt)Fe$_2$(CO)$_4$(κ^2-bpy) (**3**), and (μ-bdt)Fe$_2$(CO)$_4$(κ^2-bpym) (**4**) were fully characterized by spectroscopic and electrochemical techniques, and the results are compared to those of a similar complex (μ-pdt)Fe$_2$(CO)$_4$(κ^2-bpy) (**1**). The structure of (**2**) was determined by single crystal X-ray diffraction showing that the ligand lies in the basal plane. IR spectra and electrochemical analyses indicate that electron density at the iron centers decreases in the order **1**>**2**>**3**>**4**. Furthermore, **2** undergoes a ligand-centered reduction at the same potential as the hexacarbonyl precursor. However, unlike the bpy derivatives **1** and **3**, the bpym complexes **2** and **4** do not catalyze electrochemical proton reduction from acetic acid.

Introduction

[FeFe]-hydrogenases are exceptionally efficient natural biocatalysts for producing hydrogen. They catalyze proton reduction with high turnover frequencies, 6000-9000 s^{-1}, under ambient conditions.[1-4] Recently, these metalloenzymes have attracted widespread attention due to their tremendous potential in energy-related applications involving utilization of molecular hydrogen as a carbon-neutral fuel. Hydrogen is a promising future energy carrier and implementation of a hydrogen based economy requires efficient catalysts for interconversion of protons and hydrogen. In current applications, this reaction is catalyzed by expensive noble metals such as platinum and palladium.[5, 6] Since hydrogenases primarily rely on first row transition metals, iron and/or nickel, to catalyze this reaction, their active sites serve as ideal templates for developing inexpensive catalysts.[7, 8] As shown in Scheme 5-1, the X-ray crystal structure shows that the active site of [FeFe]-hydrogenases, commonly referred to as the H-cluster, is a unique six-iron cluster that is comprised of two subunits: a redox-active [4Fe4S] cubane that serves as a conduit for shuttling electrons, and a butterfly [Fe_2S_2] subsite where the catalytic reaction takes place.[9, 10] The two iron centers in the [Fe_2S_2] unit are linked by a bridging dithiolate (-SCH_2NHCH_2S-) and are ligated to the diatomic ligands carbon monoxide (CO) and cyanide (CN^-) that are otherwise biologically uncommon. One of the iron atoms of the [Fe_2S_2] cluster, defined as the proximal iron (Fe_p), is connected to the cuboidal [4Fe4S] cluster *via* a cysteinyl thiolate, and the other iron center (distal iron, Fe_d) contains an open coordination site for substrate binding. Other interesting features of the enzyme include a proton-channel, gas-channel, and several [4Fe4S] cubanes for electron transport to and from the active site.

The $[Fe_2S_2]$ cluster bears remarkable resemblance to a well known organometallic compound $(\mu\text{-}S_2C_3H_6)Fe_2(CO)_6$ that has been exploited by synthetic chemists to build a multitude of biomimetic diiron complexes and provided a better understanding of the structure-function relationship of the enzyme.[11-13] While the hexacarbonyl models have been demonstrated to be poor electrocatalyst for proton reduction, replacing CO ligands with better σ-donor ligands has led to better structural and functional models that are more efficient electrocatalysts. However, in contrast to the natural system that utilizes the $Fe^{II}Fe^{I}$ redox state for proton reduction catalysis, most diiron model complexes rely on the $Fe^{I}Fe^{0}$ redox state, leading to a requirement for high overpotentials for electrocatalytic proton reduction.[14] Furthermore, theoretical studies have indicated that electron density is delocalized throughout all six irons of the H-cluster,[15, 16] but redox-active cofactors are rarely incorporated in diiron models.[17-21]

Non-innocent ligands have attracted considerable interest because changing the oxidation state of the ligand can modulate the electronic properties of the metal center and thus facilitate catalytic redox transformations.[22] For diiron model systems, redox active ligands can serve as a proxy for the [4Fe4S] cluster. In particular, when a reducible organic ligand is appended to the diiron unit, reduction of the complex can occur either on the ligand or the Fe center or the electron(s) can be delocalized over the entire metal-ligand framework. Such interaction between metal and ligand may lower the large overpotential required for proton reduction catalysis. Heterocyclic α-diimine ligands such as 2,2'-bipyridine (bpy) and 2,2'-bipyrimidine (bpym) have found extensive application in inorganic and organometallic chemistry owing to their chelating ability, π-accepting character and redox-activity.[23-26] Both ligands can be readily reduced by two one-electron

processes to first produce the radical anion and then the dianion.[27] Since replacement of CH by N lowers the energy of the molecular orbitals of the ligands, 2,2'-bipyrimidine is easier to reduce than 2,2'-bipyridine. The ligand 2,2'-bipyrimidine also acts as a better π-acceptor, stabilizing reduced metal center(s) by delocalizing the extra electron density into the empty π* orbitals. Moreover, recent computational studies have suggested that electronic asymmetry provided by chelating ligands in diiron complexes is important for attaining robust, functional models which makes the aforementioned ligands good candidates for building catalysts.[28]

Here, we report synthesis and characterization of three new diiron complexes each with a non-innocent α-diimine ligand: (μ-pdt)$Fe_2(CO)_4(\kappa^2$-bpym) (**2**), (μ-bdt)$Fe_2(CO)_4(\kappa^2$-bpy) (**3**), and (μ-bdt)$Fe_2(CO)_4(\kappa^2$-bpym) (**4**) (pdt = propane-1,3-dithiolate, bdt = benzene-1,2-dithiolate). We have investigated the effect of the nitrogen ligands and bridging dithiolates on the electronic and catalytic properties of the complexes by spectroscopic techniques and cyclic voltammetry, and the results are compared to the related diiron analogue (μ-pdt)$Fe_2(CO)_4(\kappa^2$-bpy) (**1**).[21]

Results and Discussion

Synthesis. Two bidentate nitrogen donor ligands, 2,2'-bipyridine (bpy) and 2,2'-bipyrimidine (bpym), were chosen because both of them are weak π-acceptors, and can participate in redox reactions. All complexes were synthesized from the corresponding diiron-hexacarbonyl-dithiolate complexes (Scheme 5-2). The synthesis of **3** was similar to that already reported for **1**.[21] Refluxing the hexacarbonyl precursor, (μ-bdt)$Fe_2(CO)_6$, in toluene resulted in the formation of the 2,2'-bipyridyl substituted derivative **3**, which was isolated in moderate yield (38%). However, this synthetic route failed to produce the

2,2'-bipyrimidine substituted derivatives leading instead to decomposition of the starting diiron complex. Reaction of 2,2'-bipyrimidine and the diiron hexacarbonyl precursor (μ-pdt)$Fe_2(CO)_6$ or (μ-bdt)$Fe_2(CO)_6$ in acetonitrile in the presence of two equivalents of Me_3NO resulted, over 2 hours, in the formation of a dark green solution. Following purification complexes **2** and **4** were isolated in moderate yields (40–45%) after purification. Although (μ-bdt)$Fe_2(CO)_6$ has been reported to undergo reactions with strong donor ligands to produce mononuclear Fe^{II} complexes of the form (bdt)Fe(CO)(L-L) or (bdt)$Fe(CO)_2L_2$ (L-L = chelating ligand, L = monodentate ligand), no such complex was isolated in the reaction with bpy and bpym.[29-31] The molecular structure of **2** was determined by X-ray diffraction analysis of a single crystal obtained from hexane/dichloromethane mixture. The crystal structure of **2** is shown in Figure 5-1, and important metric parameters are summarized in Table 5-1. The structure shows that the bpym ligand coordinates one iron center in a basal-basal mode, consistent with the small bite angle of the ligand (N-Fe-N = 80.26°).[32] The bond angles indicate that the both iron centers have distorted square pyramidal first coordination sphere, and each of the two irons centers is in an eclipsed confirmation. As observed also for the bpy system of complex **1**, the inter-ring C-C bond (C11-C12) in the bpym ligand of **2** is slightly shorter (1.474 Å) than the same bond in free ligand (1.511 Å).[21, 33] The LUMO of the ligand is a π* orbital with an in-phase overlap between the *p*-orbitals of the two carbon atoms linking the two rings.[34] Therefore, increased electron density on the LUMO due to π-backdonation from the metal to the ligand results in greater double bond character of the C-C bond.[21, 33, 35] While the Fe-Fe bond of **2** (2.5558 Å) is longer than the parent hexacarbonyl precursor (2.5103 Å),[36] it is slightly shorter than that reported for similar

diiron complexes with donor bidentate ligands such as bis-phosphine or di-carbene.[37-40] This suggests that bpym, owing to its low lying π* orbitals and the concomitant π-acceptor ability, lowers the electron density on the diiron center.

Spectroscopic Characterization. Complexes **1-4** were characterized spectroscopically by FTIR, UV-vis and NMR, and the results are summarized in Tables 5-2 and 5-3. As shown in Figure 5-2, the IR spectra of all of the complexes in dichloromethane consist of three characteristic bands in the C-O stretching region, similar to analogous diiron complexes with chelating donor ligands.[40-42] The average of the IR stretching frequencies of the CO ligands is usually considered a reliable indicator of the electron densities about the metal centers. Thus, the shifts of the C-O bands on changing ligands provide an estimate of the donating ability of the ligands. In general, comparison of the IR spectra of **1–4** reveal that replacing bpy with bpym results in significant strengthening of the C-O bonds as demonstrated by an shift of the average of the C-O stretching bands by 9 cm^{-1} towards higher energy for complexes **2** and **4**. One hypothesis is that the stronger π-acceptor strength of bpym relative to bpy withdraws more electron density from the iron core at the expense of backbonding into carbonyls. In essence backbonding into bpym substitutes for backbonding into the CO ligands. This leads to stronger C-O bonds in **2** and **4** relative to **1** and **3**. The average value of the CO bands for **2** is similar to that of the bis-phosphine analogue, (μ-pdt)$Fe_2(CO)_4(\kappa^2$-dppe) (dppe = $Ph_2PCH_2CH_2PPh_2$),[43] indicating that electron density on the diiron center of the bpym complex is similar to that of the dppe analogue. On the other hand, changing the bridging ligand from pdt to bdt led to a blue-shift of the C-O stretching bands by an average of 13 cm^{-1} as a result of the lower electron densities on the Fe centers caused by electron delocalization over the aromatic ring of

bdt. According to the IR stretching frequencies of the complexes, the electron density of the diiron core increases in the order **4** < **3** < **2** < **1**.

Three types of electronic transitions must be considered in describing the UV-vis spectra of low-spin iron complexes containing α-diimine ligands: ligand centered π–π* bands in the high energy UV region, metal to ligand charge transfer (MLCT) bands, and weak metal-centered d-d transitions.[27, 44] As shown in Figure 5-3, the UV-vis spectra of the complexes with the bpy ligand (**1** and **3**) consist of an intense band at *ca.* 295 nm that can be attributed to a bpy π–π* transition. In the case of the complexes with the bpym ligand (**2** and **4**), this ligand centered transition requires higher energy and consequently appears at shorter wavelengths region (<250 nm). The spectra of all four complexes feature an intense band in the region 340–350 nm ($\varepsilon > 10^3$ $M^{-1}cm^{-1}$) that is likely associated with the Fe-S core (Table 5-2). Since the energies of MLCT transition bands are dependent on the energy of the LUMO of the diimine ligand, they are likely to occur at a lower energy for **2** and **4** than **1** and **3**, respectively.[27] The charge transfer bands at 391 and 603 nm in the spectrum of **1** are red-shifted to 449 and 634 nm, respectively, in the spectrum of **2**. Similarly, red-shifts of the charge transfer bands are also observed when comparing the spectra of **3** and **4** in the regions 390–430 nm and 550–650 nm (Figure 5-3 and Table 5-2). The metal-centered d-d transitions with relatively low molar absorptivity are likely masked by the intense charge transfer bands.

The ^{1}H NMR spectra of **1** and **2** show the expected signals for the propane-1,3-dithiolate bridge in the region 1.2–2.2 ppm, slightly upfield compared to the parent hexacarbonyl complex. In contrast, the ^{1}H NMR signals for the aromatic protons of benzene-1,2-dithiolate in complexes **3** and **4** appear at 7.08-7.09 and 6.59 ppm, chemical

shifts nearly identical to the corresponding hexacarbonyl starting material.[45] More interestingly, the chemical shifts of the resonances of the α-diimine ligands (bpy and bpym) in **1–4** relative to the non-coordinated free ligand provide a qualitative description of the nature of the bonding between the Fe and the ligand. As listed in Table 5-3, the NMR spectra of the bpy derivatives, **1** and **3**, consist of four resonances in the aromatic region, consistent with symmetrical coordination of bpy. It is noticeable that, relative to the free ligand, the resonances attributable to the protons at positions 3, 4 and 5 of the bpy, shifted upfield in both complexes. However, the resonance of the proton on the carbon adjacent to the coordinated nitrogen, H(6), is shifted downfield for **1** and upfield for **3**. Similarly, while upfield shifts are observed for the resonances of H(4) and H(5) of the bpym ligand in **2** and **4**, the resonance of the proton [H(6)] next to the coordinated nitrogen undergoes a small downfield shift in **2** and upfield shift in **4**. The underlying reason for this difference is not yet clear. Overall, the NMR data suggest that π-back donation from the electron rich Fe^{I} center to the empty π* of the α-diimine ligand leads to an increase in π-electron density over the ligand.

Electrochemistry. To evaluate the influence of the two α-diimine ligands and the two S-S linkers on the redox properties of the diiron clusters, cyclic voltammograms of the complexes were measured in acetonitrile. Voltammograms of **1–4** are shown in Figure 5-4, and the redox potentials tabulated in Table 5-4. We have previously reported that **1** undergoes a two-electron reduction at -2.06 V with one metal-centered reduction and the other likely a ligand-centered reduction.[21] As shown in Figure 5-4, cyclic voltammograms of **2** show two irreversible reductive waves at E_p = -1.76 and -2.25 V as well as a small oxidative wave at E_p = -1.55 V during the return scan. Interestingly, when

the reductive scan is stopped prior to the second reduction, the first reductive event (E_p = -1.76 V) becomes reversible with $E_{1/2}$ = -1.72 V (i_p^c/i_p^a = 1.1), and the oxidative wave at -1.55 V disappears. Comparison of the reduction peak currents suggests that if we assume that the first reduction is a one-electron process, then the second reduction involves transfer of two-electrons (i_p^{red1} = 27 μA and i_p^{red2} = 54 μA; $i_p^{red2}/\ i_p^{red1}$ = 2). Ordinarily, displacement of two CO ligands from the hexacarbonyl complex (μ-pdt)$Fe_2(CO)_6$ with better donor ligands and/or weak π-accepting ligands lead to increased electron density on the Fe centers making the complex more difficult to reduce. However, this reasoning clearly does not hold for **2** which is reduced at potentials almost identical to those of the all-CO parent compound (Table 5-4). This despite the significant shift of average ν(CO) upon replacement of two CO ligands by bpym (76 cm^{-1}) indicating increased electron density in the iron core. According to previous studies, the free ligand, 2,2'-bipyrimidine, undergoes a primary reversible one-electron reduction (bpym/$bpym^{1-}$) at -2.12 V and a subsequent irreversible one-electron reduction ($bpym^{1-}$/$bpym^{2-}$) at -2.83 V.[27] Assuming that the diiron center withdraws electron density from the ligand making its reduction easier, these results suggest that the first reduction of **2** is likely centered on the bpym ligand. The second reduction at -2.24 V, two-electron process, likely corresponds to one metal-centered reduction forming a Fe^IFe^0 species and one ligand centered reduction corresponding to the $bpym^{1-}$/$bpym^{2-}$ couple. It is worth noting that, relative to the hexacarbonyl analogue, the negative shift of the reduction potential of the metal based reduction is 500 mV for **2**, largest among all of the diiron complexes discussed here. However, the physical mechanism responsible for the large shift of the metal based reduction is still unclear. The presence of the small oxidation wave at -1.55

V on the return scan suggests an EC process in which the three electron reduced species, $Fe^{0}Fe^{I}(bpym^{2-})$, undergoes a fast chemical reaction generating a product with a new reduction potential, detected as the oxidative peak at -1.55 V.

Cyclic voltammograms of complex **3** in acetonitrile features an irreversible reduction at E_p = -1.71 V indicating that, relative to the parent hexacarbonyl complex, $(\mu\text{-bdt})Fe_2(CO)_6$, coordination of the bpy ligand results in a 440 mV negative shift of the reduction potential. This shift is higher than the 320 mV observed for the pdt complex, **1**. On the other hand, substitution of $(\mu\text{-bdt})Fe_2(CO)_6$ with bpym results in only of 310 mV shift of the first reduction as observed for complex **4**. This is in keeping with the better π-accepting ability of the bpym ligand relative to bpy and also consistent with the FTIR results. Previous electrochemical investigations have shown that the diiron-hexacarbonyl complexes with aromatic dithiolates are reduced to dianions in a reversible two-electron process.[31, 46] Therefore, based on the previous reports on electrochemical properties of the parent hexacarbonyl analogue, $(\mu\text{-bdt})Fe_2(CO)_6$, it is reasonable to suggest that the reductions of **3** and **4** are two-electron processes forming the dianions $[\mathbf{3}]^{2-}$ and $[\mathbf{4}]^{2-}$, respectively.[46, 47] It is interesting to note that in voltammograms from **3** and **4**, unlike those from the pdt analogues, distinct reduction waves for ligand-centered reductions were not observed. However, the electrochemical reversibility observed for the two electron reduction of the hexacarbonyl analogue is completely lost upon introduction of the α-diimine ligands suggesting lower stability of the reduced complexes in the presence of the donor ligands. The poor electron donating ability of the bdt bridge results in significantly less negative reduction potentials for **3** and **4** than the pdt analogues, and thus makes them potentially attractive candidates for proton reduction catalysts.

Complexes **1–4** all undergo irreversible oxidation in the range -0.14 to -0.27 V. Based on previous electrochemical studies on similar diiron complexes, this oxidation peak can be assigned to $Fe^{II}Fe^{I}/Fe^{I}Fe^{I}$ couple of the complexes.[14] Furthermore, ratios of the oxidative peak currents [$i_p^{ox}(Fe^{II}Fe^{I}/Fe^{I}Fe^{I})$] to the peak currents for the reduction of the complexes ($i_p^{red}$for metal-centered and/or ligand-centered reductions in the range -1.5 to -2.3 V) were calculated for **1–4** which clearly indicate that the observed oxidations are one-electron processes (Table 5-4). The complexes with the bpym ligand, **2** and **4**, are more difficult to oxidize by 70–100 mV than the corresponding bpy complexes, **1** and **3**, respectively. This is consistent with the relative donating abilities of the ligands.

Electrochemical proton reduction. The abilities of the complexes **1–4** to electrocatalyze hydrogen production from acetic acid (0–40 mM) in acetonitrile was investigated by cyclic voltammetry. Although IR and NMR studies show that none of the complexes undergo reaction with acetic acid at low acid concentrations (0–10 mM) in the resting redox state, we expected that reduction of the complexes would make them sufficiently basic to bind protons and catalyze the reduction. Since the reduction potential for each complex is more negative than the standard reduction potential of acetic acid in acetonitrile (-1.36 V), such electrocatalysis is thermodynamically possible.[48] Furthermore, we have reported that **1** can act as an homogeneous electrocatalyst for proton reduction from acetic acid with considerably less overpotential than similar diiron analogues.[21] As shown in Figure 5-5A, sequential addition of acetic acid (from 5 mM to 20 mM) to an acetonitrile solution of complex **2** did not increase the current of the two primary reductive waves at -1.72 and -2.24 V, indicating catalysis does not take place. In particular, upon addition of acetic acid, the first reduction peak shifted by 90 mV to more

positive potential without affecting the peak current, and the reduction became completely irreversible even when the scan was stopped prior to the second reduction. These results hint towards an EC process occurring at the first reduction event in the presence of acid. First a ligand centered reduction produces $\mathbf{2}^-$; then a protonation of the bpym ligand of $\mathbf{2}^-$ occurs to give **2H** which is apparently not active towards any proton reduction catalysis. This result implies a lack of efficient electronic communication between the ligand and the iron center because the ligand-centered reduction does not increase the basicity of the diiron core sufficiently to facilitate metal based protonation. Thus, no catalysis was observed. While the **2H** intermediate appears to undergo further two-electron reduction at more negative potentials (beyond -2.2 V), the three electron reduced species is probably unstable towards excess acid. Observed decomposition of **2** in the presence of excess acetic acid (above 20 mM) using IR supports the hypothesis. However, even in the concentration range 5 mM–20 mM, in which the complex is moderately stable, no significant electrocatalytic activity is observed.

The bdt-bridged analogues, **3** and **4**, are reduced at milder potentials than the analogous pdt complexes. As shown in Figure 5-6B, in the case of complex **3**, addition of acetic acid did not increase the peak current of the primary reductive wave at -1.71 V. Instead a new catalytic wave appeared at E_p = -2.05 V, the potential of which was shifted to more negative values upon incremental increase of acetic acid concentration. It is worth noting that the onset of catalytic peak current for **3** is only at a slightly more positive potential than that of **1** although the primary reduction of **3** occurs at considerably more positive potential (350 mV). For a more detailed comparison, the catalytic peak currents for both complexes (**1** and **3**) were plotted against concentrations

of AcOH (Figure 5-7A). This analysis reveals an exponential dependence of catalytic current on acid concentration, suggesting a first order reaction with respect to the acid. Assuming first order dependence on catalyst concentration, bimolecular catalytic rate constants of 0.8×10^2 and 3×10^2 $M^{-1}s^{-1}$ can be estimated for **1** and **3**, respectively, from the slope of the linear plot of catalytic peak current (i_{cat}) *vs*. $[AcOH]^{1/2}$ (Figure 5-7B).[49] The overpotential for the process, which is defined as the difference between the standard reduction potential of the acid and the half-wave potential for the catalytic wave, is *ca*. 620 mV for **3** which is similar to that observed for **1** (680 mV).[48] Importantly direct reduction of acetic acid on the glassy carbon electrode is negligible in this potential range (-1.9 to -2.2 V). On the other hand, as shown in Figure 5-5B, the electrochemical response of complex **4** towards acetic acid is similar to that of **2**. While the addition of acetic acid did not affect the primary reduction wave of **4** at -1.58 V, a new reduction wave appears at *ca*. -2 V which grows only slightly with increasing acid concentration. In fact, a plateau in catalytic current was observed quickly at the relatively low acid concentration of 4 mM. Although the complexes with the bpym ligand have more positive reduction potentials than the bpy analogues and might be expected to be more potent catalysts, they exhibit essentially no electrocatalytic activity towards proton reduction from acetic acids.

Conclusions

In summary, we have synthesized four different $[(\mu\text{-SRS})\{Fe(CO)_3\}\{Fe(CO)(N–N)\}]$ (N–N = bidentate α-diimine ligand) complexes with two dithiolate-bridges and two chelating N-donor ligands. To our knowledge, complexes **3** and **4** are the first examples of benzene-1,2-dithiolate bridged asymmetric diiron complexes with chelating ligands.

The primary purpose of our study was to evaluate the influence of the redox non-innocent, chelating α-diimine ligands 2,2'-bipyridine and 2,2'-bipyrimidine on the electrochemical properties of the diiron models of [FeFe]-hydrogenases. Since bpym has lower energy empty π* orbitals compared to bpy, it is easier to reduce and it acts as a better π-acceptor ligand. This distinction in electronic properties of the two ligands is reflected in the IR and electrochemical results which clearly indicate that replacing bpy with bpym led to higher ν(CO) frequencies and more positive reduction potentials for the complexes. In particular, complex **2** undergoes one-electron, ligand-centered reduction at the same potential as the hexacarbonyl precursor despite the substitution of two CO ligands with the better electron donating bpym ligand. However, this reduction of the ligand in **2** does not increase the electron density of the diiron site sufficiently for proton reduction catalysis. Complex **4** was also inactive towards electrocatalytic proton reduction. This suggests that although coordination of bpym increases the electron density on the diiron center to the same extent as of bis-phosphine ligands, the electronic properties of bpym are unsuitable for catalysis.

The second goal of this study was to investigate the impact of replacement of the aliphatic pdt ligand with benzene-1,2-dithiolate on diiron model complexes with chelating donor ligands. Since bdt is a significantly weaker donor than the alkyldithiolates, it can potentially compensate for the negative shift of reduction potential caused by strong donor ligands on the iron center while maintaining the basicity of the diiron core. Although the bdt bridged complex **3** is reduced at more positive potentials than the pdt complex, the potential at which proton reduction catalysis occurs and the rate of catalysis are similar for the two complexes. In short, the results demonstrate that the

electronic properties of the diiron models can be tuned by using different dithiolate-bridges and α-diimine ligands, but the impact of those variations on improving catalytic activity of the complexes is minimal.

Experimental Section

All reactions were performed under an inert atmosphere (nitrogen or argon) using a double manifold Schlenk vacuum line. The complexes (μ-pdt)$Fe_2(CO)_6$[36] and (μ-bdt)$Fe_2(CO)_6$[45] were prepared according to literature methods. All anhydrous solvents and chemicals were of the highest available grades from Aldrich and were used as received. NMR spectra were recorded at room temperature on a Varian Liquid-State NMR spectrometer (400 or 500 MHz for ^1H). NMR chemical shifts are quoted in ppm; spectra are referenced to tetramethylsilane. FTIR spectra were recorded on a Bruker Vertex 70 spectrophotometer using a stainless steel sealed liquid spectrophotometer cell with CaF_2 windows. UV-vis measurements were performed on a Hewlett-Packard 8453 spectrophotometer using quartz cuvettes with a 1 cm pathlength.

Synthesis of (μ-pdt)$Fe_2(CO)_4(\kappa^2$-bpym), (2). The metalloprecursor (μ-pdt)$Fe_2(CO)_6$ (451 mg, 1.16 mmol) and trimethylamine-N-oxide (260 mg, 2.34 mmol) were dissolved in acetonitrile (10 mL) and stirred in the dark at room temperature for 15 min. Then the solution was anaerobically transferred to a suspension of 2,2'-bipyrimidine (370 mg, 2.33 mmol) in acetonitrile (5 mL) and heated to reflux in the dark for two hours. The reaction mixture was concentrated under reduced pressure, and the dark residue was purified *via* silica gel chromatography using 1:1 hexane/ethyl acetate with 1% triethylamine as eluent to give the desired product as a dark green solid. Yield: 230 mg, 41%. ^1H NMR (400 MHz, $CDCl_3$): δ = 9.04 (dd, 2H), 8.89 (dd, 2H), 7.30 (t, 2H), 2.20–2.17 (dt, 2H), 2.08 (m,

1H), 1.65 (td, 2H), 1.27 (m, 1H). IR (CH_2Cl_2, cm^{-1}): 2014, 1946, 1907. R_f = 0.32 (1:4 hexane/ethyl acetate, 1% NEt_3).

Synthesis of (μ-bdt)$Fe_2(CO)_4(\kappa^2$-bpy), (3). A solution of (μ-bdt)$Fe_2(CO)_6$ (174 mg 0.41 mmol) and 2,2'-bipyridine (130 mg, 0.83 mmol) in toluene (12 mL) was refluxed under argon until evolution of carbon monoxide ceased (2 h). The reaction mixture was concentrated under reduced pressure, and the dark residue was purified by column chromatography on silica gel. A dark bluish green solution eluted with 1:1 hexane/dichloromethane. After collection of this fraction and removal of the solvent, the desired complex was collected as a dark reddish brown solid. Yield: 80 mg, 38%. ^{1}H NMR (400 MHz, CD_2Cl_2): δ = 8.36 (s, 2H), 8.08 (s, 2H), 7.79 (s, 2H), 7.22 (s, 2H), 7.09 (s, 2H), 6.59 (s, 2H). IR (CH_2Cl_2, cm^{-1}): 2016, 1949, 1916.

Synthesis of (μ-bdt)$Fe_2(CO)_4(\kappa^2$-bpym), (4). A solution of (μ-bdt)$Fe_2(CO)_6$ (160 mg, 0.38 mmol) and trimethylamine-N-oxide (85 mg, 0.76 mmol) in acetonitrile (10 mL) was stirred in the dark under nitrogen for 15 min. Then 2,2'-bipyrimidine (90 mg, 0.57 mmol) was added anaerobically to the reaction mixture and stirred for 2 h. The dark green reaction mixture was concentrated under reduced pressure and thoroughly washed with hexane until the washings were colorless. The residues was redissolved in dichloromethane (25 mL) and filtered through celite followed by silica. Finally, upon evaporation of the solvent, the desired complex was obtained as a green powder. Yield: 90 mg, 45%. ^{1}H NMR (400 MHz, CD_2Cl_2): δ = 8.89 (br, 2H), 8.62 (s, 2H), 7.29 (br, 2H), 7.08 (s, 2H), 6.59 (s, 2H). IR (CH_2Cl_2, cm^{-1}): 2022, 1958–1927 (broad).

X-ray crystallography. Cell parameter measurements and single-crystal diffraction data collection were performed at low temperature (123 K) with a Bruker Smart APEX

diffractometer. Graphite monochromated Mo Kα radiation (λ = 0.71073 Å) in the ω–φ scanning mode was used for the measurements. The structure was solved by direct methods and refined by fullmatrix least-squares on F^2. The following is the list of the programs used: data collection, Bruker Instrument Service v2010.9.0.0; cell refinement and data reduction, SAINT V7.68A; structure solution and refinement, SHELXS-97; molecular graphics, XShell v6.3.1; preparation of material for publication, Bruker APEX2 v2010.9-1.30. Details of crystal data and parameters for data collection and refinement are listed in Table 5-5.

Electrochemistry. Electrochemical experiments were performed using either a CHI 1200A or a PG-STAT 128N Autolab electrochemical analyzer. A conventional three-electrode cell was used for recording cyclic voltammograms. The working electrode was a 3 mm diameter glassy carbon disk polished with 1 mm and 0.3 mm deagglomerated alpha alumina, successively, and sonicated for 15 min in ultrapure water prior to use. The supporting electrolyte was $[NBu_4][PF_6]$ (0.1 M in acetonitrile). The reference was a Ag/Ag^+ electrode prepared by immersing a silver wire anodized with AgCl in an acetonitrile solution of 0.1 M $[NBu_4][PF_6]$. A platinum wire was used as counter electrode. The cyclic voltammograms were recorded either inside a glovebox or on the benchtop under an argon atmosphere. All potentials are reported relative to the ferrocene couple (Fc^+/Fc) as reference. Concentrations of the complexes were determined spectrophotometrically based on the following extinction coefficients: ε(603 nm) = 3500 M^{-1} cm^{-1} (complex **1**), ε(634 nm) = 1950 $M^{-1}cm^{-1}$ (complex **2**), ε(520 nm) = 2400 $M^{-1}cm^{-1}$ (complex **3**), and ε(636 nm) = 1950 $M^{-1}cm^{-1}$ (complex **4**).

Table 5-1. Selected bond lengths (Å) and bond angles (°) for **2**

Bond lengths			
Fe1-Fe2	2.5558	Fe2-S2	2.2094
Fe1-C2	1.8005	Fe2-C1	1.7611
Fe1-C3	1.7808	Fe2-N1	1.9932
Fe1-C4	1.7875	Fe2-N3	1.9924
Fe1-S1	2.2823	C11-C12	1.4737
Fe1-S2	2.2780	N1-C11	1.352
Fe2-S1	2.2079	N3-C12	1.357
Bond angles			
C2-Fe1-C3	93.0805	Fe1-S2-Fe2	69.4178
Fe1-S1-Fe2	69.3654	N1-Fe2-N3	80.2595

Table 5-2. UV-vis absorptions and CO vibrational stretching frequencies for complexes **1-4** and relevant related diiron complexes

Complex	**ν(CO), cm^{-1}**	**Average ν(CO), cm^{-1}**	**λ, nm (ε, $M^{-1}cm^{-1}$)**
(μ-pdt)$Fe_2(CO)_6$	2072, 2033, 1993	2032	325, 452 (shoulder)
(μ-bdt)$Fe_2(CO)_6$ [45]	2080, 2044, 2004	2043	-
1[21]	2007, 1937, 1896	1947	298, 342, 391 (shoulder, 5200), 519 (2700), 603 (3500), 685 (shoulder, 2500)
2	2014, 1946, 1907	1956	339 (5500), 449 (3700), 634 (1950)
3	2016, 1949, 1916	1960	292, 350 (2800), 390 (shoulder), 520 (2400), 625 (broad shoulder, 1900)
4	2022, 1958–1927 (broad)	1969	347 (4100), 429 (3100), 636 (1950)
(μ-pdt)$Fe_2(CO)_4$(dppe)[43]	2019, 1949, 1904	1957	-
(μ-pdt)$Fe_2(CO)_4(I_{Me}\text{-}CH_2\text{-}I_{Me})$[39]	1996, 1920, 1872	1929	-

Table 5-3. ^{1}H NMR chemical shifts of 2,2'-bipyridine and 2,2'-bipyrimidine

Position	2,2'-bpy	1	3	2,2'-bpym	2	4
3	8.43	8.03	8.08	-	-	-
4	7.82	7.74	7.79	8.98	8.89	8.62
5	7.31	7.23	7.22	7.43	7.30	7.29
6	8.65	8.73	8.36	8.98	9.04	8.89

Table 5-4. Electrochemical data for the ligands, diiron hexacarbonyl precursors, and complexes **1–4** in acetonitrile

Compound	E_{ox}, V [a]	E_{red}, V [a]	(i_p^{red}/i_p^{ox}) [b]	Note
2,2'-bpy	-	-2.63 (r), -3.13 (i)	NA[c]	Ref. [50, 51]
2,2'-bpym	-	-2.12 (r), -2.83 (i)	NA[c]	Ref. [27]
(μ-pdt)$Fe_2(CO)_6$	+0.74 (i)	-1.74 (r), -2.35 (i)	ND[d]	Ref. [52]
(μ-bdt)$Fe_2(CO)_6$	-	-1.27 (r)	NA[d]	Ref. [47]
1	-0.21(i)	-2.06 (i)	2.1	Ref. [21]
2	-0.14 (i)	-1.72 (r), -2.24 (i)	1.0, 2.1	This work
3	-0.27 (i)	-1.71 (i)	1.8	This work
4	-0.17 (i), 0.73 (p)	-1.58 (i)	1.9	This work

[a] (i), (r) and (p) denote irreversible, reversible and partially reversible redox processes, respectively; [b] ratio of the peak currents for the reduction in the range -1.58 to -2.23 V and the oxidation in the range -0.14 to -0.27 V; [c] NA = not applicable; [d] ND = not determined.

Table 5-5. Crystallographic experimental data for **2**

Parameter	**2**
Empirical formula	$C_{15}H_{12}Fe_2N_4O_4S_2$, $(CH_2Cl_2)_{1/2}$
Formula weight	534.11
Temperature	123 (2)
Wavelength	0.71073
a (Å)	27.052
b (Å)	10.961
c (Å)	13.676
α (°)	90
β (°)	90
γ (°)	90
Volume ($Å^3$)	4054.8

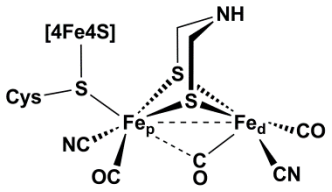

Scheme 5-1. Active site of [FeFe]-hydrogenase (H-cluster)

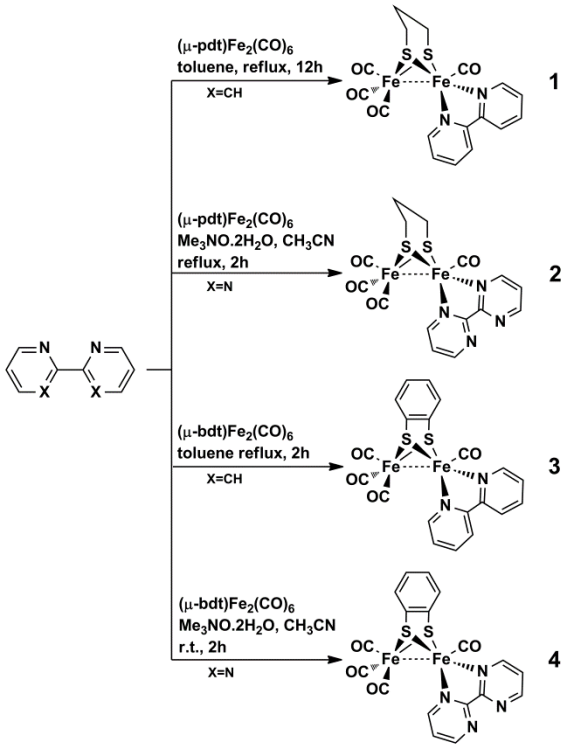

Scheme 5-2. Synthetic routes to complexes **1–4** from hexacarbonyl precursors and bidentate N-donor ligands.

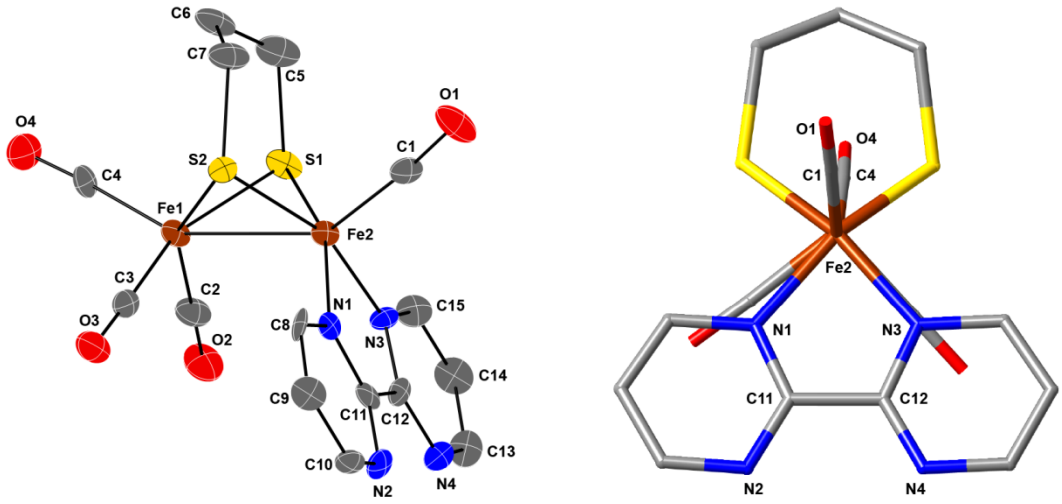

Figure 5-1. X-ray crystal structure of 2. Molecular structure of **2**: (left) thermal ellipsoid representation (50 % probability level); (right) rotated stick view indicating the eclipsed conformation of the two iron centers. Hydrogen atoms have been omitted for clarity.

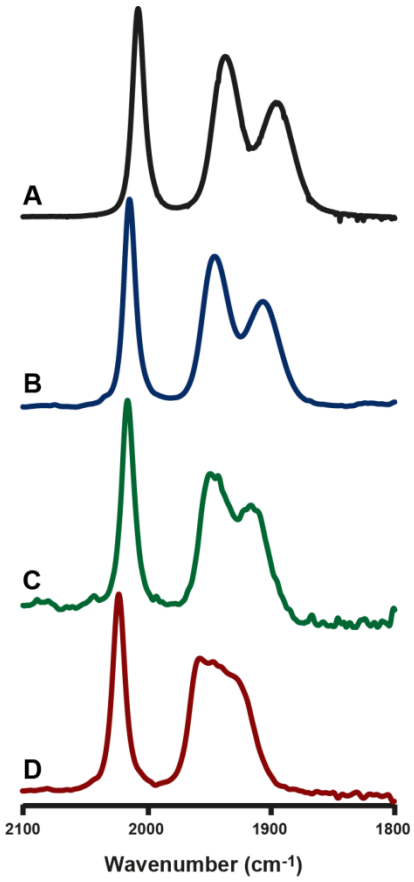

Figure 5-2. Comparative FTIR spectra for the diiron complexes 1–4 with 2,2'-bpy and 2,2'-bpym ligands. IR spectra of (A) **1** (black trace), (B) **2** (blue trace), (C) **3** (green trace), and (D) **4** (red trace) in dichloromethane.

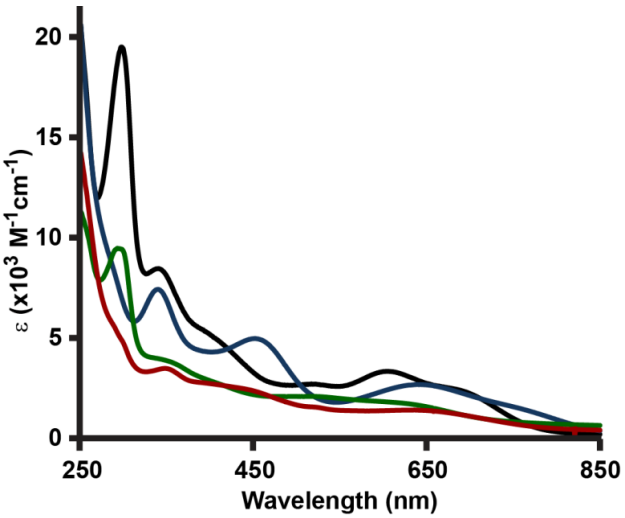

Figure 5-3. Comparative optical spectra for diiron complexes 1–4. UV-vis spectra of **1** (black trace), **2** (blue trace), **3** (green trace), and **4** (red trace) in acetonitrile at room temperature. Spectra were collected from solutions of approximately 0.1 mM complex.

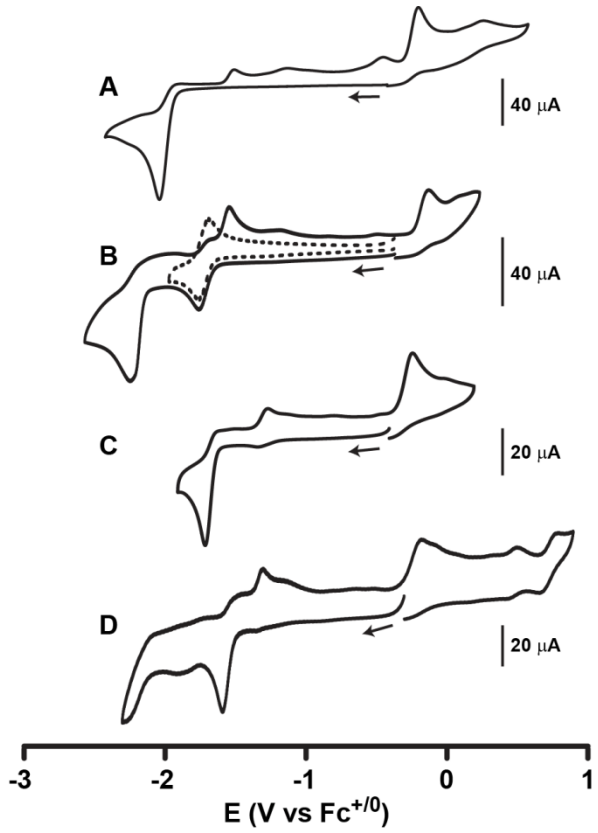

Figure 5-4. Cyclic voltammograms of diiron complexes 1–4. Cyclic voltammograms of (A) **1** (1.2 mM), (B) **2** (1.3 mM), (C) **3** (0.88 mM), and (D) **4** (1.6 mM) measured in 0.1 M $[NBu_4][PF_6]$/ acetonitrile at potential scan rate 0.2 Vs^{-1}. Arrows indicate the starting potential and scan direction.

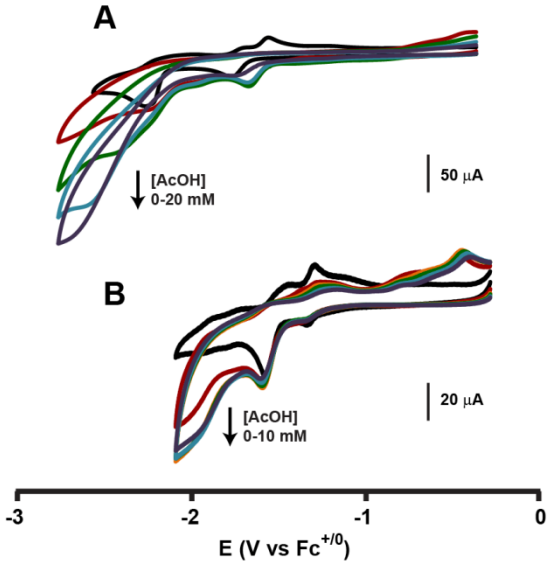

Figure 5-5. Cyclic voltammograms of 2 and 4 in the presence of AcOH. Cyclic voltammograms of **2** (A; 1.3 mM) and **4** (B; 1.6 mM) with various concentrations of acetic acid. Acid concentrations used are 2, 4, 6, 8, 10 mM for complex **4** and 5, 10, 15, 20 mM for complex **2**. Other experimental conditions are as described in Figure 5-4.

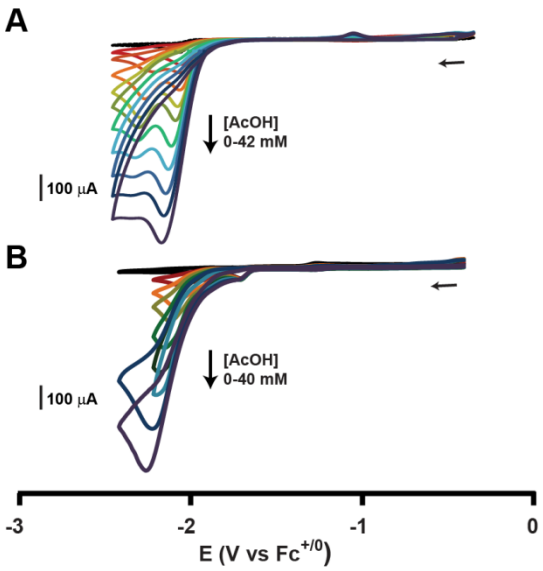

Figure 5-6. Electrocatalytic proton reduction from AcOH by 1 and 3. Cyclic voltammograms of **1** (A; 1.4 mM) and **3** (B; 0.88 mM) with various concentrations of acetic acid. Acid concentrations used are 2, 4, 6, 10, 15, 20, 30, 40 mM for complex **3** and 1.4, 2.8, 5.6, 8.4, 11.2, 16.8, 22.4, 28, 33.6, 42 mM for complex **1**. Other experimental conditions are as described in Figure 5-4.

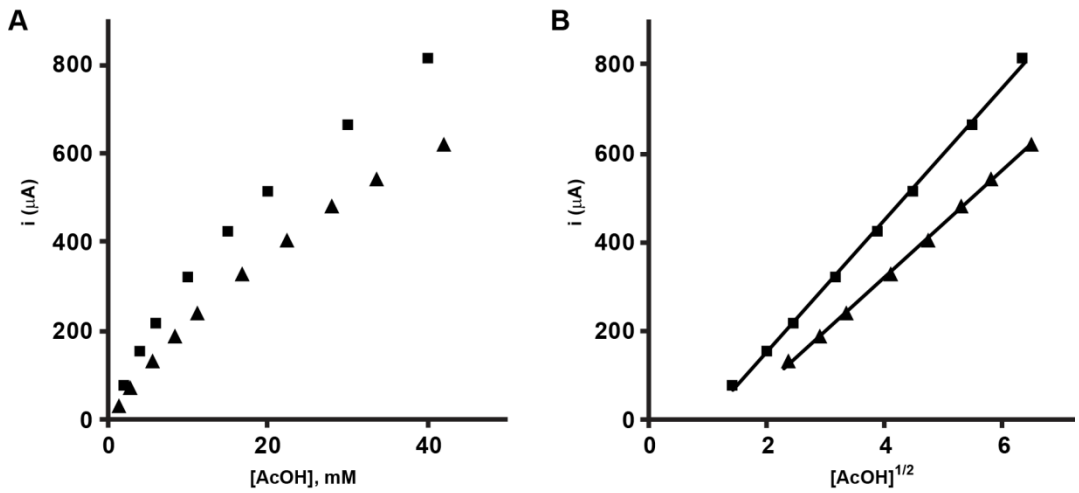

Figure 5-7. Plots of catalytic peak currents as functions of [AcOH] and $[AcOH]^{1/2}$.

(A) Dependence of i_{cat} on concentration of acetic acid added to a solution of **1** (1.4 mM, ▲) and **3** (0.88 mM, ■), and (B) plot of i_{cat} as a function of $[AcOH]^{1/2}$ for **1** (▲, $k = 0.78\times10^2\ M^{-1}s^{-1}$) and **3** (■, $k = 3\times10^2\ M^{-1}s^{-1}$).

References

1. Happe, R. P.; Roseboom, W.; Pierik, A. J.; Albracht, S. P. J.; Bagley, K. A., *Nature* **1997,** 385, 126-126.

2. Cammack, R.; Frey, M.; Robson, R., *Hydrogen as a Fuel: Learning from Nature*. Talor & Francis: London & New York, 2001.

3. Frey, M., *Chembiochem* **2002,** 3, 153-160.

4. Evans, D. J.; Pickett, C. J., *Chem. Soc. Rev.* **2003,** 32, 268-275.

5. Antolini, E., *Energy Environ. Sci.* **2009,** 2, 915-931.

6. Serov, A.; Kwak, C., *Appl. Catal., B* **2009,** 90, 313-320.

7. Adams, M. W. W.; Stiefel, E. I., *Science* **1998,** 282, 1842-1843.

8. Cammack, R., *Nature* **1999,** 397, 214-215.

9. Peters, J. W.; Lanzilotta, W. N.; Lemon, B. J.; Seefeldt, L. C., *Science* **1998,** 282, 1853-1858.

10. Nicolet, Y.; Piras, C.; Legrand, P.; Hatchikian, C. E.; Fontecilla-Camps, J. C., *Structure* **1999,** 7, 13-23.

11. Gloaguen, F.; Rauchfuss, T. B., *Chem. Soc. Rev.* **2009,** 38, 100-108.

12. Heinekey, D. M., *J. Organomet. Chem.* **2009,** 694, 2671-2680.

13. Tard, C.; Pickett, C. J., *Chem. Rev.* **2009,** 109, 2245-2274.

14. Felton, G. A. N.; Mebi, C. A.; Petro, B. J.; Vannucci, A. K.; Evans, D. H.; Glass, R. S.; Lichtenberger, D. L., *J. Organomet. Chem.* **2009,** 694, 2681-2699.

15. Schwab, D. E.; Tard, C.; Brecht, E.; Peters, J. W.; Pickett, C. J.; Szilagyi, R. K., *Chem. Commun.* **2006**, 3696-3698.

16. Bruschi, M.; Greco, C.; Fantucci, P.; De Gioia, L., *Inorg. Chem.* **2008,** 47, 6056-6071.

17. Tard, C.; Liu, X. M.; Ibrahim, S. K.; Bruschi, M.; De Gioia, L.; Davies, S. C.; Yang, X.; Wang, L. S.; Sawers, G.; Pickett, C. J., *Nature* **2005,** 433, 610-613.

18. Si, Y.; Charreteur, K.; Capon, J.-F.; Gloaguen, F.; Petillon, F. Y.; Schollhammer, P.; Talarmin, J., *J. Inorg. Biochem.* **2010,** 104, 1038-1042.

19. Camara, J. M.; Rauchfuss, T. B., *Nat. Chem.* **2012,** 4, 26-30.

20. Liu, Y.-C.; Yen, T.-H.; Tseng, Y.-J.; Hu, C.-H.; Lee, G.-H.; Chiang, M.-H., *Inorg. Chem.* **2012,** 51, 5997-5999.

21. Roy, S.; Groy, T. L.; Jones, A. K., *Dalton Trans.* **2013,** 42, 3843-3853.

22. Allgeier, A. M.; Mirkin, C. A., *Angew. Chem. Int. Ed.* **1998,** 37, 894-908.

23. Balzani, V.; Juris, A.; Venturi, M.; Campagna, S.; Serroni, S., *Chem. Rev.* **1996,** 96, 759-834.

24. Kaes, C.; Katz, A.; Hosseini, M. W., *Chem. Rev.* **2000,** 100, 3553-3590.

25. Armentano, D.; de Munno, G.; Guerra, F.; Faus, J.; Lloret, F.; Julve, M., *Dalton Trans.* **2003**, 4626-4634.

26. Concepcion, J. J.; Jurss, J. W.; Brennaman, M. K.; Hoertz, P. G.; Patrocinio, A. O. v. T.; Murakami Iha, N. Y.; Templeton, J. L.; Meyer, T. J., *Acc. Chem. Res.* **2009,** 42, 1954-1965.

27. Ernst, S.; Kaim, W., *J. Am. Chem. Soc.* **1986,** 108, 3578-3586.

28. Tye, J. W.; Darensbourg, M. Y.; Hall, M. B., *Inorg. Chem.* **2006,** 45, 1552-1559.

29. Kaur-Ghumaan, S.; Schwartz, L.; Lomoth, R.; Stein, M.; Ott, S., *Angew. Chem. Int. Ed.* **2010,** 49, 8033-8036.

30. Beyler, M.; Ezzaher, S.; Karnahl, M.; Santoni, M.-P.; Lomoth, R.; Ott, S., *Chem. Commun.* **2011,** 47, 11662-11664.

31. Gao, S.; Fan, J.; Sun, S.; Song, F.; Peng, X.; Duan, Q.; Jiang, D.; Liang, Q., *Dalton Trans.* **2012,** 41, 12064-12074.

32. Adam, F. I.; Hogarth, G.; Richards, I.; Sanchez, B. E., *Dalton Trans.* **2007**, 2495-2498.

33. Fernholt, L.; Romming, C.; Samdal, S., *Acta Chem. Scand.* **1981,** 35A, 707-715.

34. Irwin, M.; Jenkins, R. K.; Denning, M. S.; Kraemer, T.; Grandjean, F.; Long, G. J.; Herchel, R.; McGrady, J. E.; Goicoechea, J. M., *Inorg. Chem.* **2010,** 49, 6160-6171.

35. Baumann, F.; Stange, A.; Kaim, W., *Inorg. Chem. Commun.* **1998,** 1, 305-308.

36. Lyon, E. J.; Georgakaki, I. P.; Reibenspies, J. H.; Darensbourg, M. Y., *Angew. Chem. Int. Ed.* **1999,** 38, 3178-3180.

37. Adam, F. I.; Hogarth, G.; Richards, I., *J. Organomet. Chem.* **2007,** 692, 3957-3968.

38. Adam, F. I.; Hogarth, G.; Richards, I.; Sanchez, B. E., *Dalton Trans.* **2007**, 2495-2498.

39. Morvan, D.; Capon, J.-F.; Gloaguen, F.; Le Goff, A.; Marchivie, M.; Michaud, F.; Schollhammer, P.; Talarmin, J.; Yaouanc, J.-J.; Pichon, R.; Kervarec, N., *Organometallics* **2007,** 26, 2042-2052.

40. Ezzaher, S.; Capon, J.-F.; Gloaguen, F.; Kervarec, N.; Petillon, F. Y.; Pichon, R.; Schollhammer, P.; Talarmin, J., *C. R. Chimie* **2008,** 11, 906-914.

41. Justice, A. K.; Zampella, G.; De Gioia, L.; Rauchfuss, T. B.; van der Vlugt, J. I.; Wilson, S. R., *Inorg. Chem.* **2007,** 46, 1655-1664.

42. Orain, P.-Y.; Capon, J.-F.; Kervarec, N.; Gloaguen, F.; Petillon, F.; Pichon, R.; Schollhammer, P.; Talarmin, J., *Dalton Trans.* **2007**, 3754-3756.

43. Ezzaher, S.; Capon, J.-F.; Gloaguen, F.; Petillon, F. Y.; Schollhammer, P.; Talarmin, J., *Inorg. Chem.* **2007,** 46, 3426-3428.

44. Palmer, R. A.; Piper, T. S., *Inorg. Chem.* **1966,** 5, 864-&.

45. Zhao, J.; Wei, Z.; Zeng, X.; Liu, X., *Dalton Trans.* **2012,** 41, 11125-11133.

46. Felton, G. A. N.; Vannucci, A. K.; Chen, J.; Lockett, L. T.; Okumura, N.; Petro, B. J.; Zakai, U. I.; Evans, D. H.; Glass, R. S.; Lichtenberger, D. L., *J. Am. Chem. Soc.* **2007,** 129, 12521-12530.

47. Capon, J.-F.; Gloaguen, F.; Schollhammer, P.; Talarmin, J., *J. Electroanal. Chem.* **2006,** 595, 47-52.

48. Fourmond, V.; Jacques, P.-A.; Fontecave, M.; Artero, V., *Inorg. Chem.* **2010,** 49, 10338-10347.

49. Savéant, J.-M., *Elements of Molecular and Biomolecular Electrochemistry: An Electrochemical Approach to Electron Transfer Chemistry*. John Wiley & Sons, Inc.: Hoboken, N.J., 2006.

50. Tokel-Takvoryan, N. E.; Hemingway, R. E.; Bard, A. J., *J. Am. Chem. Soc.* **1973,** 95, 6582-6589.

51. Ohsawa, Y.; Hanck, K. W.; DeArmond, M. K., *J. Electroanal. Chem.* **1984,** 175, 229-240.

52. Chong, D. S.; Georgakaki, I. P.; Mejia-Rodriguez, R.; Samabria-Chinchilla, J.; Soriaga, M. P.; Darensbourg, M. Y., *Dalton Trans.* **2003**, 4158-4163.

Chapter 6

A pentacoordinate trigonal bipyramidal iron complex as a functional model of [FeFe]-hydrogenase

Souvik Roy[†§], Thomas L. Groy[†], Shobeir K. S. Mazinani[†§], Pilarisetty Tarakeshwar[†], Vladimiro Mujica[†§], Anne K. Jones[†§*]

[†]Department of Chemistry and Biochemistry; [§]Center for Bio-Inspired Solar Fuel Production; Arizona State University, Tempe, AZ 85287

Abstract

Two pentacoordinate mononuclear iron carbonyls, (bdt)Fe(CO)P_2 (bdt = benzene-1,2-dithiolate; P_2 = 1,1'-diphenylphosphinoferrocene (**1**), methyl-2-{bis(diphenylphosphinomethyl)amino}acetate (**2**)) were prepared as biomimetic models for the distal iron (Fe_d) of the active site of [FeFe]-hydrogenase. X-ray crystal structures of the complexes reveal that, despite similar ν(CO) stretching bands, they have different geometries. The iron center of **1** is in a distorted trigonal bipyramidal arrangement and that of **2** is in a distorted square pyramidal geometry. Electrochemical investigation shows that both complexes can catalyze electrochemical proton reduction from acetic acid at mild overpotential, 0.17 and 0.38 V for **1** and **2**, respectively. Although coordinatively unsaturated, the complexes display only weak, reversible binding affinity towards CO (1 bar). However, ligand centered protonation by a strong acid, HBF_4-OEt_2, triggered quantitative CO uptake by **1** to form a dicarbonyl analogue **[1(H)-CO]**$^+$, which was reversibly converted back to **1** upon deprotonation by NEt_3. DFT calculations suggest that the iron center in both **1** and **2** is largely of Fe^I character due to non-innocence of bdt ligand. Ligand based protonation interrupts the extensive electron delocalization over the Fe and bdt, and thus, makes **1(H)**$^+$ susceptible to external CO binding.

Introduction

Hydrogen produced from solar energy and water offers the tantalizing opportunity to produce a storable, renewable fuel on a scale comparable to global energy challenges.[1] However, developing efficient and renewable catalysts for this transformation has proven challenging. Thus hydrogenases, the biological catalysts for reversible proton reduction to hydrogen, have caught the attention of a broad range of researchers.[2, 3] Since the elucidation of the structures of both [NiFe]- and [FeFe]-hydrogenases revealed that these enzymes feature organometallic active sites including the diatomic ligands CO and CN (Figure 1),[4-7] inorganic chemists have sought to produce both structural and functional models in an effort to understand and reproduce these enzymes.[8] However, although natural hydrogenases have turnover frequencies exceeding 1000 s^{-1} at potentials close to the thermodynamic reduction potential of the proton, synthetic models seldom come close to this exquisite reactivity.[9, 10]

The active site of [FeFe]-hydrogenases, referred to as the H-cluster, is a unique six iron cluster consisting of a [4Fe4S] cluster bridged *via* a cysteinyl thiolate to a diiron subsite.[5, 6] This diiron subcluster, although biologically unprecedented, is highly reminiscent of known organometallic complexes. As shown in Figure 6-1, it consists of a dithiolate ligand bridging the two iron ions as well as the strong π-acceptors CO and CN^- at each iron center. The proximal iron, Fe_p, so designated due to its relative proximity to the [4Fe4S] center, is a coordinatively saturated, octahedral site. On the other hand, hydrogen binding or production occurs at the distal iron, Fe_d, an electron deficient, five-coordinate, pseudo-square pyramidal center featuring a terminal open coordination site.

Organometallic complexes of the type $[(\mu\text{-}SR_2)Fe_2(CO)_6]$ and their derivatives in which one or more of the carbonyls have been replaced with strongly σ-donating ligands such as phosphines, have been used extensively as both structural and functional mimics of [FeFe]-hyrogenases.[3, 11, 12] Although the natural enzyme features iron centers in square pyramidal environments that are inverted relative to one another such that a terminal open coordination site is available, the irons in these model complexes are in the so-called "eclipsed" geometry in which the two pyramids have the same orientation. In this geometry, the bridging, as opposed to terminal, position is most reactive, facilitating formation of stable but unreactive bridging hydrides.[13-15] Thus the models tend to be poor catalysts for proton reduction and require substantial overpotentials for the catalysis. Development of mononuclear iron complexes with an open coordination site can, in principle, overcome this difficulty and mimic the reactivity of the distal iron site of the enzyme if an appropriate ligand set can be found to simulate the electronic environment of the second missing metal.

Although synthetic efforts immediately following the elucidation of the crystal structure of [FeFe]-hydrogenases produced a series of coordinatively saturated mononuclear iron complexes as spectroscopic models for the H-cluster,[16-18] relatively few five coordinate models have been reported. Liaw and coworkers demonstrated the synthesis of a pentacoordinate, 16-electron Fe(II) complex$[Fe(CO)_2(CN)(S,NH\text{-}C_6H_4)]^-$ and showed that it readily reacted to form hexacoordinate complexes or dimers.[19] They did not, however, investigate the catalytic activity of this compound. Darensbourg and coworkers have also produced pentacoordinate iron dicarbonyls using the strongly π-donating, redox noninnocent ligand 2-amido-thiophenylate as models for the

mononuclear Fe-containing hydrogenases.[20, 21] Only recently have Ott and coworkers used the related, redox non-innocent, benzene-1,2-dithiolate (bdt) ligand together with a chelating phosphine to create coordinatively unsaturated monocarbonyl models of the distal iron site of [FeFe]-hydrogenases and show that these compounds are active in electrocatalytic proton reduction.[22, 23]

In this paper, we present a new coordinatively unsaturated, five-coordinate Fe(II)-carbonyl in a P_2S_2 coordination environment that employs two chelating ligands to stabilize an unusual trigonal bipyramidal geometry. The phosphines are provided by 1,1'-{bis(diphenyl)phosphino}ferrocene (dppf), and the steric constraints of the ferrocene moiety in this ligand cause it to have one of the largest bite angles observed for a chelating phosphine. On the other hand, benzene-1,2-dithiolate (bdt), well known for its redox non-innocence associated with the conjugation of the sulfur donors to the aromatic ring, provides the sulfur ligands. The result is that [(κ^2-dppf)Fe(CO)(κ^2-bdt)] (**1**) **e**lectrocatalytically reduces protons from the weak acid acetic acid with unprecedentedly low overpotentials. Furthermore, the protonated complex binds exogenous CO, a reaction seldom seen in model compounds but well known for the enzyme. The electrocatalytic properties of this complex are directly compared to those of an analogous square-based pyramidal compound [(κ^2-NP_2)Fe(CO)(κ^2-bdt)] (**2**) for NP_2 = methyl-2,-{bis(diphenylphosphinomethyl)amino}acetate, and electronic explanations for the differing reactivities of the two complexes are considered.

Results and Discussion

Synthesis and spectroscopic characterization. Two pentacoordinate iron(II)-carbonyl complexes each with a chelating bis-phosphane and benzene-1,2-dithiol (bdt) were

synthesized starting from $FeCl_2$: (κ^2-dppf)Fe(CO)(κ^2-bdt) (**1**) and (κ^2-NP_2)Fe(CO)(κ^2-bdt) (**2**) where dppf is 1,1'-bis(diphenylphosphino)ferrocene and NP_2 is methyl-2-{bis(diphenylphosphinomethyl)amino}-acetate (Scheme 6-1). The bdt ligand was employed both for its strong π-donor propensity and its redox non-innocence. Similarly, the ligand dppf was chosen because it is both chelating and redox-active. Furthermore, dppf, among common chelating bis-phosphane ligands, has one of the widest bite angles. This angle has a major influence on the structure of the resulting complex and the corresponding catalytic properties.[24-27] For comparison, to evaluate the impact of dppf on the electronic and catalytic properties of the $Fe^{II}S_2P_2$ center, **2**, which features an N-containing bis-phosphane ligand (NP_2) instead of dppf, was synthesized. The ligand NP_2 is easily obtained by reaction of two equivalents of Ph_2PCH_2OH with glycine methyl ester in refluxing ethanol.[28] As shown in Scheme 1, treatment of a methanolic solution of anhydrous $FeCl_2$ with a solution of the appropriate bis-phosphane in THF and benzene-1,2-dithiol in the presence of a base (triethylamine) under a CO atmosphere afforded the desired diamagnetic complexes, **1** and **2** in 65% and 60% isolated yields, respectively. A single resonance is observed in the $^{31}P\{^1H\}$ NMR spectrum at 66.32 ppm for **1** and 50.21 ppm for **2**.

In a tetrahydrofuran (THF) solution, **1** is reddish brown with visible absorbances at 467 nm (ε = 4433 M^{-1} cm^{-1}) and 745 nm (ε = 974 M^{-1} cm^{-1}) (Figure 6-2). Another very intense band in the UV range 250–300 nm arising from the π-π* transition of the phenyl groups was also present. The 467 nm band features a prominent shoulder on the lower energy side, and, by comparison to the spectrum of **2** (vide infra) likely consists of two distinct charge transfer transitions. The 745 nm band is thought to arise from a d-d

transition. By comparison, despite a similar coordination environment and metal oxidation state, **2** is dark green in a THF solution with absorption maxima at 437 nm ($\varepsilon = 4537\ M^{-1}\ cm^{-1}$) and 579 nm ($\varepsilon = 2883\ M^{-1}\ cm^{-1}$). These bands are tentatively assigned as charge transfers involving the Fe center and the benzene-1,2-dithiolate ligand.

IR spectra of both **1** and **2** in dichloromethane consist of a single peak in the CO-stretching region at 1918 or 1915 cm^{-1}, respectively (Figure 6-3A and 6-3B, bottom panel). The energy of this absorbance is comparable to that of related Fe^{II} complexes such as (κ^2-dppp)Fe(CO)(Cl_2bdt) (dppp = diphenylphosphinopropane, Cl_2bdt = 3,6-dichloro-1,2-benzenedithiolate).[22] The remarkable similarity of the CO-stretching frequencies for the two complexes indicates that changing the bis-phosphane ligand has little detectable impact on the Fe-CO bonding interactions.

Crystal Structures. The structures of **1** and **2** were determined by single-crystal X-ray diffraction and are shown in Figure 6-4. Selected bond distances and angles are given in Tables 6-1 and 6-2 and additional crystallographic information is available in Table 6-3. Crystals were grown by slow diffusion of hexane into a dichloromethane (**1)** or chloroform (**2**) solution of complex. The two complexes feature remarkably different geometries about the central iron atom. Complex **2** is a distorted square pyramid (SP) with an axial CO ligand while complex **1** is a distorted trigonal bipyramid (TBP) with CO, phosphorus and sulfur in the equatorial positions and phosphorus and sulfur in the apical positions. The geometries of the complexes were further characterized by Addison's τ value, defined as $\tau = (\beta - \alpha)/60$ for which β is the larger of the angles between the trans ligands on the basal plane of a SP or the angle between the two axial ligands for a TBP. The parameter α is defined as the smaller of the angles between the

trans ligands on the basal plane of a SP or the larger of the basal angles for a TBP.[29] For pentacoordinate complexes, τ value is a measure of the degree of distortion from ideal SP (τ = 0) or ideal TBP (τ = 1) geometry. The calculated value of τ is 0.099 for **2** (based on β(S1-Fe1-P2) = 165.1427˚ and α(S2-Fe1-P1) = 159.2057˚) and 0.721 for **1** (based on β(S2-Fe1-P1) = 171.7433˚ and α(S1-Fe1-P2) = 128.4776˚) corroborating the geometry assignmentts of the complexes described above. As noted above, dppf has a much larger bite-angle (P-Fe-P = 101.17˚) than NP_2 (87.49˚), and this difference is likely responsible for the geometric differences about the irons of **1** and **2**. For complex **1**, the three equatorial ligands show a significant distortion from symmetrical arrangement with bond angles of 134.58˚ (C-Fe-S), 128.48˚ (S-Fe-P), and 96.69˚ (P-Fe-C). The two axial ligands, thiolate and phosphane, are also slightly distorted from a linear arrangement with an S-Fe-P angle of 171.74˚. We note that **1** is a diamagnetic, Fe^{II} complex. Perfect TBP geometry does not permit a diamagnetic ground state for a d^6 metal, but the observed distorted geometry is consistent with the S = 0 ground state.[30, 31] Despite the metal coordination geometry differences, the Fe-C and C-O bond lengths of **1** and **2** are very similar to one another. This is consistent with the similar ν(CO) stretching frequencies observed for the two complexes. Additionally, as shown in Table 6-2, the C-C bond lengths of the benzene-1,2-dithiolato ligand show an alternating pattern of two shorter C-C bonds (average 1.37 Å for **1** and 1.38 Å for **2**) and four longer ones (average 1.40 Å for **1** and **2**) for both **1** and **2**. Moreover, the two C-S bonds are also not identical. The average C-S bond lengths, 1.74 Å for **1** and 1.75 Å for **2,** are slightly shorter than typical bond lengths for the C-S single bonds (1.76 - 1.77 Å) in benzene-1,2-dithiolate, suggesting that in the metallocomplexes the C-S bond orders are greater than one.[32-34]

The observed distortions of the bdt ligand represent clear evidence that it is partially oxidized and possesses substantial 1,2-dithiobenzosemiquinonate, π-radical character.[34, 35] Concomitantly, the physical oxidation state of the Fe center in both complexes should be less than +2. The distortion of the ligand is more obvious for **1** indicating that the bdt ligand is more oxidized and the pentacoordinate Fe center is more reduced in this complex than in **2**.

Reactivity towards CO. To investigate whether the open coordination site on complexes **1** and **2** is accessible for external ligand binding, reactions of **1** and **2** with CO were studied. Figure 6-3A shows the FTIR spectrum of a solution of **1** after it was saturated by bubbling with CO for ten minutes. In addition to the 1918 cm^{-1} signal of the parent complex, two new CO stretching bands are observed at 1996 and 2020 cm^{-1} indicating formation of an $Fe(CO)_2S_2P_2$ complex, **1-CO**. The presence of two new bands indicates that the CO ligands are in a *cis* orientation. The ^{31}P NMR spectrum obtained under the same conditions also includes both the 66.32 ppm resonance of the starting material and a new signal at 62.59 ppm, providing additional evidence for formation of **1-CO**. Following removal of CO from the solution by purging with nitrogen, the signals associated with **1-CO** were no longer present. This demonstrates that binding of external CO to **1** is a reversible process. The analogous reaction for **2** was also observed *via* identification of new CO stretches at 1995 and 2021 cm^{-1} (Figure 6-3B). The complex **2-CO** also reverted reversibly to **2** upon removal of the CO. We note, however, that formation of **2-CO** was less complete than formation of **1-CO**. The complex **2-CO** was not produced in quantities sufficient to be detected by ^{31}P NMR. Furthermore, the ratios of the intensities of the CO stretching bands in the IR spectrum also suggest that the

majority of **2** remains unreacted. The difference in reactivities of the two complexes may be attributable to the geometries about the iron centers. Formation of a *cis* dicarbonyl from **2** will require a substantial distortion so that one of the extant ligands moves to a position *trans* to a carbonyl. However, such a large rearrangment is not required for the reaction of **1**.

A quantitative reaction between **1** and CO was observed if the strong acid HBF_4-OEt_2 was also present. The newly formed complex, **[1(H)-CO]**$^+$, is red in solution and has characteristic CO stretching vibrations at 2089 and 2043 cm^{-1} (Figure 6-3C). Complex **1** could be reversibly regenerated from **[1(H)-CO]**$^+$ by purging the solution with nitrogen and addition of triethylamine. An analogous reaction of **2** was not observed under the same conditions. The relative intensities of and energy gap between the two signals associated with CO stretching in the IR spectrum of **[1(H)-CO]**$^+$ are reminiscent of the well characterized *cis,cis,cis*-$Fe(CO)_2(dppe)(SPh)_2$ which has analogous peaks at 2017 and 1970 cm^{-1}.[36] Most notable is that the stretching frequencies of **[1(H)-CO]**$^+$ are 73 cm^{-1} higher in energy compared to this reference compound. This shift can be explained by the requirement for acid for this reaction. Since bdt complexes of transition metals can have mixed metal-ligand character frontier orbitals (*vide infra*), the complex is likely protonated at one of the sulfurs resulting in a substantially weaker ligand and increasing the electrophilicity of the metal center.[37-39] The result is less back-bonding into the π^* LUMO of the CO and a stronger C–O bond reflected in a higher energy stretch. Such enhanced electrophilicity of a d^6 metal ion on ligand protonation is not unprecedented.[20, 40] Hence we postulate that the protonated dicarbonyl species is *cis,cis,cis*-$[Fe(CO)_2(\kappa^2\text{-dppf})(bdt\text{-}H)]^+$.

Electrochemistry and catalysis. The effects of the change in geometry on the redox behavior of the complexes were probed by cyclic voltammetry. Electrochemical analysis of **1** and **2** in 0.1 M $[NBu_4][PF_6]$/THF was performed under an argon atmosphere. The number of electrons involved in the observed redox processes was determined on the basis of peak separations (ΔE_p). As shown in Figure 6-5, cyclic voltammograms of **1** show a reversible reduction wave at $E_{1/2}$ = -1.65 V (i_p^c/i_p^a = 1.01, ΔE_p = 0.144 V) and two reversible oxidation waves at $E_{1/2}$ = +0.13 V (i_p^c/i_p^a = 0.90, ΔE_p = 0.140 V) and +0.44 V (i_p^c/i_p^a = 0.98, ΔE_p = 0.137 V) *vs.* $Fc^{+/0}$ (Fc = ferrocene). Upon comparison of the peak separations to that of the $Fc^{+/0}$ couple under the same conditions, 0.156 V, we conclude that all three transitions are one-electron redox processes. The reduction wave at -1.65 V can be attributed to the $Fe^{II/I}$ couple corresponding to the pentacoordinate Fe center. The oxidation waves at +0.13 and +0.44 V can be assigned to the $Fe^{III/II}$ couples for the Fe center in dppf and the pentacoordinate Fe center. The oxidation wave at +0.13 V is likely associated with the oxidation of the Fe^{II} center in dppf since quasi-reversible oxidation of free dppf occurs at $E_{1/2}$ = 0.183 V in 1,2-dichloroethane.[41, 42] On the other hand, cyclic voltammograms of **2** reveal that it undergoes a reversible one-electron reduction at $E_{1/2}$ = -1.86 V (i_p^c/i_p^a = 1.04, ΔE_p = 0.164 V) and an irreversible one-electron oxidation at $E_{1/2}$ = +0.32 V. By analogy to **1**, the reduction and oxidation waves are likely to be $Fe^{II/I}$ and $Fe^{III/II}$ couples, respectively. Notably, reduction of the pentacoordinate Fe^{II} center in **2** occurs at more negative potential than **1** due to the change from TBP to SP geometry. More interestingly, in contrast to the two reversible $Fe^{III/II}$ couples in trigonal bipyramidal **1**, the $Fe^{III/II}$ couple in square pyramidal **2** is

irreversible, indicating coordination of dppf leads to improved stability of oxidized complex in $Fe^{III}Fe^{II}$ and $Fe^{III}Fe^{III}$ states. In case of **2**, oxidation of the pentacoordinate Fe^{II} center might be associated with a geometry change or subsequent reaction with solvent molecules or ligand dissociation.

The electrocatalytic proton reduction activities of **1** and **2** were investigated in THF in the presence of acetic acid *(*$pK_{a(THF)}$ = 24.42) and *p*-toluenesulfonic acid (*p*-TsOH). As shown in Figure 6-6, sequential addition of acetic acid from 0.2 M to 1.4 M renders the reduction wave for the $Fe^{II/I}$ couple irreversible and leads to an increase in current. This is characteristic of electrocatalytic proton reduction since direct proton reduction from acetic acid at the glassy carbon electrode is negligible in this potential range (Figure 6-7).[43,44] The overpotentials for proton reduction by the two complexes, determined using the method reported by Artero and co-workers, were relatively small, only 0.17–0.2 V and 0.38–0.43 V for **1** and **2**, respectively (Table 6-4).[45] The half-wave potentials for the catalytic current, used for the overpotential calculation, were determined as the potential corresponding to the maximum value of (di/dE), *i.e.* the first derivative of the current data from the cyclic voltammograms. Notably, a mononuclear iron complex $\{\kappa^2\text{-}(Ph_2PCH_2N(X)CH_2PPh_2)\}Fe(CO)(\kappa^2\text{-bdt})$ (X = 1,1-diethoxy-ethyl) similar to **2** was reported to reduce protons from acetic acid in acetonitrile with overpotential in the range 0.23–0.27 V.[22] The kinetics of proton reduction were evaluated by considering the effect of catalyst concentration and acid concentration on observed activity (see Figures 6-8 and 6-9). Figure 6-8 shows that catalytic peak current, i_{cat}, depends linearly on catalyst concentration, [cat], for both **1** and **2**. This demonstrates a first-order dependence of the catalytic current on the concentration of the catalyst at fixed

acid concentrations as described by eq. 1 in which *n* is the number of electrons involved in the catalytic reaction, *A* is the area of the electrode, *D* is the diffusion coefficient of the catalyst, *k* is the rate constant and *x* is the order of the reaction with respect to acid.[46] Figure 6-9 shows that the ratio of catalytic current to reductive peak current measured in the absence of acid, i_{cat}/i_p, is also linear with respect to acid concentration for catalyst concentrations in the range 0.74–1.13 mM for **1** and 0.47–1.35 mM for **2**. This indicates the reaction is second-order with respect to acid concentration as described by eq. 2, for a scan rate υ of 0.1 V s^{-1}. At the highest acid concentration investigated (1.6 M), a value of i_{cat}/i_p of 35 was obtained for **2** (0.6 mM), corresponding to a turnover frequency of 241 s^{-1}. A much slower rate was observed for **1** (0.74 mM) with a turnover frequency of 10 s^{-1} at 1.8 M acetic acid.

$$i_{cat} = nFA[cat]\sqrt{D(k[acid]^x)} \quad (1)$$

$$i_{cat}/i_p = (n/0.4463)\sqrt{RT(k[acid]^x)/F\upsilon} \quad (2)$$

The electrocatalytic activities of the two complexes were also studied in the presence of the stronger acid, *p*-TsOH. Irreversible catalytic waves corresponding to the reduction of protons are observed at the potentials of the **1/1**$^-$ and **2/2**$^-$ couples (Figure 6-10). The catalytic peak current is largely independent of catalyst concentration (panel B of Figure 6-11) for **1** over the investigated range (0.28–0.83 mM) and increases linearly with increasing concentration of *p*-TsOH (panel A of Figure 6-11). A similar result has been reported for the mononuclear iron complex analogous to **2** incorporating a different NP_2 ligand N,N-bis{(diphenylphosphino)methyl}-2,2-diethoxyethanamine.[22] Interestingly, for both **1** and **2**, at low concentration of *p*-TsOH (1-2 eq. of the catalyst), a new reduction wave at 150 mV less negative potential is observed together with the

original $Fe^{II/I}$ couple which grows with increasing acid concentration (Figure 6-12). However, at higher acid concentration (more than 2 eq.), the two peaks merge to produce a single catalytic wave. The observation that this new peak emerges for both complex **1** and **2** excludes the possibility that it is associated with protonation at the amine group of the NP_2 ligand in **2**. Association between either the sulfurs or the aromatic ring of the bdt ligand and the proton/acid is, however, a distant possibility.

Computational Studies. To complement the experimental results on the pentacoordinate iron complexes, density functional theory (DFT) calculations were carried out on **1** and **2**. Calculations were performed using the B3LYP hybrid functional, and the DFT-optimized structures, which agree well with the corresponding crystal structures, were confirmed as energy minima. Table 6-5 presents a comparison of the calculated and experimental metric parameters, and Figure 6-13 shows the calculated frontier molecular orbitals for the two complexes. Complexes **1** and **2** both have HOMOs that are delocalized over the Fe and much of the bdt ligand, emphasizing the importance of the redox non-innocence of this ligand to the electronic structure of the complex. In particular, the HOMOs are a bonding combination of iron d orbitals and sulfur p(π) orbital(s), and an antibonding combination of sulfur and the adjacent carbon atoms, implying strong electron delocalization over the iron and the bdt ligand (see overlap population in Table 6-6). It is worth noting, however, that the Fe-S interactions are not equivalent for the two complexes. The HOMO of **1** includes interactions only between the Fe and S1, likely a result of the unusual geometry. On the other hand, the HOMO of **2** includes substantial contributions from both sulfurs of the bdt ligand. Furthermore, the HOMOs of **1** and **2** bear considerable resemblance to the HOMO of the free bdt^{2-} ligand or the SOMO of the

free ligand in the π-radical anion form ($bdt^{-\bullet}$).[47, 48] From the molecular orbital approach, the metal dithiolate interaction in the complexes can best be described as transfer of electron density from the HOMO of a bdt^{2-} ligand to empty Fe *d* orbitals. Alternatively, the bonding pattern can also be thought of as an Fe^{I} center antiferromagnetically coupled to a radical anion $bdt^{\bullet-}$ ligand, leading to diamagnetic complexes. It is particularly important to note that only one sulfur atom contributes to the HOMO of **1**, but both sulfur atoms have significant contributions to the HOMO of **2**. On the other hand, the orbital density profiles shown in Figure 6-13 and the percentage orbital contribution given in Table 6-6 indicate that the LUMOs are dominated primarily by contributions from the Fe *d* orbitals with the sulfur and phosphorus atoms playing a minor role, and almost no contribution from the rest of the ring structure. This suggests that reduction of the complexes results in substantial accumulation of charge at the metal center yielding a highly basic iron site for interaction with protons. Furthermore, the significant iron character of the LUMOs (51% and 43% for **1** and **2**, respectively) is consistent with the abilities of these complexes to reversibly bind CO.

To correlate the observed trends in the reactivity of the two complexes with CO in the presence of acid, DFT calculations were also undertaken for the protonated complexes $\mathbf{1(H)}^{+}$ and $\mathbf{2(H)}^{+}$, assuming compositional integrity following protonation. For complex **1**, protonation is most likely to occur at either the Fe center or the thiolate sulfur with the highest contribution to the HOMO. The possibilities for **2** are more numerous since both the sulfurs contribute to the HOMO and it features an amine group in the NP_2 ligand that could also serve as a protonation site. Calculations for $\mathbf{1(H)}^{+}$ with the proton localized on the Fe indicate that it is 13 kcal/mol higher in energy than a $\mathbf{1(H)}^{+}$ complex

with a thiolate protonated. Likewise, in the case of **2**, an N-protonated species is 6.4 kcal/mol higher in energy than the S-protonated species. Therefore, the rest of the computational studies were carried out assuming that protonation occurs exclusively at the thiolate sulfur. The geometry optimized structure of $\mathbf{1(H)}^+$ shows that protonation results in only minor changes about the Fe center; in particular, the τ value of $\mathbf{1(H)}^+$, 0.65, is not significantly different from that of **1**, 0.72 (Table 6-5). In contrast, upon protonation, **2** undergoes considerable distortion from its nearly square pyramidal geometry (τ = 0.09) to a hybrid of square pyramidal and trigonal bipyramidal geometries (τ = 0.42). Furthermore, electron density profiles of the HOMO and LUMO of $\mathbf{1(H)}^+$ and $\mathbf{2(H)}^+$ reveal stark differences that are important for understanding their different reactivities towards CO. The HOMO of $\mathbf{1(H)}^+$ is localized entirely on the ferrocene moiety, while the HOMO of $\mathbf{2(H)}^+$ is delocalized over the entirety of the bdt ligand with minimal contribution from the Fe atom. The bonding pattern in the bdt ligand and the orbital contributions in the HOMO suggest that in $\mathbf{2(H)}^+$, the bdt ligand is non-innocent and, consequently, the physical oxidation state of the Fe center is less than +2. On the other hand, computational results suggest that addition of a proton to **1** likely disrupts the electron delocalization between the bdt ligand and the Fe center, reinstating the aromaticity of the C_6H_4-ring of the protonated bdt ligand. Therefore, $\mathbf{1(H)}^+$ to behaves more like a typical, coordinatively unsaturated Fe^{II}, d^6 complex. This difference in the electronic structures of $\mathbf{1(H)}^+$ and $\mathbf{2(H)}^+$ is likely responsible for the fact that protonation induced CO uptake is observed only for **1**.

Conclusions

In summary, we have synthesized two pentacoordinate $Fe^{II}(CO)S_2P_2$ complexes using benzene-1,2-dithiol and two different chelating bis-phosphane ligands: NP_2 and dppf. In contrast to the SP complex formed with NP_2, the wider bite-angle of dppf provides access to a pentacoordinate iron carbonyl in TBP geometry, leading to significant changes in both the electronic and the chemical properties of the complex. This is highlighted by the differences in their reactivity towards CO, reduction potentials, electrocatalytic activity, and energies of charge-transfer bands. The TBP complex requires considerably less overpotential to reduce protons, but the overall rate is very slow. The strong electron donor ligands, thiolates and phosphanes, make the iron basic enough to electrocatalyze proton reduction but render the metal insufficiently electrophilic for efficient binding of external ligands such as H_2 or CO that might be expected for a coordinatively unsaturated d^6 metal center.[49] Computational studies indicate that the bdt ligand is "non-innocent" in both complexes, and, as a result of the extensive π-overlap between the metal and the ligand, the physical oxidation state of the iron is less than +2. The flexibility of the π-interaction between iron and bdt in complex **1** is demonstrated by the ligand-protonation induced CO uptake by **1** to produce an 18-electron hexacoordinate iron dicarbonyl. This model complex of [FeFe]-hydrogenase might serve as a template for developing reversible iron catalysts capable of binding and activating H_2 as well as catalyzing electrochemical proton reduction.

Experimental Section

All reactions were carried out under an atmosphere of nitrogen using standard Schlenk and vacuum-line techniques unless otherwise noted. Anhydrous dichloromethane and

methanol were purchased from Sigma-Aldrich and deuterated solvents from Cambridge Isotope Laboratories. Tetrahydrofuran was dried by distilling overnight over sodium and benzophenone. All starting materials were obtained commercially and used without further purification. ^{1}H, ^{13}C and ^{31}P NMR spectra were recorded at room temperature on a Varian Liquid-State NMR spectrometer (400 or 500 MHz for ^{1}H). NMR chemical shifts are quoted in ppm; spectra were referenced to tetramethylsilane for ^{1}H and ^{13}C NMR. The ^{31}P NMR spectra were referenced to external phosphoric acid at 0 ppm. FTIR spectra were recorded on a Bruker vertex 70 spectrophotometer using a stainless steel sealed liquid spectrophotometer cell with CaF_2 windows. UV-vis measurements were performed on a Hewlett-Packard 8453 spectrophotometer using quartz cuvettes with a 1 cm pathlength.

Synthesis of methyl 2-(bis(diphenylphosphinomethyl)amino)acetate, NP_2. To a degassed solution of formaldehyde (37 wt.% in water; 1 mL, 12.3 mmol) in absolute ethanol (10 mL), diphenylphosphine (1.9 mL, 10.9 mmol) was added dropwise under argon. The reaction mixture was stirred at room temperature for 30 min followed by addition of a degassed solution of glycine methyl ester hydrochloride (0.7 g, 5.6 mmol) in 40% aqueous ethanol (5 mL). The cloudy reaction mixture became clear on stirring for 2 h. Volatile materials were removed under reduced pressure to afford a colorless oily residue. The crude product was purified *via* column chromatography on silica with hexane/ethyl acetate/triethylamine (66:33:1) as eluent to afford NP_2 as a colorless oil. Yield: 2.4 g (85%). $R_f = 0.85$ (1:1 hexane/ethyl acetate, 1% NEt_3). ^{1}H NMR (400 MHz, $CDCl_3$): $\delta = 7.38$ (m, 8H), 7.26 (m, 12H), 3.81 (s, 2H), 3.7 (d, 4H), 3.61 (s, 3H). $^{13}C\{^{1}H\}$

NMR (100 MHz, $CDCl_3$): δ = 171.21, 137.58, 137.46, 133.09, 132.90, 128.57, 128.37, 128.34, 128.30, 58.02, 55.65, 51.28. $^{13}P\{^1H\}$ NMR (161.8 MHz, $CDCl_3$): δ = -27.19.

Synthesis of (dppf)Fe(CO)(bdt), 1. To an anaerobic solution of anhydrous $FeCl_2$ (60.3 mg, 0.48 mmol) in anhydrous methanol (8 mL), 1,1'-bis(diphenylphosphino)ferrocene (280 mg, 0.5 mmol) in THF (4 mL) was added dropwise under a CO atmosphere. After stirring the reaction mixture for 30 min at room temperature, a degassed solution of benzene-1,2-dithiol (0.07 mL, 0.6 mmol) and triethylamine (0.17 mL, 1.2 mmol) in methanol (3 mL) was added dropwise. The reaction turned to violet and then to dark brown. After stirring for 1 h at room temperature, the solvent was removed under reduced pressure and the residue was purified *via* column chromatography on silica with hexane/dichloromethane (1:2) as eluent. The product was obtained as dark brown powder. Yield: 244 mg (65%). R_f = 0.4 (1:1 hexane/CH_2Cl_2). ^1H NMR (400 MHz, CD_2Cl_2): δ = 8.04 (dd, *J* = 6.0, 3.2 Hz, 2H), 7.59 (m, 4H), 7.41-7.36 (m, 8H), 7.18-7.10 (m, 10H), 4.89 (s, 2H), 4.48 (s, 2H) 4.24 (s, 2H), 4.12 (s, 2H). $^{13}C\{^1H\}$ NMR(100 MHz, CD_2Cl_2): δ = 134.98, 132.71, 130.39, 129.50, 129.32, 127.76, 127.41, 121.38, 76.96, 74.92, 74.79, 72.60, 71.40. $^{31}P\{^1H\}$ NMR (161.8 MHz, CD_2Cl_2): δ = 66.32. IR (CH_2Cl_2, cm^{-1}): ν(CO) 1918. APCI mass spectrum (positive mode): 751.0198 $[(M\text{-}CO+H)^+]$.

Synthesis of (NP_2)Fe(CO)(bdt), 2. To an anaerobic solution of anhydrous $FeCl_2$ (75 mg, 0.6 mmol) and NP_2 ligand (264 mg, 0.56 mmol) in anhydrous methanol (11 mL) under a CO atmosphere, benzene-1,2-dithiol (0.07 mL, 0.6 mmol) and triethylamine (0.17 mL, 1.2 mmol) was added. The color of the solution turned black. After stirring at room temperature for 2 h, the solvent was removed under reduced pressure and the residue was purified *via* column chromatography on silica with hexane/ethyl acetate (4:1) as eluent.

The desired compound was obtained as a green solid. Yield: 240 mg (60%). R_f = 0.3 (3:1 hexane/ethyl acetate). ^{1}H NMR (400 MHz, CD_2Cl_2): δ = 7.99 (dd, *J* = 6, 3.2 Hz 2H), 7.64 (m, 4H), 7.50 (m, 6H), 7.15 (m, 6H), 7.09 (dd, *J* = 6, 3.2 Hz, 2H), 6.96 (t, *J* = 7.6 Hz, 4H), 4.05-3.97 (m, 2H), 3.86-3.80 (m, 2H), 3.70 (s, 3H), 3.59 (s, 2H). ^{13}C NMR (100 MHz, CD_2Cl_2): δ = 133.68 (t), 132.74 (t), 130.46 (s), 129.83 (s), 129.05 (s), 128.42 (t), 127.82 (t), 121.34 (s), 62.00 (t), 56.73 (s) 56.57 (s), 51.64 (s). ^{31}P NMR (161.8 MHz): δ = 50.21. IR (CH_2Cl_2, cm^{-1}): ν(CO) 1915. APCI mass spectrum (positive mode): m/z = 710.0799 [$(M+H)^+$], 682.0787 [$(M-CO+H)^+$].

Reaction of 1 with CO in the presence of $HBF_4.OEt_2$. A solution of **1** (3.2 mg, 4.1 μmol) in CH_2Cl_2 (2 mL) was saturated with CO and $HBF_4.OEt_2$ (0.2 mL 0.074 M solution in CH_2Cl_2, 14.3 μmol, 3.6 equivalent) was added dropwise to the reaction mixture. After stirring for 10 min at room temperature, the color of the solution changed from dark brown to red. Formation of the CO adduct [**1(H)-CO**]$^+$ was indicated by IR and ^{31}P NMR. Addition of triethylamine (0.04 mL, 28.6 μmol) to the reaction mixture followed by purging with N_2 led to release of CO and quantitative regeneration of **1**. IR (CH_2Cl_2): ν(CO) 2089, 2043. ^{31}P {^{1}H} NMR (161.8 MHz, CD_2Cl_2): δ = 4.92.

X-ray crystallography. The crystal was mounted on the end of a thin glass fiber using Apiezon type N grease and optically centered. Cell parameter measurements and single-crystal diffraction data collection were performed at low temperature (123 K) with a Bruker Smart APEX diffractometer. Graphite monochromated Mo Kα radiation (λ = 0.71073 Å) in the ω–φ scanning mode was used for the measurements. The structure was solved by direct methods and refined by fullmatrix least-squares on F^2. The following is the list of the programs used: data collection, Bruker Instrument Service v2010.9.0.0; cell

refinement and data reduction, SAINT V7.68A; structure solution and refinement, SHELXS-97; molecular graphics, XShell v6.3.1; preparation of material for publication, Bruker APEX2 v2010.9-1.30. Details of crystal data and parameters for data collection and refinement are listed in Table 6-3.

Electrochemistry. All electrochemical experiments were carried out using a CHI 1200A electrochemical analyzer. A conventional three-electrode cell was used for recording cyclic voltammograms. The working electrode was a 3 mm diameter glassy carbon disk polished with 1 mm and 0.3 mm deagglomerated alpha alumina, successively, and sonicated for 15 min in ultrapure water prior to use. The supporting electrolyte was $[NBu_4][PF_6]$ (0.1 M in THF). The Ag/Ag^+ reference electrode was prepared by immersing a silver wire anodized with AgCl in an THF solution of 0.1 M $[NBu_4][PF_6]$. A platinum wire was used as counter electrode. Deaeration of the solutions was performed by bubbling argon through the solution for 15 min after which an atmosphere of Ar was maintained during the course of electrochemical measurements. All potentials are reported relative to the ferrocene couple (Fc^+/Fc) as reference. Concentrations of the complexes were determined spectrophotometrically based on the following extinction coefficients: ε(467 nm) = 4433 M^{-1} cm^{-1} and ε(437 nm) = 4537 $M^{-1}cm^{-1}$ for **1** and **2**, respectively.

Determination of catalytic overpotential. Theoretical half-wave potentials $E_{1/2}^T$ were calculated using eq. 3 as defined by Fourmond *et al*. in which $E_{1/2}^0$ is the standard potential for the reduction of protons, $C_{0(HA)}$ is the bulk concentration of the acid, $C_{H_2}^0$ is the concentration of dissolved H_2 (at $p(H_2) = 10^5$ Pa) and ε_D is a measure of the rate of diffusion of the products with respect to that of the reactant (eq. 4).[45]

$$E^{T}_{1/2(HA/H_2,A^-)} = E^{0}_{(H^+/H_2)} - 0.059\,pK_{a(HA)} + \varepsilon_D - \frac{0.059}{2}\log\frac{C_{0(HA)}}{C^{0}_{H_2}} \quad (3)$$

$$\epsilon_D = \frac{RT}{3F}\ln\frac{8D_A{}^{-2}D_{H_2}}{D^3_{AH}} \approx 0.04\,V \quad (4)$$

The standard reduction potential of protons in THF was calculated by Danielle and co-workers using $HClO_4$ as acid and Pt microelectrodes.[58] Since $HClO_4$ is a weak acid in THF (pK_a = 7.7), the reported value of $E_{1/2}$ (-440 mV *vs* Fc^+/Fc) is not equal to $E^0_{(H^+/H_2)}$. The reported value was interpreted as $E^T_{1/2(HA/H_2,A^-)}$ and the actual value of $E^0_{(H^+/H_2)}$ in THF was corrected using eq. xx. The concentration of $HClO_4$ used by Daniele and coworkers for the determination of $E_{1/2}$ is 6 mM. Substituting $C_{0(HClO_4)}$= 6 mM, $C^0_{H_2}$= 3.3 mM,[59] ε_D= 40 mV, pK_a= 7.7, and $E^T_{1/2}$= -440 mV into eq. 3 gives, $E^0_{H^+/H_2}$ = -0.018 V which was used to calculate theoretical half-wave potentials $E^T_{1/2}$ for different concentrations of acetic acid. The experimental and theoretical half-wave potentials for reduction of AcOH in THF (0.1M $[NBu_4][PF_6]$ as supporting electrolyte) on a glassy carbon electrode catalyzed by **1** and **2** are listed in Table 6-4.

Computational Details. Density functional theory (DFT) calculations were carried out using the Becke gradient-corrected exchange functional and Lee−Yang−Parr correlation functional with three parameters (B3LYP) and the 6-31G* basis set.[50-56] In light of recent studies indicating the improved performance of the BP86 and TPSS functionals in describing transition metal containing systems, the geometries and energies of **2** were also calculated using these functionals and the larger TZVPP basis sets.[55, 57] These results are shown in Table 6-7 which indicate that the B3LYP/6-31G* level of theory is most reliable for the systems investigated in this study. The "overlap population" parameter

listed in Table 6-6 is a measure of the nature of the interaction between the orbitals involved. Thus, a positive overlap population represents a bonding interaction, a negative overlap population corresponds to an anti-bonding interaction, and a zero overlap population indicates no bonding between the fragments.

Acknowledgements: This research was supported through the Center for Bio-Inspired Solar Fuel Production, an Energy Frontier Research Center funded by the U.S. Department of Energy, Office of Science, Office of Basic Energy Sciences under Award Number DE-SC0001016.

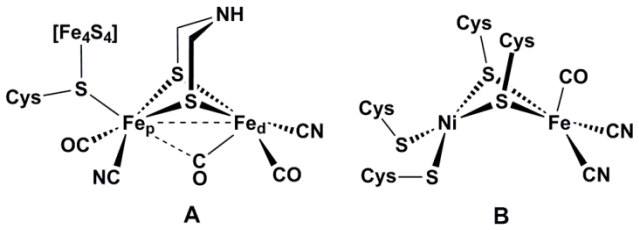

Figure 6-1. Structures of the active sites of [FeFe]- and [NiFe]-hydrogenase. The active site of (A) [FeFe]-hydrogenase (H-cluster) and (B) [NiFe]-hydrogenase. Fe_d and Fe_p denote the distal and proximal iron, respectively, in the H-cluster.

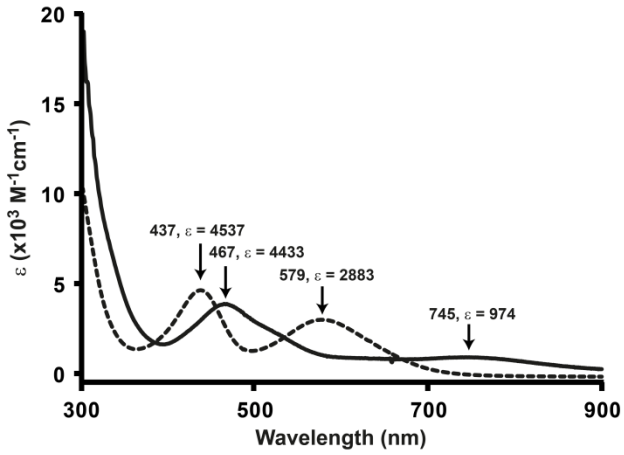

Figure 6-2. Comparative optical spectra of 1 and 2. UV-vis spectra of **1** (solid line) and **2** (dashed line) in THF at room temperature. Spectra were collected from THF solutions of approximately 0.1 mM complex.

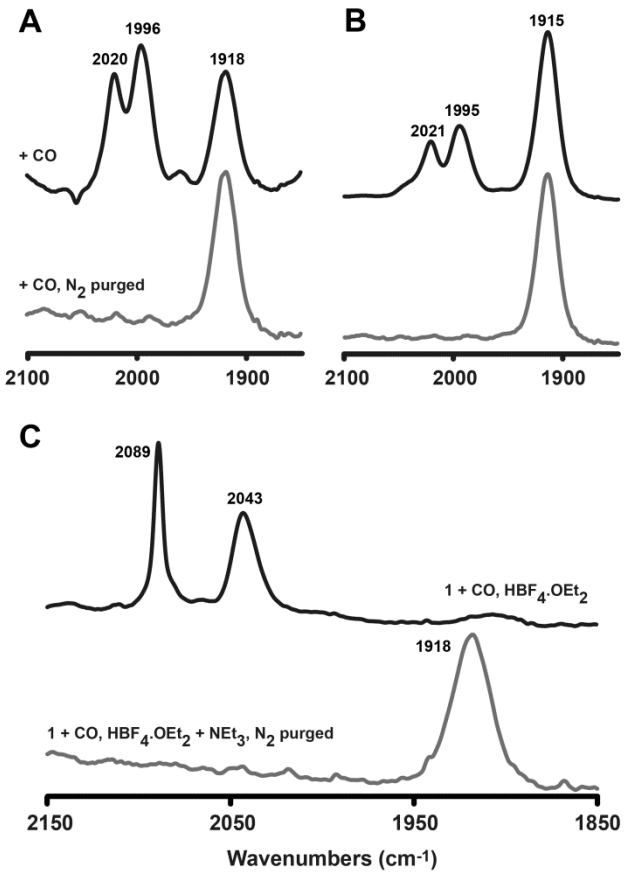

Figure 6-3. Comparative FTIR spectra of 1 and 2 under CO atmosphere. IR spectra in the presence and absence of CO for **1** (A) and **2** (B) in absence of acid. (C) Analogous spectra for **1** in the presence of 3 equiv. HBF_4. Black traces show the IR spectra after bubbling CO through the solutions of the complexes; Grey traces show the IR spectra after purging the solution with nitrogen to remove CO (A and B) and after addition of NEt_3 (C). Spectra were collected in CH_2Cl_2.

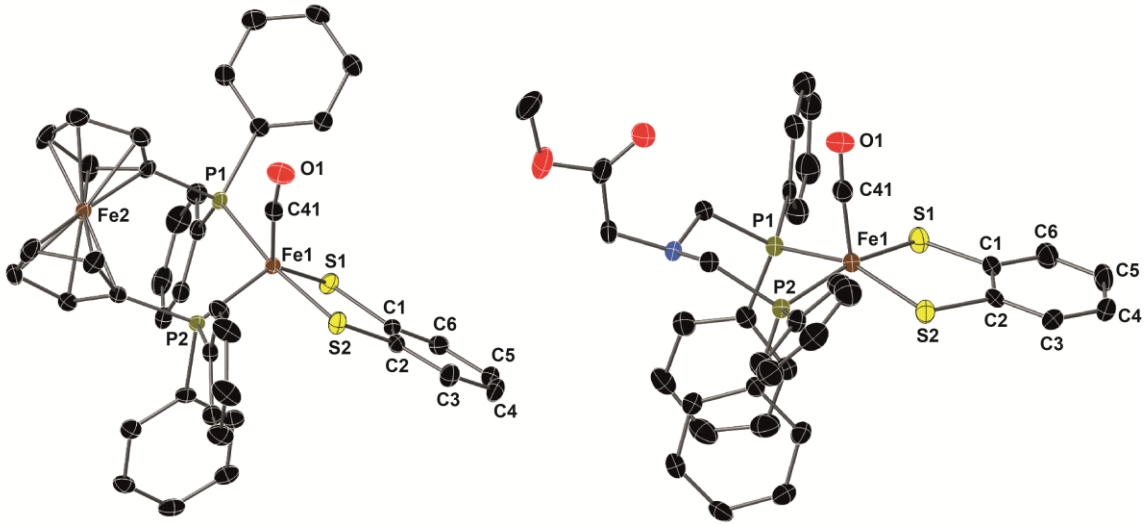

Figure 6-4. X-ray crystal structures of 1 and 2. Molecular Structures of **1** (left) and **2** (right) with thermal ellipsoids drawn at 50% probability level; hydrogen atoms have been omitted for clarity; color code: iron (brown), carbon (black), sulfur (yellow), phosphorus (green), oxygen (red), nitrogen (blue).

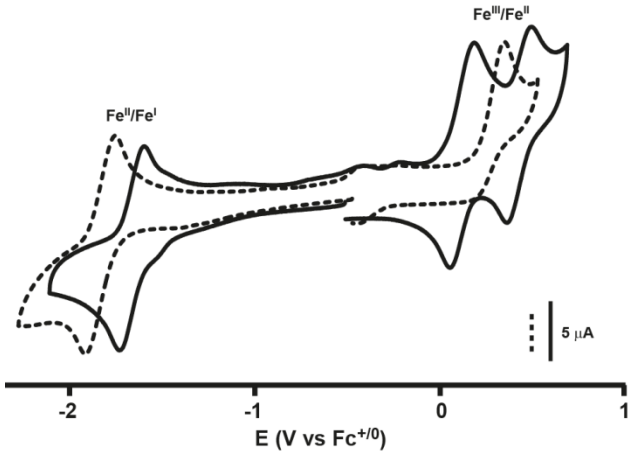

Figure 6-5. Cyclic voltammograms of 1 and 2. Cyclic voltammograms of **1** (solid line; 0.48 mM) and **2** (dashed line; 1.5 mM) in 0.1 M $[NBu_4][PF_6]$/ THF at a scan rate of 0.2 Vs^{-1}.

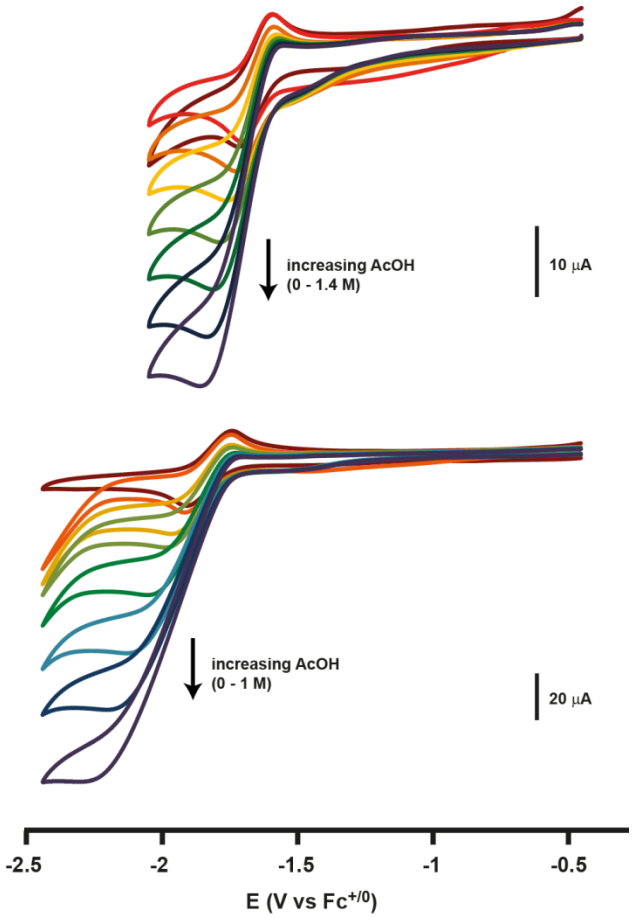

Figure 6-6. Electrocatalytic proton reduction from AcOH by 1 and 2. Cyclic voltammograms of **1** (top; 0.56 mM) and **2** (bottom; 1.25 mM) with various concentrations of acetic acid. The acid concentrations used are 0.2, 0.4, 0.6, 0.8, 1, 1.2, 1.4 M for complex **1** and 0.05, 0.1, 0.2, 0.4, 0.6, 0.8, 1 M for complex **2**. Other experimental conditions are as described in Figure 6-5.

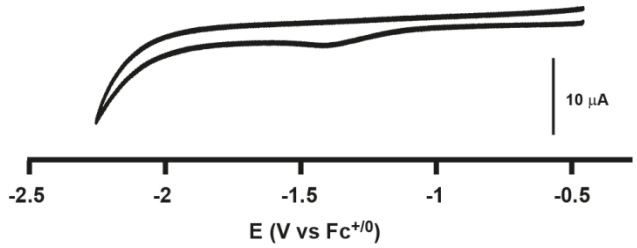

Figure 6-7. Direct reduction of AcOH at the electrode. Cyclic voltammogram of AcOH (1.8 M) in absence of catalysts using glassy carbon electrode. Other experimental conditions are as described in Figure 6-5.

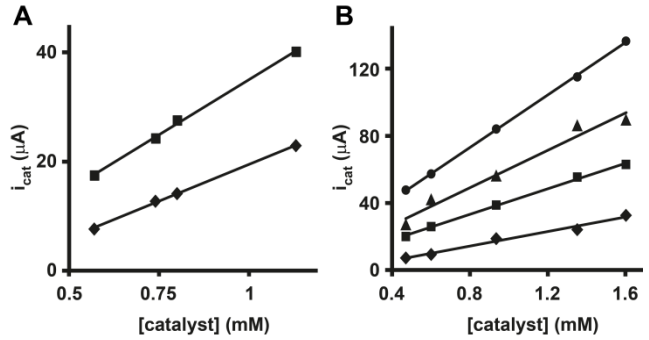

Figure 6-8. Plots of catalytic peak current (i_{cat}) against [catalyst]. Dependence of $\mathbf{i_{cat}}$ on catalyst concentration for (A) **1** and (B) **2** at constant acetic acid concentrations. Other experimental conditions are as described in Figure 6-5 with a scan rate of 0.1 Vs^{-1}. The straight lines shown are the best fit lines. The concentrations of AcOH used: (A) 1 M (♦) and 1.5 M (■); (B) 0.2 M (♦), 0.4 M (■), 0.6 M (▲), and 0.8 M (●).

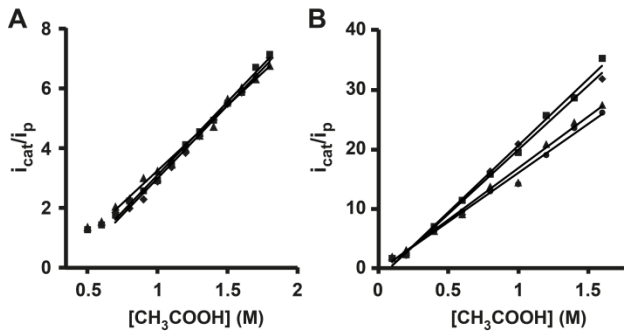

Figure 6-9. Plots of (i_{cat}/i_p) against [AcOH]. Dependence of $\mathbf{i_{cat}/i_p}$ on the concentration of acetic acid added in the experiment of **1** (A) and **2** (B). The straight lines shown are the best fit lines. The catalyst concentrations used: (A) 0.74 mM (■, k = 4.67), 0.8 mM (♦, k = 4.67), and 1.13 mM (▲, k = 3.73); (B) 0.47 mM (♦, k = 91), 0.6 mM (■, k = 96.9), 0.93 mM (▲, k = 58.9), and 1.35 mM (●, k = 53) where k is the trimolecular rate constant. Other experimental conditions are as described in Figure 6-5 with a scan rate of 0.1 Vs^{-1}.

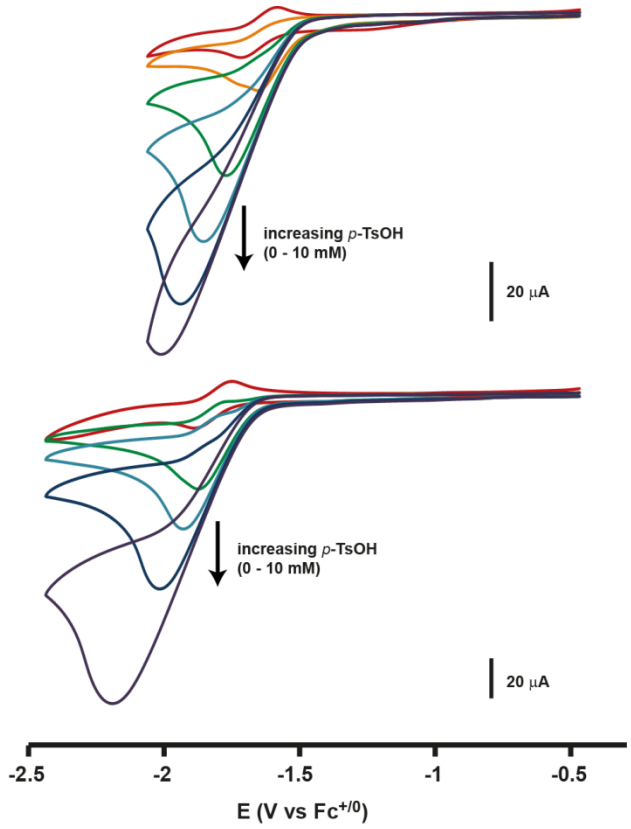

Figure 6-10. Electrocatalytic proton reduction from *p*-TsOH by 1 and 2 Cyclic voltammograms of **1** (top; 0.83 mM) and **2** (bottom; 0.88 mM) in the presence of *p*-TsOH. Acid concentrations are 2, 4, 6, 8, 10 mM for complex **1** and 1, 2, 3, 5, 10 mM for complex **2**. Other experimental conditions are as described in Figure 6-5.

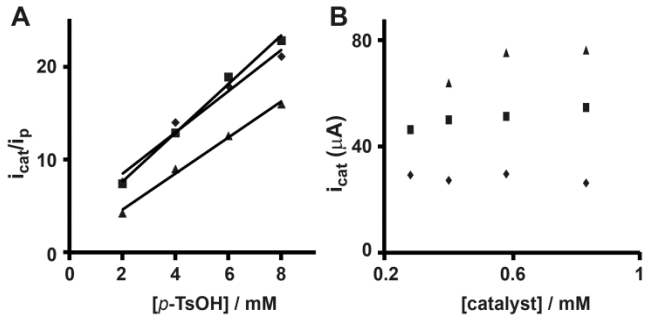

Figure 6-11. Plots of (i_{cat}/i_p) against [*p*-TsOH] and i_{cat} against [1]. (A) Dependence of $\mathbf{i_{cat}/i_p}$ on the concentration of *p*-TsOH added to the solution of **1**; concentration of catalyst used: 0.40 mM (♦), 0.58 mM (■), and 0.83 mM (▲) (B) Dependence of $\boldsymbol{i_{cat}}$ on concentration of **1** at fixed acid concentrations, 2 mM (♦), 4 mM (■), and 6 mM (▲). Other experimental conditions are as described in Figure 6-5 with a scan rate of 0.1 Vs^{-1}.

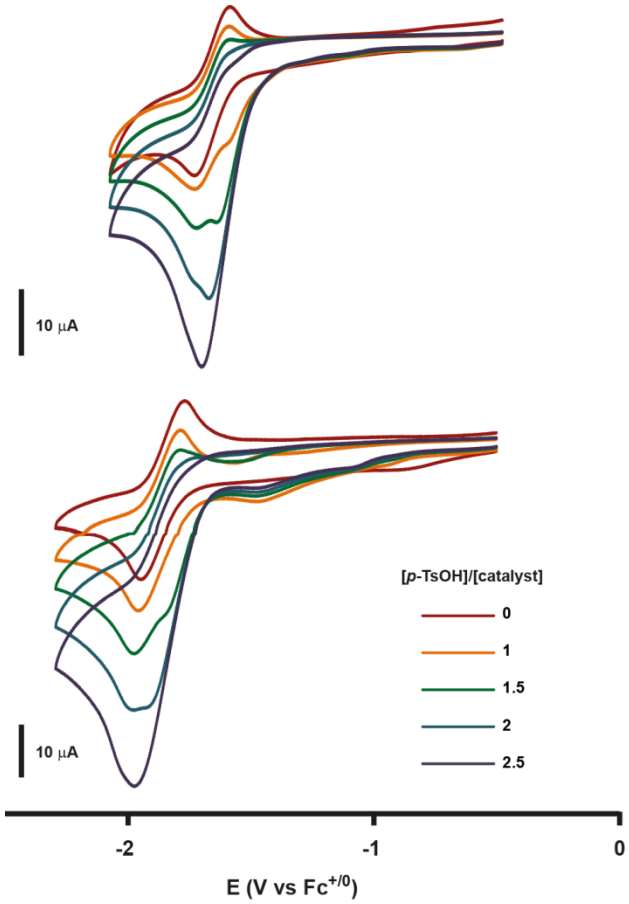

Figure 6-12. Cyclic voltammograms of 1 and 2 in the presence of 0–2.5 equivalents of [*p*-TsOH]. Cyclic voltammograms of **1** (top; 0.95 mM) and **2** (bottom; 1.39 mM) in the presence of varying *p*-TsOH concentrations ([*p*-TsOH]/[**1**] = 0–2.5. Other experimental conditions are as described in Figure 6-5.

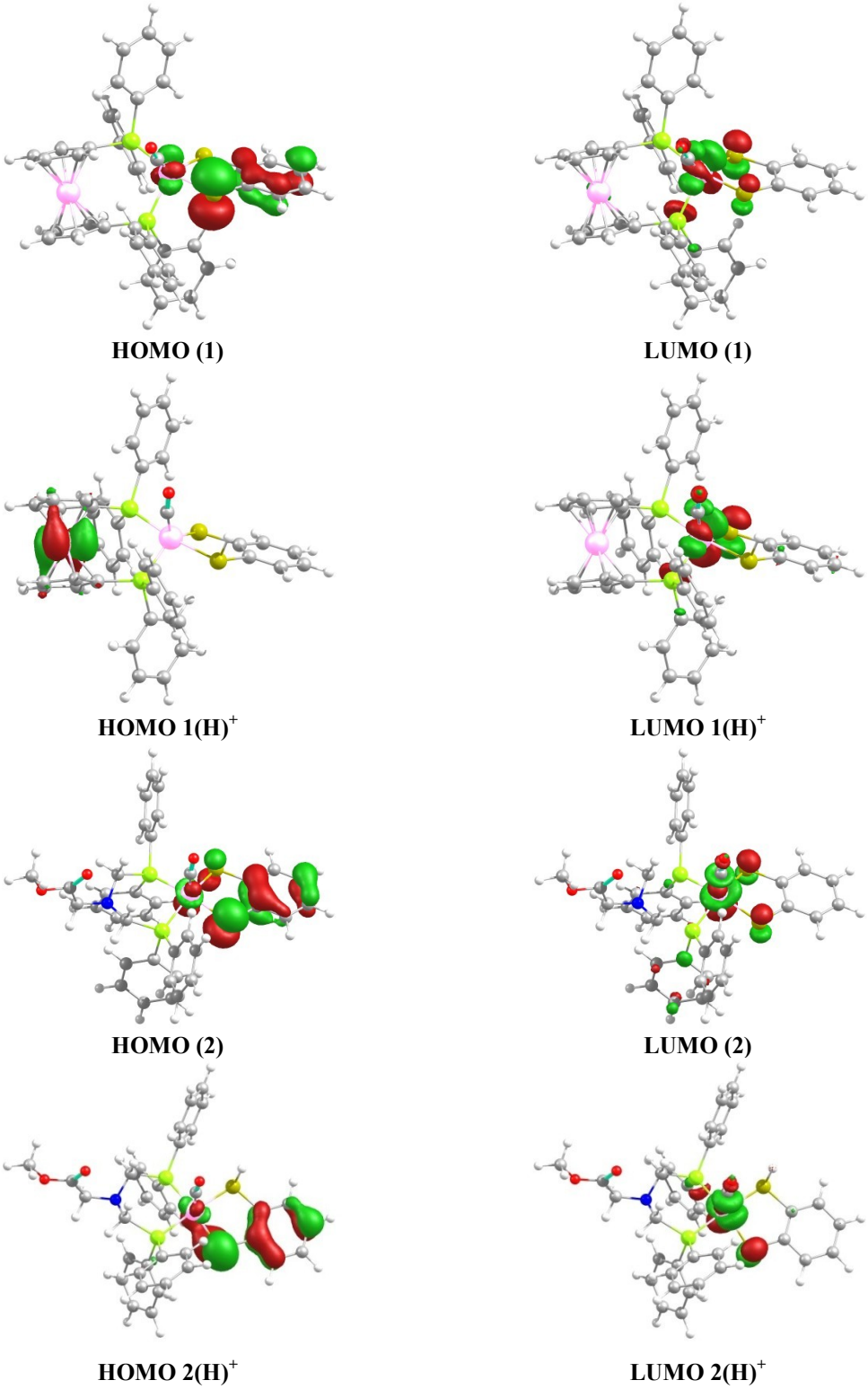

Figure 6-13. Frontier molecular orbitals of 1, 2, 1(H)$^+$ and 2(H)$^+$. Electron density profiles of the HOMOs and LUMOs of **1**, **1(H)**$^+$, **2**, and **2(H)**$^+$.

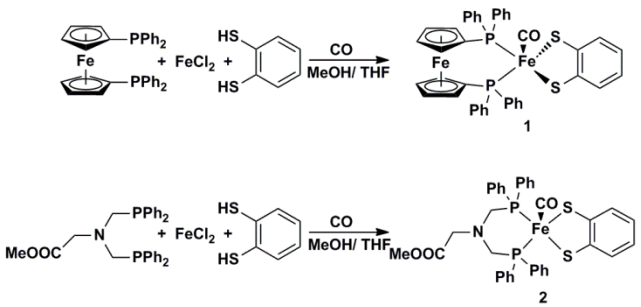

Scheme 6-1. Synthesis of complexes **1** and **2** from $FeCl_2$, the appropriate bis-phosphane ligand, benzene-1,2-dithiol, and CO.

Table 6-1. Selected bond lengths (Å) and bond angles (˚) for **1** and **2**.

Bond lengths	**1**	**2**
Fe1-S1	2.1719(7)	2.2007(12)
Fe1-S2	2.2243(7)	2.1767(12)
Fe1-P1	2.2405(7)	2.2222(12)
Fe1-P2	2.2241(7)	2.2249(12)
Fe1-C41	1.732(3)	1.715(4)
C41-O41	1.162(3)	1.154(5)
Bond angles	**1**	**2**
P2-Fe-P1	101.18(2)	87.49(4)
S1-Fe1-S2	89.21(2)	89.31(4)
C41-Fe1-S1	134.57(8)	101.30(14)
C41-Fe1-S2	88.52(8)	106.58(14)
C41-Fe1-P1	90.19(8)	94.11(14)
C41-Fe1-P2	96.69(8)	93.28(14)
S1-Fe1-P2	128.48(3)	165.14(5)
S2-Fe1-P1	171.74(3)	159.2(5)
O1-C41-Fe1	173.4(2)	176.7(4)

Table 6-2. Bond distances (Å) within the benzene-1,2-dithiolate ligand in complexes **1** and **2**.

Bond lengths	**1**	**2**
C1-C6	1.398(3)	1.412(6)
C1-C2	1.404(3)	1.386(6)
C2-C3	1.410(3)	1.407(6)
C3-C4	1.365(3)	1.373(6)
C4-C5	1.401(4)	1.394(7)
C5-C6	1.380(3)	1.385(6)
C1-S1	1.745(2)	1.746(3)
C2-S2	1.735(2)	1.757(4)

Table 6-3 Selected X-ray crystal data for **1** and **2**

Parameter	**1**	**2**
Empirical formula	$C_{41}H_{32}Fe_2OP_2S_2$	$C_{36}H_{34}FeNO_3P_2S_2$, $CHCl_3$
Formula weight	778.43	828.91
Temperature (K)	123(2)	123.(2)
Wavelength (Å)	0.71073	0.71073
Z	4	4
Crystal system	Monoclinic	Monoclinic
Space group	P1 21/n 1	P1 21/c 1
a (Å)	9.7375(6)	10.9358 (18)
b (Å)	20.8536(13)	19.445(3)
c (Å)	16.8851(11)	17.386(3)
α (°)	90	90
β (°)	95.2680(10)	94.357(2)
γ (°)	90	90
Volume ($Å^3$)	3414.2(4)	3686.4(10)
μ (mm^{-1})	1.100	0.865
Density (g cm^{-3})	1.514	1.494
Goodness-of-fit	1.019	1.070
R_1, wR_2 [$I > 2\sigma(I)$]	0.0296, 0.0653	0.0535, 0.1326
R_1, wR_2 (all data)	0.0460, 0.0714	0.0843, 0.1552

Table 6-4. Experimental half-wave potentials for reduction of AcOH (pKa = 24.42) in THF catalyzed by **1** (0.56 mM) and **2** (1.25 mM), theoretical half-wave potentials in THF, and the overpotentials for **1** and **2**.

[AcOH] C_0/M	Potential ($E_{1/2}$) /V *vs* $Fc^{+/0}$				
	Calculated ($E^T_{1/2}$)	1		2	
		Experimental ($E^E_{1/2}$)	Overpotential ($E^T_{1/2} - E^E_{1/2}$)	Experimental ($E^E_{1/2}$)	Overpotential ($E^T_{1/2} - E^E_{1/2}$)
0.05	-1.454	-	-	-1.832	0.378
0.1	-1.463	-1.633	0.17	-1.84	0.377
0.2	-1.472	-1.647	0.175	-1.853	0.381
0.4	-1.480	-1.653	0.173	-1.864	0.384
0.6	-1.486	-1.662	0.176	-1.88	0.394
0.8	-1.489	-1.68	0.191	-1.902	0.413
1	-1.492	-1.685	0.193	-1.92	0.428
1.2	-1.495	-1.69	0.195	-	-
1.4	-1.497	-1.703	0.203	-	-

Table 6-5. Comparison of selected structural data for **1**, **2**, **1(H)**$^+$, and **2(H)**$^+$ obtained from single crystal X-ray analysis and DFT calculations

Bond lengths (Å) and bond angles (°)	X-ray structure		Calculated (B3LYP/6-31G*)			
	1	**2**	**1**	**2**	**1(H)**$^+$	**2(H)**$^+$
Fe1-S1	2.1719(7)	2.2007(12)	2.218	2.229	2.194	2.357
Fe1-S2	2.2243(7)	2.1767(12)	2.285	2.239	2.386	2.192
Fe1-P1	2.2405(7)	2.2222(12)	2.297	2.263	2.320	2.284
Fe1-P2	2.2241(7)	2.2249(12)	2.256	2.256	2.321	2.288
Fe1-C1	1.732(3)	1.715(4)	1.735	1.706	1.742	1.733
C1-O1	1.162(3)	1.154(5)	1.162	1.165	1.158	1.157
C1-C6	1.398(3)	1.412(6)	1.407	1.411	1.404	1.397
C1-C2	1.404(3)	1.386(6)	1.407	1.409	1.399	1.399
C2-C3	1.410(3)	1.407(6)	1.409	1.409	1.397	1.404
C3-C4	1.365(3)	1.373(6)	1.388	1.391	1.394	1.393
C4-C5	1.401(4)	1.394(7)	1.405	1.407	1.399	1.399
C5-C6	1.380(3)	1.385(6)	1.389	1.391	1.393	1.394
C1-S1	1.745(2)	1.746(3)	1.764	1.757	1.780	1.794
C2-S2	1.735(2)	1.757(4)	1.757	1.758	1.794	1.781
P2-Fe-P1	101.18(2)	87.49(4)	102.4	89.3	100.8	92.9
S1-Fe1-S2	89.21(2)	89.31(4)	88.4	89.3	87.2	86.9
C1-Fe1-S1	134.57(8)	101.30(14)	137.9	102.4	130.4	93.3
C1-Fe1-S2	88.52(8)	106.58(14)	86.3	99.1	89.4	119.5
C1-Fe1-P1	90.19(8)	94.11(14)	89.9	96.0	89.5	92.8
C1-Fe1-P2	96.69(8)	93.28(14)	97.0	97.9	96.3	93.8
S1-Fe1-P2	128.48(3)	165.14(5)	124.7	159.7	132.9	172.6
S2-Fe1-P1	171.74(3)	159.2(5)	168.8	164.9	171.8	147.6
O1-C1-Fe1	173.4(2)	176.7(4)	172.6	173.4	170.5	173.0

Table 6-6. Orbital contributions (%) and overlap populations of different fragments of **1**, **1(H)**$^+$, **2**, and **2(H)**$^+$ to the corresponding HOMOs and LUMOs

Atoms or molecular fragments		HOMO (energy, eV)				LUMO (energy, eV)			
		1 (-4.79)	**1(H) (-8.16)**	**2 (-4.81)**	**2(H) (-8.47)**	**1 (-1.72)**	**1(H) (-5.06)**	**2 (-1.48)**	**2(H) (-4.96)**
Fe1	*s*	0	0	0	1	1	0	0	0
	p	3	0	5	3	4	8	7	9
	d_{z^2}	10	0	11	6	11	23	21	36
	dxz	3	0	0	0	2	3	22	10
	dyz	0	0	1	1	12	9	0	2
	$d_{x^2-y^2}$	0	0	0	1	22	19	0	0
	d_{xy}	6	0	0	1	4	0	0	4
	Total *d*	19	0	12	9	51	55	43	52
Fe2 (ferrocene)	*s*	0	0	-	-	0	0	-	-
	p	0	0	-	-	0	0	-	-
	d	0	79	-	-	1	1	-	-
S1	*s*	0	0	0	0	0	0	0	0
	p	0	0	9	1	8	9	8	2
	d	0	0	0	0	0	0	0	0
S2	*s*	0	0	0	0	0	0	0	0
	p	41	0	26	37	6	1	7	10
	d	0	0	0	0	0	0	0	0
CO	*s*	0	0	0	0	1	2	4	4
	p	0	0	1	1	2	2	2	2
	d	0	0	0	0	0	0	0	0
P1	*s*	0	0	0	0	0	0	0	0
	p	1	0	2	1	2	2	4	5
	d	0	0	0	0	0	0	1	0
P2	*s*	0	0	0	0	1	0	0	0
	p	0	0	1	1	7	6	4	3
	d	0	0	0	0	1	0	1	0
Phenyl ring (bdt)	Total	32	0	40	39	5	5	4	5
Cp rings of dppf (**1**)/ NP_2 ligand (**2**)	Total	0	20	0	0	2	1	0	0
Phenyl rings (PPh_2)	Total	2	1	3	7	9	5	16	5
Proton (H)	Total	-	0	-	0	-	1	-	1
Overlap Populations									
Fe1-S1		0.00	0.00	0.02	-0.01	-0.08	-0.08	-0.07	0.02
Fe1-S2		0.02	0.00	0.04	0.04	-0.04	0.01	-0.07	-0.08
Fe-C		0.00	0.00	-0.01	-0.01	0.02	0.00	0.00	0.01
Fe-P1		0.03	0.00	0.02	0.01	0.00	0.04	0.05	0.03
Fe-P2		0.00	0.00	0.01	0.01	-0.04	0.02	0.05	0.04

Table 6-7. Comparison of the optimized geometries of **2** evaluated using different functionals and basis sets with the experimentally obtained geometry.

Bond lengths (Å) and bond angles (°)	**X-ray**	**BP86/ 6-31G***	**BP86/ TZVPP**	**TPPS/ 6-31G***	**TPPS/ TZVPP**	**B3LYP/ 6-31G***
Fe1-S1	2.201	2.211	2.211	2.208	2.206	2.227
Fe1-S2	2.177	2.202	2.199	2.206	2.198	2.222
Fe1-P1	2.225	2.232	2.230	2.229	2.229	2.292
Fe1-P2	2.222	2.237	2.236	2.229	2.224	2.285
Fe1-C1	1.715	1.709	1.711	1.716	1.716	1.723
C1-O1	1.154	1.185	1.173	1.182	1.170	1.164
P2-Fe-P1	87.5	91.1	90.1	89.0	88.9	91.1
S1-Fe-S2	89.3	88.8	88.8	89.1	89.0	88.9
C1-Fe-S1	101.3	101.5	101.5	102.3	101.8	100.0
C1-Fe-S2	106.6	106.8	105.8	104.6	105.1	103.3
C1-Fe-P1	94.1	94.8	96.1	95.2	95.8	96.7
C1-Fe-P2	93.3	94.1	93.4	94.4	94.3	94.6
S1-Fe-P2	165.1	163.7	165.1	162.2	163.9	163.3
S2-Fe-P1	159.2	159.1	158.1	161.0	159.0	162.1
O1-C1-Fe	176.7	175.8	175.5	175.9	175.7	175.9

References

1. Armstrong, F. A. *Science* **2013,** *339*, 658.

2. Vignais, P. M.; Billoud, B. *Chem. Rev.* **2007,** *107*, 4206.

3. Tard, C. d.; Pickett, C. J. *Chem. Rev.* **2009,** *109*, 2245.

4. Volbeda, A.; Charon, M.-H.; Piras, C.; Hatchikian, E. C.; Frey, M.; Fontecilla-Camps, J. C. *Nature* **1995,** *373*, 580.

5. Peters, J. W.; Lanzilotta, W. N.; Lemon, B. J.; Seefeldt, L. C. *Science* **1998,** *282*, 1853.

6. Nicolet, Y.; Piras, C.; Legrand, P.; Hatchikian, C. E.; Fontecilla-Camps, J. C. *Structure* **1999,** *7*, 13.

7. Happe, R. P.; Roseboom, W.; Pierik, A. J.; Albracht, S. P. J.; Bagley, K. A. *Nature* **1997,** *385*, 126.

8. Evans, D. J.; Pickett, C. J. *Chem. Soc. Rev.* **2003,** *32*, 268.

9. Jones, A. K.; Sillery, E.; Albracht, S. P. J.; Armstrong, F. A. *Chem. Commun.* **2002**, 866.

10. Madden, C.; Vaughn, M. D.; Diez-Perez, I.; Brown, K. A.; King, P. W.; Gust, D.; Moore, A. L.; Moore, T. A. *J. Am. Chem. Soc.* **2012,** *134*, 1577.

11. Felton, G. A. N.; Mebi, C. A.; Petro, B. J.; Vannucci, A. K.; Evans, D. H.; Glass, R. S.; Lichtenberger, D. L. *J. Organomet. Chem.* **2009,** *694*, 2681.

12. Gloaguen, F.; Rauchfuss, T. B. *Chem. Soc. Rev.* **2009,** *38*, 100.

13. Darensbourg, M. Y.; Lyon, E. J.; Zhao, X.; Georgakaki, I. P. *Proc. Natl. Acad. Sci. USA* **2003,** *100*, 3683.

14. Siegbahn, P. E. M.; Tye, J. W.; Hall, M. B. *Chem. Rev.* **2007,** *107*, 4414.

15. Armstrong, F. A. *Curr. Opin. Chem. Biol.* **2004,** *8*, 133.

16. Darensbourg, D. J.; Reibenspies, J. H.; Lai, C.-H.; Lee, W.-Z.; Darensbourg, M. Y. *J. Am. Chem. Soc.* **1997,** *119*, 7903.

17. Hsu, H.-F.; Koch, S. A.; Popescu, C. V.; M√ºnck, E. *J. Am. Chem. Soc.* **1997,** *119*, 8371.

18. Lai, C.-H.; Lee, W.-Z.; Miller, M. L.; Reibenspies, J. H.; Darensbourg, D. J.; Darensbourg, M. Y. *J. Am. Chem. Soc.* **1998,** *120*, 10103.

19. Liaw, W.-F.; Lee, N.-H.; Chen, C.-H.; Lee, C.-M.; Lee, G.-H.; Peng, S.-M. *J. Am. Chem. Soc.* **2000,** *122*, 488.

20. Liu, T.; Li, B.; Popescu, C. V.; Bilko, A.; Pérez, L. M.; Hall, M. B.; Darensbourg, M. Y. *Chem. Eur. J.* **2010,** *16*, 3083.

21. Shima, S.; Pilak, O.; Vogt, S.; Schick, M.; Stagni, M. S.; Meyer-Klaucke, W.; Warkentin, E.; Thauer, R. K.; Ermler, U. *Science* **2008,** *321*, 572.

22. Beyler, M.; Ezzaher, S.; Karnahl, M.; Santoni, M.-P.; Lomoth, R.; Ott, S. *Chem. Commun.* **2011,** *47*, 11662.

23. Gardner, J. M.; Beyler, M.; Karnahl, M.; Tschierlei, S.; Ott, S.; Hammarstrom, L. *J. Am. Chem. Soc.* **2012,** *134*, 19322.

24. Bandoli, G.; Dolmella, A. *Coord. Chem. Rev.* **2000,** *209*, 161.

25. Bandoli, G.; Trovo, G.; Dolmella, A.; Longato, B. *Inorg. Chem.* **1992,** *31*, 45.

26. Butler, I. R.; Cullen, W. R.; Kim, T. J.; Rettig, S. J.; Trotter, J. *Organometallics* **1985,** *4*, 972.

27. Longato, B.; Pilloni, G.; Valle, G.; Corain, B. *Inorg. Chem.* **1988,** *27*, 956.

28. Durran, S. E.; Elsegood, M. R. J.; Hawkins, N.; Smith, M. B.; Talib, S. *Tetrahedron Lett.* **2003,** *44*, 5255.

29. Addison, A. W.; Rao, T. N.; Reedijk, J.; van Rijn, J.; Verschoor, G. C. *J. Chem. Soc., Dalton Trans.* **1984**, 1349.

30. Nguyen, D. H.; Hsu, H.-F.; Millar, M.; Koch, S. A.; Achim, C.; Bominaar, E. L.; Munck, E. *J. Am. Chem. Soc.* **1996,** *118*, 8963.

31. Hsu, H.-F.; Koch, S. A.; Popescu, C. V.; Munck, E. *J. Am. Chem. Soc.* **1997,** *119*, 8371.

32. Ray, K.; Begum, A.; Weyhermuller, T.; Piligkos, S.; van Slageren, J.; Neese, F.; Wieghardt, K. *J. Am. Chem. Soc.* **2005,** *127*, 4403.

33. Ray, K.; Bill, E.; Weyhermuller, T.; Wieghardt, K. *J. Am. Chem. Soc.* **2005,** *127*, 5641.

34. Ray, K.; Weyhermuller, T.; Goossens, A.; Craje, M. W. J.; Wieghardt, K. *Inorg. Chem.* **2003,** *42*, 4082.

35. Bachler, V.; Olbrich, G.; Neese, F.; Wieghardt, K. *Inorg. Chem.* **2002,** *41*, 4179.

36. Takacs, J.; Marko, L.; Parkanyi, L. *J. Organomet. Chem.* **1989,** *361*, 109.

37. Waters, T.; Wang, X.-B.; Woo, H.-K.; Wang, L.-S. *Inorg. Chem.* **2006,** *45*, 5841.

38. Benedito, F. L.; Petrenko, T.; Bill, E.; Weyhermuller, T.; Wieghardt, K. *Inorg. Chem.* **2009,** *48*, 10913.

39. Solis, B. H.; Hammes-Schiffer, S. *J. Am. Chem. Soc.* **2012,** *134*, 15253.

40. Heiden, Z. M.; Gorecki, B. J.; Rauchfuss, T. B. *Organometallics* **2008,** *27*, 1542.

41. Corain, B.; Longato, B.; Favero, G.; Ajo, D.; Pilloni, G.; Russo, U.; Kreissl, F. R. *Inorg. Chim. Acta* **1989,** *157*, 259.

42. Pilloni, G.; Longato, B.; Corain, B. *J. Organomet. Chem.* **1991,** *420*, 57.

43. Felton, G. A. N.; Glass, R. S.; Lichtenberger, D. L.; Evans, D. H. *Inorg. Chem.* **2006,** *45*, 9181.

44. Felton, G. A. N.; Vannucci, A. K.; Chen, J.; Lockett, L. T.; Okumura, N.; Petro, B. J.; Zakai, U. I.; Evans, D. H.; Glass, R. S.; Lichtenberger, D. L. *J. Am. Chem. Soc.* **2007,** *129*, 12521.

45. Fourmond, V.; Jacques, P.-A.; Fontecave, M.; Artero, V. *Inorg. Chem.* **2010,** *49*, 10338.

46. Helm, M. L.; Stewart, M. P.; Bullock, R. M.; DuBois, M. R.; DuBois, D. L. *Science* **2011,** *333*, 863.

47. Ray, K.; Weyhermuller, T.; Neese, F.; Wieghardt, K. *Inorg. Chem.* **2005,** *44*, 5345.

48. Ray, K.; Petrenko, T.; Wieghardt, K.; Neese, F. *Dalton Trans.* **2007**, 1552.

49. Kubas, G. J. *Chem. Rev.* **2007,** *107*, 4152.

50. Francl, M. M.; Pietro, W. J.; Hehre, W. J.; Binkley, J. S.; Gordon, M. S.; DeFrees, D. J.; Pople, J. A. *J. Chem. Phys.* **1982,** *77*, 3654.

51. Lee, C.; Yang, W.; Parr, R. G. *Phys. Rev. B* **1988,** *37*, 785.

52. Becke, A. D. *J. Chem. Phys.* **1993,** *98*, 5648.

53. Stephens, P. J.; Devlin, F. J.; Chabalowski, C. F.; Frisch, M. J. *J. Phys. Chem.* **1994,** *98*, 11623.

54. Rassolov, V. A.; Pople, J. A.; Ratner, M. A.; Windus, T. L. *J. Chem. Phys.* **1998,** *109*, 1223.

55. Brothers, S. M.; Darensbourg, M. Y.; Hall, M. B. *Inorg. Chem.* **2011,** *50*, 8532.

56. Neese, F. *WIREs Comput. Mol. Sci.* **2012,** *2*, 73.

57. Ye, S.; Neese, F. *Inorg. Chem.* **2010,** *49*, 772.

58. Daniele, S.; Ugo, P.; Mazzocchin, G.-A.; Bontempelli, G. *Anal. Chim. Acta* **1985,** *173*, 141.

59. Brunner, E. *J. Chem. Eng. Data* **1985,** *30*, 269.

REFERENCES

1. Adams, M. W. W.; Stiefel, E. I., *Science* **1998,** 282, 1842-1843.

2. Peters, J. W.; Lanzilotta, W. N.; Lemon, B. J.; Seefeldt, L. C., *Science* **1998,** 282, 1853-1858.

3. Cammack, R., *Nature* **1999,** 397, 214-215.

4. Lyon, E. J.; Georgakaki, I. P.; Reibenspies, J. H.; Darensbourg, M. Y., *Angew. Chem. Int. Ed.* **1999,** 38, 3178-3180.

5. Nicolet, Y.; Piras, C.; Legrand, P.; Hatchikian, C. E.; Fontecilla-Camps, J. C., *Structure* **1999,** 7, 13-23.

6. Peters, J. W.; Lanzilotta, W. N.; Lemon, B. J.; Seefeldt, L. C., *J. Inorg. Biochem.* **1999,** 74, 44-44.

7. Gloaguen, F. d. r.; Lawrence, J. D.; Rauchfuss, T. B., *J. Am. Chem. Soc.* **2001,** 123, 9476-9477.

8. Frey, M., *Chembiochem* **2002,** 3, 153-160.

9. Chong, D. S.; Georgakaki, I. P.; Mejia-Rodriguez, R.; Samabria-Chinchilla, J.; Soriaga, M. P.; Darensbourg, M. Y., *Dalton Trans.* **2003**, 4158-4163.

10. Mejia-Rodriguez, R.; Chong, D.; Reibenspies, J. H.; Soriaga, M. P.; Darensbourg, M. Y., *J. Am. Chem. Soc.* **2004,** 126, 12004-12014.

11. Li, P.; Wang, M.; He, C.; Li, G.; Liu, X.; Chen, C.; Åkermark, B.; Sun, L., *Eur. J. Inorg. Chem.* **2005,** 2005, 2506-2513.

12. Tye, J. W.; Lee, J.; Wang, H. W.; Mejia-Rodriguez, R.; Reibenspies, J. H.; Hall, M. B.; Darensbourg, M. Y., *Inorg. Chem.* **2005,** 44, 5550-5552.

13. Na, Y.; Wang, M.; Jin, K.; Zhang, R.; Sun, L., *J. Organomet. Chem.* **2006,** 691, 5045-5051.

14. Tye, J. W.; Darensbourg, M. Y.; Hall, M. B., *Inorg. Chem.* **2006,** 45, 1552-1559.

15. Capon, J.-F.; Ezzaher, S.; Gloaguen, F.; Petillon, F. Y.; Schollhammer, P.; Talarmin, J.; Davin, T. J.; McGrady, J. E.; Muir, K. W., *New J. Chem.* **2007,** 31, 2052-2064.

16. Jones, A. K.; Lichtenstein, B. R.; Dutta, A.; Gordon, G.; Dutton, P. L., *J. Am. Chem. Soc.* **2007,** 129, 14844-14845.

17. Barton, B. E.; Rauchfuss, T. B., *Inorg. Chem.* **2008,** 47, 2261-2263.

18. Pandey, A. S.; Harris, T. V.; Giles, L. J.; Peters, J. W.; Szilagyi, R. K., *J. Am. Chem. Soc.* **2008,** 130, 4533-4540.

19. Song, L.-C.; Wang, H.-T.; Ge, J.-H.; Mei, S.-Z.; Gao, J.; Wang, L.-X.; Gai, B.; Zhao, L.-Q.; Yan, J.; Wang, Y.-Z., *Organometallics* **2008,** 27, 1409-1416.

20. Capon, J.-F.; Gloaguen, F.; Petillon, F. Y.; Schollhammer, P.; Talarmin, J., *Coord. Chem. Rev.* **2009,** 253, 1476-1494.

21. Felton, G. A. N.; Mebi, C. A.; Petro, B. J.; Vannucci, A. K.; Evans, D. H.; Glass, R. S.; Lichtenberger, D. L., *J. Organomet. Chem.* **2009,** 694, 2681-2699.

22. Gloaguen, F.; Rauchfuss, T. B., *Chem. Soc. Rev.* **2009,** 38, 100-108.

23. Green, K. N.; Hess, J. L.; Thomas, C. M.; Darensbourg, M. Y., *Dalton Trans.* **2009**, 4344-4350.

24. Tard, C. d.; Pickett, C. J., *Chem. Rev.* **2009,** 109, 2245-2274.

25. Apfel, U.-P.; Rudolph, M.; Apfel, C.; Robl, C.; Langenegger, D.; Hoyer, D.; Jaun, B.; Ebert, M.-O.; Alpermann, T.; Seebach, D.; Weigand, W., *Dalton Trans.* **2010,** 39, 3065-3071.

26. Jablonskyte, A.; Wright, J. A.; Pickett, C. J., *Dalton Trans.* **2010,** 39, 3026-3034.

27. Nanda, V.; Koder, R. L., *Nat. Chem.* **2010,** 2, 15-24.

28. Singleton, M. L.; Reibenspies, J. H.; Darensbourg, M. Y., *J. Am. Chem. Soc.* **2010,** 132, 8870-8871.

29. Surawatanawong, P.; Tye, J. W.; Darensbourg, M. Y.; Hall, M. B., *Dalton Trans.* **2010,** 39, 3093-3104.

30. Roy, S.; Shinde, S.; Hamilton, G. A.; Hartnett, H. E.; Jones, A. K., *Eur. J. Inorg. Chem.* **2011,** 2011, 1050-1055.

31. Sano, Y.; Onoda, A.; Hayashi, T., *Chem. Commun.* **2011,** 47, 8229-8231.

32. Singleton, M. L.; Crouthers, D. J.; Duttweiler, R. P., III; Reibenspies, J. H.; Darensbourg, M. Y., *Inorg. Chem.* **2011,** 50, 5015-5026.

33. Tschierlei, S.; Ott, S.; Lomoth, R., *Energy Environ. Sci.* **2011,** 4, 2340-2352.

34. Frederix, P. W. J. M.; Kania, R.; Wright, J. A.; Lamprou, D. A.; Ulijn, R. V.; Pickett, C. J.; Hunt, N. T., *Dalton Trans.* **2012,** 41, 13112-13119.

35. Sano, Y.; Onoda, A.; Hayashi, T., *J. Inorg. Biochem.* **2012,** 108, 159-162.

36. Zhao, J.; Wei, Z.; Zeng, X.; Liu, X., *Dalton Trans.* **2012,** 41, 11125-11133.

37. Berggren, G.; Adamska, A.; Lambertz, C.; Simmons, T. R.; Esselborn, J.; Atta, M.; Gambarelli, S.; Mouesca, J. M.; Reijerse, E.; Lubitz, W.; Happe, T.; Artero, V.; Fontecave, M., *Nature* **2013,** 499, 66-69.

38. Lemon, B. J.; Peters, J. W., *Biochemistry* **1999,** 38, 12969-12973.

39. Nicolet, Y.; Piras, C.; Legrand, P.; Hatchikian, C. E.; Fontecilla-Camps, J. C., *Structure* **1999,** 7, 13-23.

40. Pierik, A. J.; Roseboom, W.; Happe, R. P.; Bagley, K. A.; Albracht, S. P. J., *J. Biol. Chem.* **1999,** 274, 3331-3337.

41. Cammack, R.; Frey, M.; Robson, R., *Hydrogen as a Fuel: Learning from Nature*. Talor & Francis: London & New York, 2001.

42. Jones, A. K.; Sillery, E.; Albracht, S. P. J.; Armstrong, F. A., *Chem. Commun.* **2002**, 866-867.

43. Armstrong, F. A., *Curr. Opin. Chem. Biol.* **2004,** 8, 133-140.

44. Tard, C.; Liu, X.; Ibrahim, S. K.; Bruschi, M.; Gioia, L. D.; Davies, S. C.; Yang, X.; Wang, L.-S.; Sawers, G.; Pickett, C. J., *Nature* **2005,** 433, 610-613.

45. Felton, G. A. N.; Glass, R. S.; Lichtenberger, D. L.; Evans, D. H., *Inorg. Chem.* **2006,** 45, 9181-9184.

46. De Lacey, A. L.; Fernandez, V. M.; Rousset, M.; Cammack, R., *Chem. Rev.* **2007,** 107, 4304-4330.

47. Fontecilla-Camps, J. C.; Volbeda, A.; Cavazza, C.; Nicolet, Y., *Chem. Rev.* **2007,** 107, 4273-4303.

48. Justice, A. K.; Rauchfuss, T. B.; Wilson, S. R., *Angew. Chem. Int. Ed.* **2007,** 46, 6152-6154.

49. Kubas, G. J., *Chem. Rev.* **2007,** 107, 4152-4205.

50. Liu, T.; Darensbourg, M. Y., *J. Am. Chem. Soc.* **2007,** 129, 7008-7009.

51. Siegbahn, P. E. M.; Tye, J. W.; Hall, M. B., *Chem. Rev.* **2007,** 107, 4414-4435.

52. Vignais, P. M.; Billoud, B., *Chem. Rev.* **2007,** 107, 4206-4272.

53. Bruschi, M.; Greco, C.; Fantucci, P.; Gioia, L. D., *Inorg. Chem.* **2008,** 47, 6056-6071.

54. Olsen, M. T.; Barton, B. E.; Rauchfuss, T. B., *Inorg. Chem.* **2009,** 48, 7507-7509.

55. Si, Y.; Charreteur, K.; Capon, J.-F.; Gloaguen, F.; Petillon, F. Y.; Schollhammer, P.; Talarmin, J., *J. Inorg. Biochem.* **2010,** 104, 1038-1042.

56. Camara, J. M.; Rauchfuss, T. B., *J. Am. Chem. Soc.* **2011,** 133, 8098-8101.

57. Camara, J. M.; Rauchfuss, T. B., *Nat. Chem.* **2012,** 4, 26-30.

58. Roy, S.; Groy, T. L.; Jones, A. K., *Dalton Trans.* **2013,** 42, 3843-3853.

59. Ray, K.; Weyhermuller, T.; Goossens, A.; Craje, M. W. J.; Wieghardt, K., *Inorg. Chem.* **2003,** 42, 4082-4087.

60. Ray, K.; Bill, E.; Weyhermuller, T.; Wieghardt, K., *J. Am. Chem. Soc.* **2005,** 127, 5641-5654.

61. Hambourger, M.; Gervaldo, M.; Svedruzic, D.; King, P. W.; Gust, D.; Ghirardi, M.; Moore, A. L.; Moore, T. A., *J. Am. Chem. Soc.* **2008,** 130, 2015-2022.

62. Shima, S.; Pilak, O.; Vogt, S.; Schick, M.; Stagni, M. S.; Meyer-Klaucke, W.; Warkentin, E.; Thauer, R. K.; Ermler, U., *Science* **2008,** 321, 572-575.

63. Fourmond, V.; Jacques, P.-A.; Fontecave, M.; Artero, V., *Inorg. Chem.* **2010,** 49, 10338-10347.

64. Liu, T.; Li, B.; Popescu, C. V.; Bilko, A.; Pérez, L. M.; Hall, M. B.; Darensbourg, M. Y., *Chem. Eur. J.* **2010,** 16, 3083-3089.

65. Beyler, M.; Ezzaher, S.; Karnahl, M.; Santoni, M.-P.; Lomoth, R.; Ott, S., *Chem. Commun.* **2011,** 47, 11662-11664.

66. Brothers, S. M.; Darensbourg, M. Y.; Hall, M. B., *Inorg. Chem.* **2011,** 50, 8532-8540.

67. Erdem, Ö. F.; Schwartz, L.; Stein, M.; Silakov, A.; Kaur-Ghumaan, S.; Huang, P.; Ott, S.; Reijerse, E. J.; Lubitz, W., *Angew. Chem. Int. Ed.* **2011,** 50, 1439-1443.

68. Ray, K.; Begum, A.; Weyhermuller, T.; Piligkos, S.; van Slageren, J.; Neese, F.; Wieghardt, K., *J. Am. Chem. Soc.* **2005,** 127, 4403-4415.

69. Ray, K.; Weyhermuller, T.; Neese, F.; Wieghardt, K., *Inorg. Chem.* **2005,** 44, 5345-5360.

70. Schwab, D. E.; Tard, C.; Brecht, E.; Peters, J. W.; Pickett, C. J.; Szilagyi, R. K., *Chem. Commun.* **2006,** 0, 3696-3698.

71. Ray, K.; Petrenko, T.; Wieghardt, K.; Neese, F., *Dalton Trans.* **2007**, 1552-1566.

72. De Lacey, A. L.; Stadler, C.; Cavazza, C.; Hatchikian, E. C.; Fernandez, V. M., *J. Am. Chem. Soc.* **2000,** 122, 11232-11233.

73. Armentano, D.; de Munno, G.; Guerra, F.; Faus, J.; Lloret, F.; Julve, M., *Dalton Trans.* **2003**, 4626-4634.

74. Darensbourg, M. Y.; Lyon, E. J.; Zhao, X.; Georgakaki, I. P., *Proc. Natl. Acad. Sci. USA* **2003,** 100, 3683-3688.

75. Bruschi, M.; Fantucci, P.; De Gioia, L., *Inorg. Chem.* **2004,** 43, 3733-3741.

76. Compton, R., *Angew. Chem. Int. Ed.* **2007,** 46, 1367-1367.

77. Adam, F. I.; Hogarth, G.; Kabir, S. E.; Richards, D., *C. R. Chimie* **2008,** 11, 890-905.

78. Ezzaher, S.; Capon, J.-F.; Dumontet, N.; Gloaguen, F.; Petillon, F. Y.; Schollhammer, P.; Talarmin, J., *J. Electroanal. Chem.* **2009,** 626, 161-170.

79. Ezzaher, S.; Capon, J.-F.; Gloaguen, F.; Petillon, F. Y.; Schollhammer, P.; Talarmin, J.; Kervarec, N., *Inorg. Chem.* **2009,** 48, 2-4.

80. Heinekey, D. M., *J. Organomet. Chem.* **2009,** 694, 2671-2680.

81. Chouffai, D.; Zampella, G.; Capon, J.-F.; De Gioia, L.; Le Goff, A.; Petillon, F. Y.; Schollhammer, P.; Talarmin, J., *Organometallics* **2012,** 31, 1082-1091.

82. Gao, S.; Fan, J.; Sun, S.; Song, F.; Peng, X.; Duan, Q.; Jiang, D.; Liang, Q., *Dalton Trans.* **2012,** 41, 12064-12074.

83. Liu, Y.-C.; Yen, T.-H.; Tseng, Y.-J.; Hu, C.-H.; Lee, G.-H.; Chiang, M.-H., *Inorg. Chem.* **2012,** 51, 5997-5999.

84. Palmer, R. A.; Piper, T. S., *Inorg. Chem.* **1966,** 5, 864-&.

85. Capon, J.-F.; Gloaguen, F.; Petillon, F. Y.; Schollhammer, P.; Talarmin, J., *Eur. J. Inorg. Chem.* **2008**, 4671-4681.

86. Ezzaher, S.; Capon, J.-F.; Gloaguen, F.; Kervarec, N.; Petillon, F. Y.; Pichon, R.; Schollhammer, P.; Talarmin, J., *Comptes Rendus Chimie* **2008,** 11, 906-914.

87. Justice, A. K.; De Gioia, L.; Nilges, M. J.; Rauchfuss, T. B.; Wilson, S. R.; Zampella, G., *Inorg. Chem.* **2008,** 47, 7405-7414.

88. Irwin, M.; Jenkins, R. K.; Denning, M. S.; Kraemer, T.; Grandjean, F.; Long, G. J.; Herchel, R.; McGrady, J. E.; Goicoechea, J. M., *Inorg. Chem.* **2010,** 49, 6160-6171.

89. Chouffai, D.; Zampella, G.; Capon, J.-F.; De Gioia, L.; Gloaguen, F.; Petillon, F. Y.; Schollhammer, P.; Talarmin, J., *Inorg. Chem.* **2011,** 50, 12575-12585.

90. Roy, S.; Shinde, S.; Hamilton, G. A.; Hartnett, H. E.; Jones, A. K., *Eur. J. Inorg. Chem.* **2011**, 1050-1055.

APPENDIX A-1

PERMISSION TO REPRODUCE CHAPTER 2 FROM EUROPEAN JOURNAL OF INORGANIC CHEMISTRY

APPENDIX A-2

PERMISSION TO REPRODUCE CHAPTER 4 FROM DALTON TRANSACTIONS

Biomimetic model for [FeFe]-hydrogenase: Asymmetrically disubstituted diiron complex with a redox-active 2,2'-bipyridyl ligand

Dalton Trans., 2013, **42**, 3843 – Reproduced by permission of

The Royal Society of Chemistry (RSC)

APPENDIX B

CO-AUTHOR APPROVAL

All co-authors have granted permission for use of the material in Chapters 2, 3, 4, 5 and 6 for the purpose of this dissertation.